THE UNIVERSITY OF MICHIGAN

COLLEGE OF ENGINEERING
Department of Mechanical Engineering
Heat Transfer and Thermodynamics Laboratory

Progress Report No. 6
(For the Period December 1962 - October 1963)

PRESSURIZATION OF LIQUID OXYGEN CONTAINERS

J. A. Clark
H. Merte, Jr.
V. S. Arpaci
W. J. Yang
P. S. Larsen
E. Lewis
H. Barakat
B. Bailey
L. Chen

ORA Project 04268

under contract with:

NATIONAL AERONAUTICS AND SPACE ADMINISTRATION
GEORGE C. MARSHALL SPACE FLIGHT CENTER
CONTRACT NO. NAS-8-825
HUNTSVILLE, ALABAMA

administered through:

OFFICE OF RESEARCH ADMINISTRATION ANN ARBOR

April 1964

TABLE OF CONTENTS

TABLE OF CONTENTS (Continued)

TABLE OF CONTENTS (Concluded)

LIST OF ILLUSTRATIONS

LIST OF ILLUSTRATIONS (Continued)

Figure

Figure

NOMENCLATURE

(Part V)

$A'(\lambda)$	defined by Eq. (29), dimensionless
C_i	mole fraction of ith component, dimensionless; $C'_{i\infty}$, $C''_{i\infty}$, C'_{is}, C''_{is}, C'_{io} and C''_{io} are defined in Figures 33 and 34.
C_p	molar specific heat, Btu/lb-mole °F
D	mass diffusivity, ft^2/hr
h_{fg}	latent heat of evaporation per mole, Btu/lb-mole
k	thermal conductivity, Btu/hr-ft °F
P	pressure, lbf/ft^2 perimeter
P_o	initial ullage pressure, lbf/ft^2
P''_∞	final ullage pressure, lbf/ft^2
p	$\sqrt{\frac{s}{D}}$
Q_c	strength of an instantaneous plane source of mass, ft
Q_t	strength of an instantaneous plane source of heat, ft - °F
q	$\sqrt{\frac{s}{\alpha}}$
s	Laplace variable, 1/hr
t	time, hr
T	temperature, °F; T'_∞, T''_∞, T_s and $T_{\infty,sat}$ are defined in Figures 33 and 34.
X(t)	location of interface at time t, ft
x	distance from the position of the liquid-vapor interface in the direction of liquid, ft

x^*	location of a unit instantaneous plane source of heat or mass from the moving liquid-vapor interface, ft
α	thermal diffusivity, ft^2/hr
γ_T	defined by Eq. (41) dimensionless
δ_T	defined by Eq. (40) dimensionless
λ	growth rate parameter of the liquid-vapor interface dimensionless
ρ	density, $lb/mole/ft^3$
σ_T	defined by Eq. (42) dimensionless
$\left(\frac{\partial C}{\partial T}\right)$	gradient of concentration with respect to temperature at constant pressure P''_∞ $1/°F$

Subscripts

i	component, i = 1,2,3...
s	at interface
sat	saturated state
o	initial state
is	at a distance from the interface
P''_∞	corresponding to final ullage pressure P''_∞

Superscripts

$(\ )'$	liquid phase
$(\ )''$	vapor phase

(Part VII)

C_p	specific heat, Btu/lbm °F
F_b	surface-area-in-contact-with-the-heating-surface fraction of the actual bubble, defined by Eq. (71), dimensionless

F_c	curvature factor, dimensionless
F_s	surface-area-in-contact-with-the liquid fraction of the actual bubble, defined by Eq. (70), dimensionless
F_v	volume fraction of the actual bubble, defined by Eq. (69), dimensionless
h_{fg}	latent heat of vaporization, Btu/lbm
k	thermal conductivity, Btu/hr-ft °F
R(t)	bubble radius, ft
R_c	critical radius, ft
T	temperature, °F
X(t)	thickness of vapor film, ft
x	coordinate axis, ft
α	thermal diffusivity, ft^2/hr
δ	thermal boundary layer thickness (or thickness of thermal diffusion for transient film boiling) ft
δ'	thermal boundary layer thickness (or thickness of thermal diffusion) for transient nucleate boiling, ft
ρ	density, lbm/ft^3
σ	surface tension of the liquid
τ	time, hr
τ_o	waiting time in transient film boiling, hr
τ_o'	waiting time in transient nucleate boiling, hr
τ_{max}	time for a vapor film to grow to the maximum thickness in transient film boiling, hr

τ_{max}	time for a bubble to grow to the maximum size in transient nucleate boiling, hr

Superscript

$(\ )'$	transient nucleate boiling, liquid phase

Subscripts

ℓ	liquid
s	solid
sat	saturated state
v	vapor
∞	at infinity

ABSTRACTS

I. The problem of a sudden temperature change of the pressurant of a liquid container is analyzed by means of the integral technique, including the axial conduction in the pressurant fluid and heat transfer from the ambient. The ratio of interfacial to peripheral heat transfer is evaluated by a numerical example.

II. The results of acceleration measurements using a new accelerometer are presented for fractional gravity and free-fall conditions. On the basis of these results, a new test package was designed and constructed which reduces the magnitude of near-zero gravity attainable from approximately $a/g = 0.01$ to $a/g = 0.001$, an order of magnitude improvement.

Data are presented for film and nucleate boiling with the 1 in. dia sphere at $a/g = 0.6$. The film boiling data is correlated well by the equation of Frederking and Clark.

Data obtained at $a/g = 1$ with a 1/4 in. dia sphere has shown a size effect in film boiling not revealed with 1/2- and 1-in. dia spheres.

New results are presented for the 1 in. dia sphere in all boiling regions with the new test package under free fall conditions where $a/g \cong 0.001$.

III. A summary of all results obtained is presented, and indicated behavior similar to that observed with water. At low heat flux, increases in system acceleration result in a decrease in the heater surface superheat, while at high flux the heater surface superheat increases with increase of the system acceleration.

This report completes the phase of the study where the acceleration vector is normal to the heating surface. Future areas of study are outlined.

IV. Analytical and experimental results for the dynamic growth of a single stationary nonsoluble gas bubble in a volatile liquid are discussed for application to gas injection cooling. The mass diffusion in the gas phase reduces bubble growth rates significantly and need be considered for a stationary bubble. Based on the previous results the proposed future investigations are outlined.

V. The source theory is applied to obtain approximate solutions for determining the time-dependent interfacial location and the rate of phase change at the interface of a suddenly pressurized, multi-component liquid-vapor system. Numerical calculations for the phase change of one- and two-component cryogenic

systems of nitrogen-nitrogen, helium-nitrogen and oxygen-nitrogen show that the approximate solutions, which are of a considerably simpler form, compare favorably with the existing exact solutions. A conclusion is reached that the approximation by the source theory is dependable for low rates of phase change. The applicability of the source theory is discussed in regard to the physical configuration of the system and the nature of the phase change.

VI. A brief outline is given of the separately reported studies of the transient laminar free-convection heat and mass transfer in closed, partially filled liquid containers. The method of approach and the scope of investigation are given.

VII. The mechanism of the transient film and nucleate boiling in a subcooled liquid is presented. An analysis is given for predicting the growth and collapse of (a) the vapor film formed on an insulating substrate during film boiling, and (b) a bubble generated in an insulating substrate during nucleate boiling in a tank suddenly filled with a cryogenic fluid. Expressions for the residence time of the vapor film on the insulating substrate and the time required for a bubble to reach its maximum radius before collapsing are obtained. Variables and physical properties which govern the residence time of the vapor film on the insulating substrate and the growth and collapse of a bubble are defined and examined. In addition, a definition is sought for the physical properties of the insulating substrate and cryogenic liquid which give low rates of growth and collapse for a vapor film and a bubble.

I. OPTIMIZATION OF PRESSURIZED-DISCHARGE PROCESSES IN CRYOGENIC CONTAINERS

Analytical Program

In the last two progress reports an approximate integral method was developed for complicated problems whose solutions are not available by exact analytical means. The procedure was applied to the insulated container subject to a sudden temperature change at the inlet temperature of the pressurant fluid including the axial condition in the pressurant fluid.

The problem will now be extended to include the heat transfer from the container to the ambient. Then the solution will be used for a comparison between the peripheral and axial conductions.

The energy equation for the wall, with the addition of the heat transfer to the ambient at zero temperature, becomes

$$\frac{d}{d\theta}\int_0^{V\theta} \rho_w c_w A_w t\, dx = \int_0^{V\theta} h_i P_i (T-t)dx - \int_0^{V\theta} h_o P_o t\, dx \qquad (1)$$

The energy equation for the fluid remains the same as in the previous analysis[1]

$$\frac{d}{d\theta}\int_0^{V\theta} \rho c A T dx = \rho c A V T_g - \int_0^{V\theta} h_i P_i (T-t)dx + kA\left(\frac{\partial T}{\partial x}\right)_{x = V\theta} \qquad (2)$$

The approximate profiles used in the previous report[1] may again be utilized

$$t(x,\theta) = \left[\left(\frac{x}{V\theta}\right) - 1\right]^2 f_2(\theta) \qquad (3)$$

$$T(x,\theta) = T_g + \left(\frac{x}{V\theta}\right)\left[\left(\frac{x}{V\theta}\right) - 2\right][T_g - f_1(\theta)] - f_1(\theta)\left(\frac{x}{V\theta}\right)^2 \qquad (4)$$

Employing the procedure of the same report,[1] the following simultaneous differential equations are obtained

$$\left(\frac{d}{d\Theta} + b_1\right)F_1 - b_1F_2 = T_g \tag{5}$$

$$-b_2F_1 + \left(\frac{d}{d\Theta} + b_2 + b_3\right)F_2 = 0 \tag{6}$$

subject to the initial conditions

$$F_1(0) = F_2(0) = 0 \tag{7}$$

where

$$F_1(\Theta) = \frac{\Theta}{3}(T_g + f_1) \quad , \qquad F_2(\Theta) = \frac{\Theta}{3} f_2 \quad ,$$

$$b_1 = \frac{h_i P_i}{\rho c A} \quad , \qquad b_2 = \frac{h_i P_i}{\rho_w c_w A_w} \quad , \qquad b_3 = \frac{h_o P_o}{\rho_w c_w A_w} \quad .$$

The solution of Eqs. (5) and (6) subject to Eq. (7) is

$$F_1(\Theta) = C_1 e^{-B_1\Theta} + C_2 e^{-B_2\Theta} + \left(\frac{b_2+b_3}{b_1 b_3}\right)T_g \tag{8}$$

$$F_2(\Theta) = C_1\left(1 - \frac{B_1}{b_1}\right)e^{-B_1\Theta} + C_2\left(1 - \frac{B_2}{b_1}\right)e^{-B_2\Theta} + \frac{b_2}{b_1 b_3} T_g \tag{9}$$

where

$$B_1 = \frac{b_1+b_2+b_3-B}{2} \quad , \qquad B_2 = \frac{b_1+b_2+b_3+B}{2} \quad , \qquad B = \sqrt{(b_1+b_2+b_3)^2 - 4b_1b_3},$$

$$C_1 = -\frac{T_g}{b_3 B}\left[\frac{(-b_1+b_2+b_3+B)(b_2+b_3)}{2b_1} + b_2\right] ,$$

$$C_2 = +\frac{T_g}{b_3 B}\left[\frac{(-b_1+b_2+b_3-B)(b_2+b_3)}{2b_1} + b_2\right] .$$

Thus using Eqs. (3), (4), (8), and (9), the local value of the ratio of the axial conduction to the heat transfer from the periphery of the container is found to be

$$\frac{q_i}{q_p} = \frac{-kA\left(\frac{\partial T}{\partial x}\right)_{x = V\theta}}{\int_0^{V\theta} h_i P_i (T-t)dx}$$

which gives

$$\frac{q_i}{q_p} = \frac{6kAb_1}{h_i P_i (V\theta)^2 B_1} \frac{\left[1+\frac{C_2}{C_1} e^{(B_1-B_2)\theta} + \frac{1}{C_1}\left(\frac{b_2+b_3}{b_1 b_3} - \frac{\theta}{3}\right) T_g e^{B_1\theta}\right]}{\left[1+\frac{C_2 B_2}{C_1 B_1} e^{(B_1-B_2)\theta} + \frac{1}{B_1 C_1} T_g e^{B_1\theta}\right]} \qquad (10)$$

A numerical example is given for the following system:

Pressurant fluid (O_2)		Container (Stainless Steel)	
k	= 0.013 Btu/hr-°F-ft	ρ	= 490 lbm/ft^3
ρ	= 0.096 lbm/ft^3	c	= 0.1 Btu/lbm-°F
c	= 0.22 Btu/lbm-°F	D_i	= 6-1/2 ft
V	= 1600 ft/hr	δ_i	= 3/8 in.
T_g	= 200°F	L	= 40 ft
h_i	= 5 Btu/hr-ft^2-°F,	h_o	= 3 Btu/hr-ft^2-°F
P_i	= πD_i = 20.42 ft		
P_o	= $\pi(D_i+2\delta)$ = 20.62 ft		
A	= $A_i = \pi D_i^2/4$ = 33.2 ft^2		

TABLE I

RATIO OF INTERFACIAL TO PERIPHERAL HEAT TRANSFER

Location	0.2L	0.4L	0.6L	0.8L
Time θ (sec)	18	36	54	72
q_i/q_p	27.7×10^{-5}	5.15×10^{-5}	1.25×10^{-5}	0.59×10^{-7}

The foregoing table shows that the axial conduction in the fluid has a negligible effect on the heat transfer problem under study. At first sight, the ratio of interfacial heat transfer to peripheral heat transfer seems smaller than anticipated. However, noting that q_i is directly proportional to the thermal conductivity, the use of a liquid instead of a gas (thermal conductivity being increased approximately 30 times) would change this ratio to 1% for 0.2L. This result appears quite reasonable for the effect of axial conduction in liquids.

II. BOILING OF A CRYOGENIC FLUID UNDER REDUCED GRAVITY

A. Measurement of Acceleration

1. KISTLER ACCELEROMETER

The Kistler Model 303 S/N 384 Servo Accelerometer, described in the previous report,[1] was received during this reporting period. This unit, which operates on a 28 ± 2 volt DC power supply, has a range of ± 1/g, a voltage sensitivity of 5.0 volts/g, a damped natural frequency of 160 cps, a linearity of 0.1% of full scale (0.001 g), and a resolution of ± 0.005% of full scale (±0.00005 g). A calibrating fixture was constructed for the accelerometer. As indicated above, the calibration curve is linear within 0.001 g; the main purpose of the calibration fixture is for calibration of the Sanborn recorder, which is not linear over its entire range.

After the characteristics of the accelerometer had been determined, it was necessary to modify the voltage output so that when high sensitivity of the Sanborn recorder was desired in the range around zero g (e.g., ± 0.1 volts for full scale deflection), the high voltage (+ 5 volts) output at the 1 g state prior to drop would not damage the galvanometer in the recorder. This was accomplished by adding a diode limiting circuit which allows prior selection and limiting of the voltage range sensed by the Sanborn recorder.

2. MEASUREMENTS

A series of test drops were made at various levels of a/g with the accelerometer mounted on the top of the test package which in turn is mounted on the test platform. The results are presented in Figures 1-7.

Figure 1 shows the output of the accelerometer with the test package in the condition used for all tests reported heretofore, during free fall. A high frequency (approximately 90 cps) oscillation is generated upon release which persists during a significant part of the drop period. This oscillation is believed due to the release of elastic energy stored in the test platform frame. A stiffening bar was installed on the frame and Figure 2, with a magnified "g" scale, indicates that it has been reduced considerably. Figure 3 shows the accelerometer output as recorded on the Sanborn 4-channel recorder, with an expanded time scale. The slight humps in the acceleration, seem also in both Figures 1 and 2, are believed to show the influence of the floor opening and a structural beam as the test platform passes by.

Several test runs with boiling were repeated to determine if the oscillation of the test platform had influenced the results. No change was detected.

For fractional gravity tests, the drop was initiated by activating a solenoid which engaged the counterweight. Thus the counterweight cable is initially subjected to the full weight of the test package. As seen in Figure 4, for nominal a/g = 0.2, oscillations occurred during the drop period due to energy storage in the counterweight cable. The amplitude of the oscillation is reduced if the drop is initiated instead by releasing the test platform, reducing the initial stress in the counterweight cable. Figure 5 shows the result of this change, which was used for subsequent tests. Figures 6 and 7 show similar effects for nominal a/g = 0.6. A beat effect is observed wherein a decreasing amplitude is followed by a phase change and an increasing amplitude.

A device is being developed to maintain a constant tension in the cable both prior to and during the drop, eliminating the sudden change which causes the oscillation.

B. New Package Design

As indicated in the previous sections, the test platform being used had shortcomings in its sensitivity to external pressure variations, guidewire drag, and its internal vibration history. The release system for counterweight drops was not too efficient when modified for dropping from the test package location. Future tests utilizing subcooled nitrogen would require a pressurized test vessel. For the above reasons a new test package was deemed desirable.

A package was designed which eliminated the above shortcomings and could be adapted to future programs. A sketch of this package is shown in Figure 8.

For "0" g tests, the inner test vessel is suspended from the upper part of the outer package via three chains and a spring loaded pawl which is prevented from withdrawing by friction. The outer package is released by a solenoid actuated yoke being withdrawn, and the weight of the inner vessel is removed from the spring-loaded pawl, thereby releasing the inner vessel. The outer package thus acts as a wind screen, eliminating the effects of variation in air pressure and drag. Since the outer package is symmetrical the guide wires, with their accompanying variable drag, have been eliminated. Measurements on the inner vessel with the accelerometer indicate that the effective force field with free fall has been reduced by an order of magnitude, to approximately .001 g. More accurate measurements of the force field than this are not practical because of background noise level. The force field has been

reduced to the level, it is believed, where the forces in the small electrical wires to the inner test vessel are becoming influential.

For fractional gravity tests the inner test vessel will rest on the bottom of the outer package. The counterweight cable passes through the solenoid operated release mechanism.

The upper end of the outer package has a welded flange so that a cover may be installed and the vessel pressurized for subcooled boiling tests.

The elimination of guide wires for the test package required a modification of the buffer mechanism to prevent the package from falling to the floor after being decelerated. This was accomplished by installing eight two-by-fours around the base of the buffer to form an inverted conical enclosure. After the test package comes to a stop, it falls over a few degrees from the vertical until the top rests against one or two of the two-by-fours. In the event of a misalignment drop, it is anticipated that the two-by-fours would tend to deflect the package back onto the buffer, reducing the probability and severity of damage. Uninstrumented drops of the test package onto the buffer have demonstrated that this system performs satisfactorily.

C. Additional Data

During this period the $a/g = 0.6$ test runs were completed, using TOS-7, a 1 in dia sphere. Several tests were conducted at $a/g = 1$ using a 1/4 in dia sphere to obtain further information on the effect of size. Also, a number of tests were conducted with the 1 in. dia sphere under free fall in the new test package, with a lower value of a/g than heretofore possible.

1. $a/g = 0.6$ 1 IN. DIA SPHERE

a. Film Boiling

These data are presented in Figure 9. The results are similar to those presented previously,[1] in that good correlation is observed with the Frederking-Clark prediction,[7] with a 1/3 power dependency of heat flux on acceleration. The reference curves for $a/g = 1$ and $a/g \approx 0$ have been modified in the nucleate and transition boiling regions to reflect the averages obtained with the majority of data. This shift in the reference curves is due to the use of pure liquid nitrogen.

In Figure 10 the film boiling data for the various fractional gravities

are plotted in the form of Nusselt number and modified Rayleigh number for comparison with the correlations. It is noted that the correlation due to Bromley[8] does not predict the behavior observed. As is seen in Figure 3 of Ref. 9, the experimental data of Bromley for film boiling of liquid nitrogen from a horizontal tube are comparable with the sphere data in the Δt range common to both. Bromley's data is carried on to high values of Δt, where laminar conditions most likely exist, and thus the 1/4 exponent on the modified Rayleigh number predicts the results better in that region. Bromley's correlation is given in Figure 14. It is noted that the two correlations intersect at a modified Rayleigh number of approximately 2×10^7, and may serve as an indication of transition from laminar to turbulent conditions.

With free fall conditions the value of the force field is known, from accelerometer measurements, to lie in the range $.01 < a/g < .03$. The data are plotted to indicate this range.

b. Nucleate and Transition Boiling

A number of tests were conducted to complete the sequence of nucleate and transitional boiling with the sphere at $a/g = 0.6$. A rather pronounced shift of the data in the transition region occurred in all these runs, as indicated in the representative data shown in Figure 11. Some erratic values of peak heat flux also were obtained.

The data appear to indicate that a definite time lag exists in the response of the thermocouple to the increasing heat flux of the transition region. This could occur if the solder joint of the thermocouple to the sphere had become defective. The thermocouple appeared to be firmly attached, but as a precautionary measure a new one was installed. Subsequent tests indicated that the problem has been rectified. It is possible that the repeated shocks of impact under test conditions may have resulted in a partial short circuit between the thermocouple wires away from the junction but within the sphere.

2. $a/g = 1$. 1/4 IN. DIA SPHERE

Figure 12 shows the data obtained in all the boiling regions with the 1/4 in. copper sphere at $a/g = 1$. Previous tests conducted with a 1/2 in. dia sphere indicated no difference in behavior from a 1 in. dia sphere. The data in the nucleate and transition region are shifted somewhat, but the maximum is unchanged. In the film boiling region, however, a pronounced increase in heat flux for a given Δt is observed, on the order of 100%.

This particular sphere was constructed with a 1/32 in. dia ss rod embedded as a support and it was thought that the presence of this rod, acting

as a fin, might influence the results. A second 1/4 in. dia sphere was constructed with no rod, using instead the attached thermocouple soldered to the center as the support.

The results with this second sphere are shown in Figure 13, and are virtually unchanged. A single, unusually high value of the maximum heat flux did result. The minimum heat flux has changed from approximately $(q/A)_{min}$ = 1700 Btu/hr-ft^2 for the 1- and 1/2-in dia spheres to $(q/A)_{min}$ = 4000 Btu/hr-ft^2 for the 1/4 in. dia sphere.

The film boiling data are presented in terms of the Nusselt number and modified Rayleigh number in Figure 14 for purposes of comparison with correlations. Bromley's definition of the modified Rayleigh number differs slightly from that of Frederking and Clark, and the data were computed in both ways to determine the significance of the difference. As is seen in Figure 14, the difference is negligible in this region.

The data lie above, but parallel to the Frederking-Clark correlation. No explanation can be given yet for the behavior with this particular size sphere, but it will be given further consideration. A fundamental change in liquid-vapor flow patterns may be taking place.

3. a/g = 0. 1 IN. DIA SPHERE WITH NEW TEST PACKAGE

Further data with the 1 in. dia sphere was obtained for free fall conditions, but now using the new test package shown in Figure 8. Based on accelerometer measurements the fractional gravity is estimated to be in the range $0 < a/g < .003$.

a. Film Boiling.

The results in the film boiling region are given in Figure 15, and the same procedure as previously followed was used. For each run, data at a/g = 1 were obtained just prior to release. During free fall, a gradual change in slope of the time-temperature data occurred and this change is represented in the plot by a range of heat flux for each particular Δt.

Except for one point early in the transition region, the heat flux continues to decrease during the course of the free fall period. This may represent the viscous decay of the residual liquid motion induced by the boiling process at a/g = 1. It may represent instead the increasing thermal resistance due to the increase in thickness of the vapor film, if the vapor generated is not removed from the vicinity of the heating surface. This latter possibility will be considered further, since it is amenable to an analytic solution.

For reference, the heat flux predicted by the Frederking-Clark correlation are included in Figure 15 for several low values of fractional gravity.

b. Nucleate and Transition Boiling

The results for the nucleate and transition region are shown in Figure 16. Upon release in the transition region the heat flux continually decreases. With release in the region of the maximum heat flux a distinct fluctuation occurs which may represent the action of the intense violent liquid motion occuring at the maximum heat flux.

D. Future Work

Preparation is being made to obtain datain all boiling regions with a flat disc used as a transient colorimeter, as described in Ref. 2. The disc will simulate a flat heating surface and will permit a study of the effect of surface orientation under the various fractional gravities in the range $0 < a/g < 1$. A new digital computer program will be prepared for data reduction purposes.

The new test vessel can be readily modified to become a closed vessel, permiting pressurization. Plans are underway for doing so. This will lead to a study of the effect of liquid subcooling on the boiling of liquid nitrogen under the various fractional gravities. Both the sphere and disc heating surface configurations will be used.

III. HEAT TRANSFER TO A CRYOGENIC FLUID IN AN ACCELERATING SYSTEM

A. General

This study has been concerned with determining the effect of system acceleration on boiling heat transfer with cryogenic fluids. The present work has specifically dealt with boiling of saturated liquid nitrogen from a flat surface, using a steady-state technique with electrical heating, and with an orienteation such that the resulting body forces are exerted in a direction perpendicular to and toward the heating surface. The acceleration was varied from $a/g = 1$ to $a/g = 18.4$, and heat flux convered the range $g/a = 2{,}000$ to $40{,}000$ Btu/hr-ft^2.

This phase of the work has been completed and the final results are presented below. Also included is a table indicating the location of the detailed results of the various tests in the previous progress reports.

B. New Test Results

The modifications to the test vessel described in Ref. 1 resulted in a reduction in the temperature difference across the underside of the main heater. Except for the lowest heat flux, the temperature difference varied from 5 to 10°F, depending upon the acceleration. No significant differences in results obtained could be attributed to a large variation of this temperature difference.

In almost all test runs conducted with acceleration, a definite shift in $T_w - T_{sat}$ at $a/g = 1$ occurred after the initial acceleration period, subsequent to which it remained quite stable. It is believed that a "conditioning" of the heater surface took place as a result of the change in bubble sizes and number of nucleating sites with increasing acceleration. In order to eliminate this additional factor in the final results, the initial acceleration was always repeated twice, and the first readings were discarded. This "condition" or "history" effect could itself furnish an interesting problem for investigation.

1. RUN 32. $q/A = 10{,}130$ Btu/hr-ft^2

Figure 17 shows the time-temperature data for the various accelerations.

The thermocouples measuring fluid temperature at two different heights gave virtually the same values at all times. ΔT_B, the temperature difference across the heater underside, defined at $\Delta T_B = T_{HB} - T_B$ varied from $\Delta T_B = -7°F$ at $a/g = 1$ to $\Delta T_B = -4°F$ at $a/g = 18.3$.

Figure 18 shows the superheat of the heater surface and of the liquid nitrogen as a function of acceleration for a given liquid depth. As may be noted from Figure 17, however, these quantities are independent of depth. The increase in $T_H - T_{sat}$ with acceleration is relatively large (1.5°F) and did not reproduce the results of two previous tests at this heat flux. In runs nos. 21 and 27 the increase in $T_H - T_{sat}$ amounted to 0.6°F and 1.0°F, respectively.

2. RUN 33. $q/A = 20{,}170$ Btu/hr-ft^2

Figures 19 and 20 show the time-temperature data and superheats, respectively, for the various accelerations. ΔT_B varied from $\Delta T_B = -7°F$ at $a/g = 1$ to $\Delta T_B = -4°F$ at $a/g = 18.3$. In Figure 20 the increase in $T_H - T_{sat}$ with acceleration is noted.

In Figure 19, immediately after subjecting the system to accelerations of $a/g = 14.7$ and $a/g = 18.3$, the surface temperature decreased to a value slightly below the steady values at $a/g = 1$ and then returned to the normal value. At higher values of heat flux this effect becomes much more pronounced, and will be discussed later.

3. RUN 35. $q/A = 30{,}100$ Btu/hr-ft^2

Figure 21 presents the time-temperature data for an increased heat flux, and Figure 22 shows the heater surface and liquid superheats as functions of acceleration. The heater surface temperature at $a/g = 1$ appeared to change slightly with time after each successive acceleration. Had sufficient time been allowed between each acceleration, a steady value would have been reached. Estimates of these values were used in plotting the data in the upper portion of Figure 22, and a slight shift for the various $a/g = 1$ values still persisted. To isolate the effect of acceleration alone, the net changes are given in the lower portion of Figure 22. The value of ΔT_B varied from $\Delta T_B = -8°F$ at $a/ = 1$ to $\Delta T_B = -5°F$ at $a/g = 18.3$.

4. RUN 36. $q/A = 5{,}010$ Btu/hr-ft^2

This run is a repeat of two previous tests (Run 23 and 29) and was intended to discover if any significant changes occurred when ΔT_B was decreased to $\Delta T_B = -11°F$ at $a/g = 1$ and $\Delta T_B = -8°F$ at $a/g = 18.3$. The results are

given in Figures 23 and 24 and are essentially the same as the previous results in that $T_H - T_{sat}$ first increases then decreases with increasing acceleration.

5. RUN 37. $q/A = 2{,}000$ Btu/hr-ft^2

Figures 25 and 26 show the results conducted at the lowest heat flux. From Figure 26 it is noted that $T_w - T_{sat}$ increased up to $a/g \approx 5$ and then exhibited a pronounced decrease with further acceleration. This is attributed to the increasing contribution to the total heat transfer of nonboiling convection, reducing the contribution of boiling and thereby requiring a lower heater surface superheat.

The value of ΔT_B varied from $\Delta T_B = -13°F$ at $a/g = 1$ to $\Delta T_B = -10°F$ at $a/g = 18.3$, somewhat larger than that at the higher heat fluxes because of the reduced boil-off rate.

6. RUN 38. $q/A = 39{,}400$ Btu/hr-ft^2

Figure 27 shows the time-temperature data for the highest heat flux imposed in these tests. The maximum heat flux is expected to be in the vicinity of $q/A = 50{,}000$ Btu/hr-ft^2 and higher heat fluxes were not employed to avoid possible destruction of the heater.

As with all of the acceleration tests, the heater surface temperature decreases as the liquid level decreases, showing the effect of changes in hydrostatic head and hence saturation temperature. The values of $T_H - T_{sat}$, however, remain virtually constant, indicating that the effect of the small pressure variation on the boiling process is negligible.

After each high acceleration test, the heater surface temperature decreased to quite a low value and then began rising again to the value existing at $a/g = 1$ prior to that particular acceleration. Thus, in the lower curve of Figure 27, $T_H - T_{sat}$ also decreases and then rises to an asymptotic value. This effect has become more pronounced with the higher heat flux.

In Figure 28 are plotted the values of heater surface superheat as a function of acceleration. The increase of $T_H - T_{sat}$ with acceleration is not as large as at lower values of heat flux, and may be related to the approach to the maximum heat flux.

C. Discussion

Table II furnishes a tabulation of the various tests conducted in this particular program which resulted in meaningful data.

TABLE II

SUMMARY OF TESTS CONDUCTED IN AN ACCELERATING SYSTEM

Test No.	a/g Range	Heat Flux Btu/hr-ft^2	Location of Results	Comments
5	1	2,500-47,000	Ref. 2 Figs. 66-70	Impure liquid nitrogen—test vessel with no guard heaters
6	1	2,500-47,000	Ref. 2 Figs. 71-75	Pure liquid notrogen—test vessel with no guard heaters
21	1-18.3	10,100	Ref. 3 Figs. 28-33	Pure liquid nitrogen—with new heater surface assembly.
22	1-18.3	20,100	Ref. 3 Figs. 34-40	
23	1-18.3	5,000	Ref. 3 Figs 41-42	
25	1	2,000-5,000	This report Fig. 29	Test vessel not completely assembled
26	1	2,000-30,000	Ref. 1 Figs. 16,17	
27	1-18.3	10,200	Ref. 1 Figs. 18,19	
29	1-18.3	5,100	Ref. 1 Fig. 20	
32	1-18.3	10,100	This report Figs. 17,18	Outer test vessel modified to reduce ΔT_B
33	1-18.3	20,200	This report Figs. 19,20	

TABLE II (Concluded)

Test No	a/g Range	Heat Flux Btu/hr-ft^2	Location of Results	Comments
34	1	2,000-30,000	This report Fig. 29	Subjected to a/g = 5.6 prior to varying flux at a/g = 1
35	1-18.3	30,100	This report Figs. 21,22	
36	1-18.3	5,000	This report Figs. 23,24	
37	1-18.3	2,000	This report Figs. 25,26	
38	1-18.3	39,400	This report Figs. 27,28	

In almost all tests subjected to high acceleration it was found necessary to discard the results of the initial acceleration because the value of $T_H - T_{sat}$ at a/g = 1 following this acceleration was reduced from that preceding it (e.g., Figures 17, 19, 23, and 27). Also, as was pointed out previously, at the higher values of heat flux the values of $T_H - T_{sat}$ at a/g = 1 immediately following each acceleration run was reduced to a low value and then slowly increased back to an asymptotic value (e.g., Figures 19, 21, and 27). It was thought that this effect might be the result of the large residual motion in the liquid induced by the high force fields. However, because of limitations in the experimental apparatus it was necessary to refill the test vessel with liquid nitrogen after each high g run, and this process would eliminate any residual liquid motion. Furthermore, were this the case, the effect would be more pronounced at the lower values of heat flux rather than the opposite.

It is believed that the effects observed above can be explained in terms of the prior history of the active or nucleating sites. A number of workers have noted a so-called hysteresis effect in nucleate boiling (e.g., Ref. 4) in which the heater surface superheat is larger when increasing the heat flux than when heat flux is decreasing. If the high heat flux due to boiling is due primarily to the turbulence promoted near the heating surface by the bubbles, then a higher heat flux requires more active sites. An active site is conceived as a minute crevice in the surface in which a vapor or gas may be trapped, serving as a nucleus for bubble growth to take place. A higher superheat is required to initiate the activation of a particular site than to sustain it, thus the hysteresis effect occurs.

It had been postulated[5] based on results obtained with water, that in-

creased system acceleration results in smaller bubble sizes at departure, with an attendant decrease in agitation. To provide for a fixed total heat flux, more nucleating sites then are required, which in turn requires an increased wall temperature. This increased wall temperature has also been observed with liquid nitrogen in the present work.

It is believed that the initial acceleration of the liquid nitrogen test system results in the activation of additional nucleating sites which thereafter remain activated, thus the observed decrease in $T_w - T_{sat}$ after this initial acceleration. At the higher values of heat flux, a relatively greater number of active sites are formed with acceleration, and when the system is brought back to $a/g = 1$ these additional sites remain temporarily activated, reducing the necessary driving force, $T_w - T_{sat}$. Some of these additional active sites may be unstable at the lower values of $T_w - T_{sat}$ and gradually disappear. Thus for a given heat flux the surface temperature must rise in order to reactivate some of them, resulting in the behavior shown in Figure 27.

The values of $T_w - T_{sat}$ at $a/g = 1$ were not always reporducible, as is seen by the various data at $a/g = 1$ plotted in Figure 29. Figure 30 is a composite plot of $T_w - T_{sat}$ versus acceleration for the various values of heat flux covered. Several of the curves were shifted so that the values at $a/g = 1$ corresponded to the curve giving the best fit of the data in Figure 29, in order that the effect of acceleration be more clearly demonstrated.

Figure 31 is a cross plot of Figure 30 and shows heat flux versus $T_w - T_{sat}$ for various system accelerations. At low heat flux, the value of $T_w - T_{sat}$ decreases with increasing acceleration owing to the increasing contribution of natural convection, while at high heat flux this temperature difference increases. This latter effect has been observed with water[5] and has been attributed to the premature removal of the vapor bubbles from the vicinity of the heating surface, reducing the turbulence induced in the liquid and resulting in a higher heater surface superheat with the condition of a constant imposed heat flux.

Also included in Figure 31 are the results from the correlation for nonboiling convection for a geometrically similar system[5] for the same system accelerations. It is noted that at the lowest heat flux, $q/A = 2{,}000$ Btu/hr-ft^2, the extensions of the nonboiling correlation coincide with the experimental data at $a/g = 15$ and $a/g = 20$, indicating that boiling is completely suppressed. With liquid nitrogen, it appears that the superheat for incipient pool boiling lies in range 6-7°F. For water,[5] this was found to be 14-15°F.

D. Future Work

The flat heater surface with the acceleration vector normal to it was selected in order to isolate the effect of acceleration on the boiling process from the additional effects of nonboiling natural convection as far as possible. In the other cases of interest, however, as in the side walls of LOX tanks subjected to vehicle acceleration and ambient heating, the acceleration vector is parallel to the heating surface, and the total heat transfer may be expected to be dependent to a greater extent on the nonboiling effects.

As the next effort, it is proposed that the effect of system acceleration on heat transfer to saturated liquid nitrogen be studied for the case where the acceleration vector is parallel to the heating surface. Figure 39 of Ref. 6 indicates the type of heater configuration contemplated. The heat flux range would cover $q/A = 1{,}000 - 40{,}000$ Btu/hr-ft^2 and the acceleration would be in the range $1 \leq a/g \leq 20$.

The same contrifuge previously used would be available, and the present test vessel, with minor modifications, could also be used. Since the process is expected to be a combination of nonboiling and boiling effects, an attempt would be made to account for the influence of acceleration by means of superposition of these phenomena in the correlation of the data.

The size of the centrifuge restricts the present study to saturated liquid nitrogen, since the additional space to achieve subcooling is not available. Should the results of this study indicate that tests with subcooled liquid would be desirable, a large contrifuge consisting essentially of a scaled-up version of the small one has been constructed and is in use in the laboratory. This unit not only is capable of handling test packages of larger size and mass at higher accelerations (100 lbm at $a/g = 1{,}000$, or 200 lbm at $a/g = 500$) but is more versatile in instrumentation capabilities, and permits high-speed photographs (25,000 frames/sec) of phenomena in the centrifuge while under rotation.

For further future efforts, consideration might be given to the modifications in present equipment necessary to utilize the transient technique for studying pool boiling of saturated liquid nitrogen at high accelerations. This would permit measurements in the maximum heat flux and film boiling regions not possible with steady-state electrical heating methods. Either spheres or flat discs, or both, could be used.

IV. INJECTION COOLING

A. Bubble Dynamics

1. PREVIOUS STUDIES

An outline of the anticipated bubble dynamic studies in connection with the gas injection cooling process was given in Ref. 2, p. 40. In accordance with this, the dynamics of the single bubble has been investigated for the case of a nonsoluble gas. First, for the stationary bubble , a quasisteady model based on the assumption of uniform gas composition at all times was solved approximately by the use of source theory (Ref. 3, p. 30 ff.). Secondly, for the single bubble moving with constant translation velocity and employing the same quasisteady assumption of uniform gas composition, an approximate solution was obtained based on the "penetration" theory (Ref. 1, p. 17 ff). Comparison of these solutions (Ref. 1, Figure 23) confirmed the anticipation that translatory motion accelerates bubble growth.

The assumption of uniform composition of the gas phase can be justified for the case of a bubble having translatory motion, owing to the induced circulation of the gas. For the stationary bubble, however, this assumption is valid only when the process of molecular diffusion of mass inside the bubble is much more rapid than the molecular diffusion and convection of heat in the liquid, providing for evaporation of the liquid component at the bubble interface. Particularly during the early stage of bubble growth the existence of a nonuniform concentration distribution in the gas phase could be expected to reduce the growth-rate. A tentative analysis, based on the theory of sources and considering a distributed gas phase, was given in Ref. 9, p. 28 ff.

2. NEW WORK

A more detailed study, reported separately,[10] includes analysis and experiment for the single bubble initially containing respectively a nonsoluble and a soluble gas. For the nonsoluble gas case, primarily of interest for the injection cooling, the solutions to bubble growth for small and intermediate values of time are obtained by the integral technique, considering a distributed gas phase, while the asymptotic solution, based on a lumped gas phase, is obtained by source theory. Analytical solutions are given to the initial behavior of bubbles containing a soluble gas, and to the collapse of soluble gas bubbles in a nonvolatile liquid. The study includes experimental results for the growth and collapse of stationary and moving single bubbles

of nitrogen, helium and, ammonia injected into water. For stationary bubbles of a nonsoluble gas, experimental bubble growth agrees well with analytical predictions based on the assumption of a distributed gas phase, indicating that this is a realistic model for this case. The experimental studies furthermore illustrate the influence of translatory bubble motion on growth and collapse rates, and the influence of liquid volatility and gas solubility on collapse rates.

In the experimental study of bubble growth, water was used instead of a cryogenic liquid to facilitate high-speed film recordings providing data for bubble size versus time. Despite the relatively large values of the governing rate-parameters

$$\text{Jacob number:} \qquad Ja = \left(\frac{\partial T}{\partial x}\right)_{P_\infty, T_\infty} \frac{\rho' C'}{\rho'' h_{fg}}$$

$$\text{Lukomskiy number:} \qquad Lu = \frac{\mathcal{D}''}{\alpha'}$$

for the H_2O-N_2 systems, the experimental results were consistent with the theoretical preductions for the stationary bubble. It can thus be concluded that inertia effects—omitted in the analysis—play a negligible part in the transient. In view of the consistently lower values of the governing parameters (Ja and Lu) for cryogenic systems, as seen from Table III, the analytical results can be expected to apply directly to such systems, for which bubble growth-rates consequently will be considerably smaller.

TABLE III

COMPARISON OF CHARACTERISTIC PARAMETERS FOR BUBBLE GROWTH
NONSOLUBLE GAS CASE

System	H_2O-N_2	H_2O-He	LOX-He	LH_2-He
T	200°F	200°F	180°R	54°R
p(atm)	~1	~1	3.1	8.1
Ja-number	100	100	12.6	2.4
Lu-number	200	600	4.6	3.33
α' (cm^2/sec)	0.00167	0.00167	0.00811	0.00125
Pseudo time-constant $t(Q = 63.2)$(sec) R_0 = 1/8-in., x_∞ = 0.8	0.072	0.030	0.575	41.5

This is illustrated in Table III, where for the stationary bubble, initially of size R_0 = 1/8-in., the pseudo time-constant t(Q = 0.632) for 63.2% completion of bubble-growth $Q = (P-1)/(P_\infty-1)$, is given. The example considers an initial gas composition of pure injection gas and a dimensionless liquid-subcooling of 0.2 (i.e., an equilibrium gas composition at the liquid temperature of $x_\infty = 0.8$).

Next, relative dimensionless bubble-growth from previous studies (see Figure 23 of Ref. 1) is compared in Figure 32 with the predictions from the new analysis.[10] It may be concluded that for the stationary bubble it is necessary to include the mass transport in the gas phase, and that this results in considerably slower growth-rates than for the lumped gas case. The predictions for the bubble having translatory motion, assuming a uniform gas composition,[1] is probably not conservative, and growth-rates smaller than those shown in Figure 32 can be expected.

Finally, the results of the analytical and experimental studies for the growth of a single bubble may be summarized as follows in regard to the gas injection cooling process.

(i) Growth rates for single stationary bubbles of a nonsoluble gas can be predicted from analysis.

(ii) Induced acceleration and translatory motion owing to buoyancy effects increases the growth-rate and need be considered.

(iii) The slow growth-rates of bubbles in cryogenic systems suggest that bubbles injected at the bottom of a vertical column are effective in cooling this over a considerable height, providing nearly uniform cooling at all times, and that for short columns the injected gas may not become fully effective.

3. FUTURE WORK

In light of the results of the analytical and experimental study for single bubbles and available experimental results for the cooling of vertical columns by gas injection the scope of the future investigations is proposed as follows.

(i) Single moving bubble.—Modification of the previous analysis[1] to account for mass transport by diffusion and convection in the gas phase, actual shape of the rising bubble and gas solubility, and experimental studies. Although very valuable for testing the analysis for the stationary bubble and showing qualitatively the influence of translatory motion, the previous experimental studies[10] need modification to provide the desired results for the moving bubble. Because of the large values of the governing parameters for bubble growth for the water-nitrogen and water-helium systems (see Table III)

a significant part of the growth (60-70%) occurred before the bubble could depart from the injector and be accelerated to a steady rise velocity (see Figures 45 and 46 of Ref. 10). The slower growth-rates for cryogenic systems imply that the major growth occurs during bubble rise, assuming the time for bubble departure unchanged. It is thus desirable to isolate the effect of translatory motion in future experiments.

(ii) Ensemble of bubbles.—Experimental study of the influence of mutual bubble interference and a finite liquid domain on the bubble growth rates.

(iii) Distributed system analysis of gas injection into a vertical liquid column.—This ultimate analysis, representing an extension of the previous analysis for the lumped system,[2,3,9] would incorporate the results of the study of single bubbles and ensembles of bubbles to enable prediction of optimum injection pattern and the influence of system geometry on the effectiveness of the cooling.

V. INTERFACE HEAT AND MASS TRANSFER IN A SUDDENLY PRESSURIZED LIQUID-VAPOR SYSTEM

A. Introduction

The dynamics of interface diffusion has recently attracted considerable attention owing to its important application in several fields of engineering. An example of such an application is the pressurization of a cryogenic liquid container. The essential feature of phase growth in general is the existence of a moving interface between two phases, with the liberation or absorption of heat on it. If the system has initially a uniform temperature distribution in each phase, the movement of the interface is characterized by the well-known $X(t) = 2\lambda\sqrt{\alpha t}$ law (the phase change grows as square root of time), which also represents the phase growth rate.

For the phase change in a suddenly pressurized one-component liquid-vapor system Thomas and Morse[11] have obtained an exact solution for the mass flux of condensate or evaporate across the interface. The interface is assumed to be at the equilibrium saturation temperature corresponding to the final ullage pressure. The integral technique is applied to obtain an approximate solution in a closed form by Knuth.[12] He has shown that the expression for the rate of the interfacial mass diffusion may be reduced to a simple linearized form if the latent heat is large in comparison with the change in enthalpy between the initial and final states, for each phase. An investigation of transient condensation of pressurant gas on insulating substrates is presented in Ref. 13. The variables and physical properties which govern the residence time of the condensate layer are examined. In Ref. 14 an analysis is made of the phase change of one-component systems in a container. The time-dependent temperature distribution, and interfacial location, and the rate of phase change at the interface are obtained in a closed form. Reference 15 presents an analysis of the phase change across the interface of a suddenly pressurized, multi-component liquid-vapor system. The time dependent temperature distribution, the interfacial growth, and the rate of condensation or evaporation at the interface are obtained.

In a previous study[9,16] the source theory was applied to obtain approximate solutions for determining (a) the growth of a vapor bubble in pure liquids and binary liquid mixtures, and (b) the growth and collapse of a noncondensing, nonsoluble-gas bubble in a pure liquid. These approximate results for case (a), which yield an explicit expression, exhibit good agreement with the existing exact solutions in the transcendental form.

This study presents the application of the source theory to the phase change across the interface of a suddenly pressurized multi-component liquid-vapor system. The nature of this problem is different from those of the previous study.[16] The former treats the interfacial heat and mass diffusion in semi-infinite regions, while the latter treats radial flow of heat and mass in spherical regions. The resulting approximate solutions compare favorably with Ref. 15 and are of a considerably simpler form.

B. Formulation of Problem

An insulated container is partially filled with a multi-component liquid in equilibrium with a mixture of its vapors at T_o, the saturation temperature corresponding to the initial system pressure P_o. A pressurant consisting of a number of components is suddenly introduced into the container resulting in the instantaneous change in the gas pressure to P''_∞ and its temperature to T''_∞. This change in the pressure level is accompanied by condensation or evaporation in which the latent heat is absorbed or supplied at the interface. Assuming both the liquid and vapor regions to be semi-infinite in extent, the study is aimed at the solution for the time-dependent interfacial location and the rate of phase change at the interface. A schematic illustration of temperature and concentration distributions in the liquid and vapor regions at several different times is presented in Figure 33.

The following assumptions are imposed on the solutions:

(i) Thermal properties are assumed independent of temperature and composition for each phase and each component.

(ii) Effects of natural convection do not exist.

(iii) At the instant of pressurization, the interface temperature and compositions immediately adjusts to that of the thermodynamic phase equilibrium at T_s, C'_{is} and C''_{is} corresponding to the final system pressure P''_∞. This contradicts the Kinetic theory in that a net mass flux is realized only if there exists a nonequilibrium state at the interface. However, it is found in Ref. 15 that the differences between interface temperature and compositions and those of equilibrium are small and may be neglected except a very short time immediately subsequent to the disturbance.

(iv) Ideal vapor and liquid phases are assumed.

(v) The mass diffusivity D for each phase remains unchanged.

With these assumptions, the equations governing heat and mass diffusion

in each phase are solved with the appropriate initial and boundary conditions for n-components in Ref. 15. The temperature and concentration distributions are coupled at the liquid-vapor interface by the assumption of equilibrium conditions at the interface. This results in a transendental equation for the determination of λ, a growth rate parameter of the interface. It is due to the complexity of this transcendental equation that an approximate solution is sought to evaluate λ by the application of the source theory.

Forster[17] has developed a method to obtain the analytical solution of the problem of diffusion in a moving medium with time-dependent boundaries. His method involves the solutions for the associated problem of diffusion in a stationary medium with stationary boundaries. Then assuming that the boundaries move stepwisely with time, the solutions for diffusion in a moving medium with moving boundaries may be obtained by the use of Green's function. Since this method has been introduced previously,[9] it is not presented here in detail.

C. Solutions

1. PHASE CHANGE IN ONE COMPONENT LIQUID-VAPOR SYSTEM

The interfacial motion due to phase change in a one-component liquid-vapor system is governed by the rate at which latent heat of vaporization can be supplied at the liquid-vapor interface.

Consider transient heat conduction in two semi-infinite regions, of which one has a heat source: Suppose that the region $x < 0$ is the liquid phase of the one component system at temperature T_o at infinity and that the region $x > 0$ is the gas phase at temperature T''_∞ at negative infinity. If there exists a unit instantaneous plane source of heat at $t = 0$ at x^* in the region $x < 0$ it is desired to determine the Green's functions for this problem. From page 363 of Ref. 18 the Laplace transform of the appropriate Green's functions for both liquid and gas temperatures may readily be written as: liquid region, $x < 0$

$$\bar{T}'(x,s) = \frac{e^{-q'|x-x^*|}}{2\alpha' q'} + \frac{(k'\sqrt{\alpha''}-k''\sqrt{\alpha'})e^{q'(x+x^*)}}{2\alpha' q'(k'\sqrt{\alpha''}+k''\sqrt{\alpha'})} + \frac{(T''_\infty-T_o)e^{q'x}}{s\left(1+\frac{k'}{k''}\sqrt{\frac{\alpha''}{\alpha'}}\right)} + \frac{T_o}{s} \tag{11}$$

gas region, $x > 0$

$$\bar{T}''(x,s) = \frac{k' e^{-q''x+q'x^*}}{q''\sqrt{\alpha'}(k'\sqrt{\alpha''}+k''\sqrt{\alpha'})} + \frac{(T_o-T_\infty'')e^{-q''x}}{s\left(1+\frac{k''}{k'}\sqrt{\frac{\alpha'}{\alpha''}}\right)} + \frac{T_\infty''}{s} \qquad (12)$$

The inverse Laplace transformation of Eqs. (11) and (12) give: liquid region, $x < 0$

$$T'(x,t) = \frac{e^{-\frac{(x-x^*)^2}{4\alpha' t}}}{2\sqrt{\pi\alpha' t}} + \frac{(k'\sqrt{a''}-k'\sqrt{\alpha'})e^{-\frac{(x+x^*)^2}{4\alpha' t}}}{2(k'\sqrt{\alpha''}+k''\sqrt{\alpha'})\sqrt{\pi\alpha' t}} + \frac{T_\infty''-T_o}{1+\frac{k'}{k''}\sqrt{\frac{\alpha''}{\alpha'}}} \operatorname{erf} -\left(\frac{x}{2\sqrt{\alpha' t}}\right) + T_o \qquad (13)$$

gas region $x > 0$

$$T''(x,t) = \frac{k'\alpha'' e^{-\frac{\left(x-x^*\sqrt{\frac{\alpha''}{\alpha'}}\right)^2}{4\alpha'' t}}}{(k'\sqrt{\alpha''}+k''\sqrt{\alpha'})\sqrt{\pi\alpha'\alpha'' t}} + \frac{T_o-T_\infty''}{1+\frac{k''}{k'}\sqrt{\frac{\alpha'}{\alpha''}}} \operatorname{erfc} \frac{x}{2\sqrt{\alpha'' t}} + T_\infty'' \qquad (14)$$

If the heat source is located at the interface $x = 0$, (i.e., $x^* = 0$) the temperature increment at the interface at time t due to an amount of heat $dQ_t(y)$ liberated on the interface at time y may be obtained from Eqs. (13) or (14) by substituting $x = 0$, $x^* = 0$ and $t-y$; hence

$$d\left(T_s - \frac{T_\infty''-T_o}{1+\frac{k'}{k''}\sqrt{\frac{\alpha''}{\alpha'}}} - T_o\right) = \frac{dQ_t(y)}{\left(1+\frac{k''}{k'}\sqrt{\frac{\alpha'}{\alpha''}}\right)\sqrt{\pi\alpha'(t-y)}} \qquad (15)$$

If the interface moves by $dx(y)$, an amount of heat

$$\rho' C_p' dQ_t(y) = \rho' h_{fg} \dot{X}(y) dy \qquad (16)$$

is released constituting a distributed plane heat source.

For the problems of phase growth in an initially uniform temperature field, the interfacial movement is characterized by the well-known expression

$$X(t) = 2\lambda\sqrt{\alpha' t} \tag{17}$$

where λ is a constant characterizing the interfacial motion and is positive for condensation, negative for evaporation.

Therefore the combination of Eqs. (15), (16), and (17) gives

$$d\left(T_s - \frac{T_\infty'' - T_o}{1+\frac{k'}{k''}\sqrt{\frac{\alpha''}{\alpha'}}} - T_o\right) = \frac{2\lambda h_{fg} dy}{C_p'\left(1+\frac{k''}{k'}\sqrt{\frac{\alpha'}{\alpha''}}\right)\sqrt{\pi y(t-y)}} \tag{18}$$

Integration of Eq. (18) gives the interfacial temperature at time t:

$$T_s = \frac{\lambda h_{fg}\sqrt{\pi}}{C_p'\left(1+\sqrt{\frac{(\rho C_p k)''}{(\rho C_p k)'}}\right)} + \frac{T_\infty'' - T_o}{1+\sqrt{\frac{(\rho C_p k)'}{(\rho C_p k)''}}} + T_o \tag{19}$$

λ, the growth rate parameter of the interfacial motion, for one component liquid-vapor system may be expressed as

$$\lambda = \frac{C_p'\left(1+\sqrt{\frac{(\rho C_p k)''}{(\rho C_p k)'}}\right)}{\sqrt{\pi} h_{fg}}\left(T_s - T_o - \frac{T_\infty'' - T_o}{1+\sqrt{\frac{(\rho C_p k)'}{(\rho C_p k)''}}}\right) \tag{20}$$

2. PHASE CHANGE IN MULTI-COMPONENT LIQUID-VAPOR SYSTEM

If both the liquid and gas phases are mixtures of multi-components, the rate of interfacial movement is controlled by the transport of heat and mass at the interface.

Consider transient mass diffusion of an n-component mixture in two semi-infinite, liquid-vapor system in which one has a mass source: Suppose that the region $x < 0$ is a liquid phase of a n-component mixture at concentration C_{io} at infinity and at the saturation concentration C'_{is} at the liquid-vapor interface $x = 0$. The region $x > 0$ is a gaseous phase of the n-component mixture at concentration $C''_{i\infty}$ at infinity and at the saturation concentration C''_{is} at the interface. If these exists a unit instantaneous phase mass source at $t = 0$ at x^* in the liquid region $x < 0$ the appropriate Green's functions in the Laplace transform for liquid and gas phases may be obtained from page 363 of Ref. 18 as:

for liquid region $x < 0$

$$\bar{C}'_i = \frac{e^{-p'|x-x^*|}}{2D'p'} + \frac{e^{p'(x+x^*)}}{2D'p'} - \sqrt{\frac{D''}{D'}}\,\frac{(C''_{is}-C''_{i\infty})}{s}\,e^{p'x} + \frac{C'_{io}}{s} \tag{21}$$

for gas region $x > 0$

$$\bar{C}''_i = \frac{C''_{is}-C'_{is}}{s}\,e^{-p''x} + \frac{C''_{i\infty}}{s} \tag{22}$$

Performing the inverse Laplace transformation on Eqs. (21) and (22), one obtains

liquid region, $x < 0$

$$C'_i(x,t) = \frac{e^{-\frac{(x-x^*)^2}{4D't}}}{2\sqrt{\pi D't}} + \frac{e^{-\frac{(x+x^*)^2}{4D't}}}{2\sqrt{\pi D't}} - \sqrt{\frac{D''}{D'}}\,(C''_{is}-C''_{i\infty})\,\mathrm{erfc}\left(\frac{-x}{2\sqrt{D't}}\right) + C'_{io} \tag{23}$$

gas region, $x > 0$

$$C''_i(x,t) = (C''_{is}-C'_{is})\,\mathrm{erfc}\,\frac{x}{2\sqrt{D't}} + C''_{i\infty} \tag{24}$$

If the mass source is located at the interface $x = 0$, the concentration increment of the liquid phase of the i-th component at the interface at time

t due to an amount of mass $\rho' dQ_{ci}(y)$ evaporated on the interface at time y may be obtained from Eq. (23) by substituting x = 0, x* = 0 and t = t-y:

$$d\left[C'_{is}+(C''_{is}-C''_{i\infty})\sqrt{\frac{D''}{D'}}-C'_{io}\right] = \frac{dQ_{ci}(y)}{\sqrt{\pi D'(t-y)}} \tag{25}$$

If the liquid-vapor interface moves by dx(y), an amount of mass of the ith component

$$\rho' dQ_{ci}(y) = \rho' \dot{X}(y) C''_{is} dy \tag{26}$$

is condensated constituting a distributed plane mass source. The combination of Eqs. (15) and (16) gives:

$$d\left[C'_{is}+(C''_{is}-C''_{i\infty})\sqrt{\frac{D''}{D'}}-C'_{io}\right] = \frac{\dot{X}(y)C''_{is}dy}{\sqrt{\pi D'(t-y)}} \tag{27}$$

Integration of Eq. (27) for the mole fraction of the ith component in the liquid phase at the interface at time t yields:

$$C'_{is} = \int_0^t \frac{\dot{X}(y)C''_{is}dy}{\sqrt{\pi D'(t-y)}} + C'_{io} - (C''_{is}-C''_{i\infty})\sqrt{\frac{D''}{D'}} \tag{28}$$

By substituting Eq. (26) into eq. (28), one gets

$$C'_{is} = \lambda\sqrt{\frac{\pi\alpha'}{D'}}\, C''_{is} + C'_{io} + (C''_{is}-C''_{i\infty})\sqrt{\frac{D''}{D'}} \tag{29}$$

This equation may be regarded as an expression for the determination of the growth rate parameter in a multi-component liquid-vapor system at isothermal state.

The interfacial temperature T_s for the ith component in the multi-component liquid-vapor system is identical with Eq. (19).

In order to couple the temperature and concentration distributions, it

is necessary to introduce an additional boundary condition, that is:

The temperature-concentration relation may be expressed by the equilibrium condition at the interface

write:

$$C'_{is} = f'_i(T_s, P''_\infty)$$
$$C''_{is} = f''_i(T_s, P''_\infty) \qquad (30)$$

The total interface mass transfer N_T is

$$N_T = \rho' \int_0^t \frac{dx}{dt}\, dt = 2\lambda\rho' \sqrt{\alpha' t} \qquad (31)$$

3. SPECIAL CASES

a. Phase Change in Binary Liquid-Vapor System

For a binary-component liquid-vapor system, if the relationship between temperature and concentration at the interface may be approximated linearly as shown in Figure 34, one obtains

$$C'_{is} = C'_{i\infty} + \left(\frac{\partial C'_i}{\partial T}\right)(T_s - T'_{\infty,sat}) \quad \text{at } P = P''_\infty \qquad (32\text{-a})$$

and

$$C''_{is} - C''_{i\infty} = \left(\frac{\partial C''_i}{\partial T}\right)(T_s - T''_{\infty,sat}) \quad \text{at } P = P''_\infty \qquad (32\text{-b})$$

Substituting Eqs. (19) and (29) into Eq. (32-a) to eliminate T_s and C'_{is}, one obtains

$$\lambda = \frac{\left(\frac{\partial C_i'}{\partial T}\right)\left[\frac{T_\infty''-T_o'}{1+\sqrt{\frac{(\rho C_p k)'}{(\rho C_p k)''}}} + T_o - T_{\infty,sat}'\right] + (C_{is}''-C_{i\infty}'')\sqrt{\frac{D''}{D'}} + C_{i\infty}'-C_{io}'}{\sqrt{\pi}\left[\sqrt{\frac{\alpha'}{D'}}\,C_{is}'' - \left(\frac{\partial C_i'}{\partial T}\right)\frac{h_{fg}}{C_p'\left(1+\sqrt{\frac{(\rho C_p k)''}{(\rho C_p k)'}}\right)}\right]} \tag{33}$$

The gas composition C_{is}'' is a function of the interface temperature T_s and can be eliminated from Eq. (33) by Eqs. (20) and (32-b), resulting in a quadratic equation in λ.

b. Zero Condensation Rate

This particularly interesting special case, $\lambda = 0$, is the case separating condensation from evaporation. From Eqs. (20), (29), and (33) it is obvious that $\lambda = 0$ if the following conditions hold:

(i) One-component liquid-vapor system

$$\frac{T_s-T_o}{T_\infty''-T_o} = \frac{1}{1+\sqrt{\frac{(\rho C_p k)'}{(\rho C_p k)''}}} \tag{34}$$

(ii) Multi-component liquid-vapor system at isothermal state

$$\frac{C_{is}'-C_{io}'}{C_{i\infty}''-C_{is}''} = \sqrt{\frac{D''}{D'}} \tag{35}$$

(iii) Binary-component liquid-vapor system

$$\left(\frac{\partial C_i'}{\partial T}\right) = \frac{(C_{i\infty}''-C_{is}'')\sqrt{\frac{D''}{D'}} + C_{io}'-C_{i\infty}'}{\frac{T_\infty''-T_\infty'}{1+\sqrt{\frac{(\rho C_p k)'}{(\rho C_p k)''}}} + T_\infty'-T_{\infty,sat}'} \tag{36}$$

Or by the substitution of Eq. (35) with i = 1 into Eq. (36), one gets

$$\left(\frac{\partial C_i'}{\partial T}\right) = \frac{\dfrac{C_{is}'-C_{io}'}{T_\infty'-T_{\infty,sat}'}}{1+\dfrac{T_\infty''-T_\infty'}{T_\infty'-T_{\infty,sat}'}\dfrac{1}{1+\sqrt{\dfrac{(\rho C_p k)'}{(\rho C_p k)''}}}} \tag{37}$$

D. Comparison of the Results by the Source Theory and the Exact

1. SOLUTIONS

The exact solutions which give the growth rate parameter as obtained in Ref. 15, may be expressed as follows:

(i) One component liquid-vapor system

$$\frac{T_s-T_o}{T_\infty''-T_o} = A'(\lambda)\,(1+\mathrm{erf}\lambda) \tag{38}$$

where

$$A'(\lambda) = \frac{\delta_t\lambda\,\mathrm{erfc}(\gamma_T\lambda) + \sigma_t e^{-\lambda^2\gamma_T^2}}{e^{-\lambda^2}\mathrm{erfc}(\gamma_T\lambda)+\sigma_T e^{-\lambda^2\gamma_T^2}(1+\mathrm{erf}\lambda)} \tag{39}$$

$$\delta_T = \frac{\sqrt{\pi}h_{fg}}{C_p'(T_\infty''-T_o)} \tag{40}$$

$$\gamma_T = \frac{\rho'}{\rho''}\sqrt{\frac{\alpha'}{\alpha''}} \tag{41}$$

$$\sigma_T = \sqrt{\frac{(\rho C_p k)''}{(\rho C_p k)'}} \tag{42}$$

(ii) Multi-component liquid vapor system at isothermal state

$$\frac{(C'_{is}-C'_{io})e^{-\left(\lambda\sqrt{\frac{\alpha'}{D'}}\right)^2}}{1+\mathrm{erf}\left(\lambda\sqrt{\frac{\alpha'}{D'}}\right)} - \frac{(C''_{is}-C''_{i\infty})\sqrt{\frac{D''}{D'}}\,e^{-\left(\lambda\frac{\rho'}{\rho''}\sqrt{\frac{\alpha'}{D''}}\right)^2}}{\mathrm{erfc}\left(\lambda\frac{\rho'}{\rho''}\sqrt{\frac{\alpha'}{D''}}\right)} = \sqrt{\pi}\rho'\lambda\sqrt{\frac{\alpha'}{D'}}\left(\frac{C''_{is}}{\rho''}-\frac{C'_{is}}{\rho'}\right) \tag{43}$$

(iii) Binary-component liquid-vapor system

$$\frac{C'_{i\infty}-C'_{io}}{1+\mathrm{erf}\left(\lambda\sqrt{\frac{\alpha'}{D'}}\right)} - \sqrt{\pi}\rho'\lambda\sqrt{\frac{\alpha'}{D''}}\left(\frac{C''_{i\infty}}{\rho''}-\frac{C'_{i\infty}}{\rho'}\right) = \left\{-\frac{\left(\frac{\partial C'_i}{\partial T}\right)e^{-\left(\lambda\sqrt{\frac{\alpha'}{D'}}\right)^2}}{1+\mathrm{erf}\left(\lambda\sqrt{\frac{\alpha'}{D'}}\right)} + \frac{\left(\frac{\partial C''_i}{\partial T}\right)\sqrt{\frac{D''}{D'}}\,e^{-\left(\lambda\frac{\rho'}{\rho''}\sqrt{\frac{\alpha'}{D''}}\right)^2}}{\mathrm{erfc}\left(\lambda\frac{\rho'}{\rho''}\sqrt{\frac{\alpha'}{D''}}\right)}\right.$$

$$\left. - \sqrt{\pi}\rho'\lambda\sqrt{\frac{\alpha'}{D''}}\left[\frac{\left(\frac{\partial C''_i}{\partial T}\right)}{\rho''}-\frac{\left(\frac{\partial C'_i}{\partial T}\right)}{\rho'}\right]\right\}\left[T_o-T_{\infty,sat}+A'(\lambda)(T''_\infty-T_o)(1+\mathrm{erf}\lambda)\right] \tag{44}$$

For the zero condensation rate, $\lambda = 0$, eqs (38) and (34), (43), and (35), and (44) and (36) become identical. If gas phase is lumped, that is $T_s = T''_\infty$, and λ is small, then both Eqs. (20) and (38) reduce to

$$\lambda = \frac{C_p'(T''_\infty-T_o)}{\sqrt{\pi}h_{fg}} \tag{45}$$

The comparison of the results by the source theory and the exact solution for this case is graphically illustrated in Figure 35. Similarly if λ is sufficiently small such that all error functions and exponential functions which are functions of λ may respectively be approximated by 0 and 1, then Eqs. (23) and (35), and (44) and (36) will also be identical.

Figure 36 shows the comparison of the results by the source theory and the exact solution of liquid-vapor nitrogen system that has been pressurized from one to three atmospheres. The agreement is good for low values of λ and $T_s \cong T''_\infty$.

The comparison for two-component liquid-vapor systems of helium-nitrogen pressurized from 4 atm to 20 atm and oxygen-nitrogen pressurized from 14.7 to 75 and 150 psia is given in Figures 37 and 38, respectively. They show that the agreement is qualitatively good and quantitatively acceptable.

2. CONCLUSIONS

The source theory which has been applied to bubble dynamics of spherical geometry in Refs. 9 and 16 is extended to the problem of interfacial heat and mass transfer in multi-component systems of semi-infinite extent. The approximate solution obtained for the growth rate parameter is of a considerably simpler form. For a one-component liquid-vapor system the comparison exhibits good agreement between the exact and approximate results for any values of the growth rate parameter, if the gas temperature at infinity does not exceed the saturation temperature by too large a degree. Numerical comparison for the binary-component liquid-vapor systems also shows that the approximation is acceptable for low values of the growth-rate parameters. From the previous[9] and the present work, the conclusion is reached that results predicted by the source theory are dependable for low values of the rate of phase change.

The applicability of the source theory is not limited to the systems of semi-infinite or spherical geometries such as bubbles. It can be extended to the systems having rectangular and rectangular parallelopiped boundaries, and to systems consisting of composite regions, etc. However, due to the complexity arising from mathematical functions related to the cylindrical coordinates, such as Bessel functions, the analysis would become rather involved if the system is of cylindrical geometry.

If phase change occurs in a system with initial temperature field, for example, the growth and collapse of bubble in subcooled boiling, the source theory would give more complicated results because the interfacial movement would not follow the $x(t) = 2\lambda\sqrt{\alpha t}$ law.

VI. TRANSIENT LAMINAR FREE-CONVECTION HEAT AND MASS TRANSFER IN CLOSED, PARTIALLY FILLED LIQUID CONTAINERS

The two-dimensional, laminar transient natural convection heat and mass transfer in a closed rectangular container having a liquid-vapor interface has been studied. Several cases with different boundary conditions, including constant wall heat flux, change in wall temperature and pressurization have been treated. These studies represent the initial stages of a program presently being conducted to study the transient velocity profiles, temperature stratification and pressure histories in such containers.

The problem is formulated from the complete Navier-Stokes equations coupled with those from the first law of thermodynamics and the conservation of mass. Boundary-layer approximations are not made since the geometry and boundary conditions invalidate complete boundary layer flow and require additional momentum considerations not usually found in boundary layer calculations. The x-momentum, the y-momentum and the continuity equations were coupled to obtain the vorticity transport equation. The solution of the governing partial differential equations, namely, the energy equation and the vorticity transport equation, was carred out numerically using the finite-difference approximation. Special attention is given to the problem of convergence and stability of the numerical solution.

Calculations have been carried on for different levels of heat flux and different values of interfacial temperature. The calculated temperature profiles show clearly thermal stratification of the liquid layer near the liquid-vapor interface. The obtained flow patterns indicated that for small time periods, the flow is of the boundary-layer type, except near the bottom and the liquid-vapor interface.

The full study, briefly summarized above, is reported separately in Ref. 19, giving the details of the analytical work and a complete discussion of the results.

VII. TRANSIENT BOILING ON INSULATING SUBSTANCES FOR CRYOGENIC APPLICATION

A. Introduction

The problem of phase change, such as bubble growth, interfacial condensation or evaporation, etc., may be analyzed as an initial value problem. The interfacial movement due to phase change in a system initially with a uniform temperature field as shown in Figure 39 is characterized by the $x(t) = 2\beta\sqrt{\alpha t}$ law (which states that the phase change grows as square root of time.) References 14, 18, and 20-25 deal with this type of problem. However, if the system is subcooled and initially has a nonuniform temperature field as illustrated in Figure 40, the phase formed grows to a certain size and then starts to collapse. This problem was treated in Refs. 13, 26, and 27.

Problems concerning heat transfer with phase change have attracted great interest during the last decade. Typical examples are boiling heat transfer and interfacial heat and mass transfer. The latter has an extensive application in the pressurization of a cyrogenic liquid tank in space vehicles.

During the initial stages of the charging process of a cryogenic liquid into a container, boiling may occur on the surface of the container. This results from an initially high temperature difference between the container surface and the cryogenic liquid. If the temperature difference is sufficiently high, film boiling occurs first on the container surface, later followed by nucleate boiling. It is desirable to reduce the boiling phenomenon in order to prevent boil-off of the cryogenic liquid. This can be accomplished by pressurizing the containers or by lining the inside surfaces of such containers with a low-density, insulating material.

In this study, the mechanism of the transient film and nucleate boiling in a subcooled liquid is presented. The transient boiling on insulating substrates in the container suddenly filled with the cryogenic liquid is analyzed. Variables and physical properties which govern the growth and collapse of (1) the vapor film on the substrate during film boiling, and (2) of a bubble on the substrate during nucleate boiling are defined and examined. In addition, a definition is sought for the physical properties of the container and cryogenic liquid which give low rates of growth and collapse of a vapor film and a bubble.

B. Transient Film Boiling

1. STATEMENT OF THE PROBLEM

The heat transfer process which occurs during film boiling in a nonuniform temperature field may be described as follows: One may imagine that the formation of vapor phase at the interface between the liquid and the superheated container surface is started by a small explosion. In order to initiate the explosion the liquid temperature at the interface has to be considerably higher than its saturation temperature T_{sat}. During the change of the liquid interfacial temperature from the initial value $T_{\ell\infty}$ to T_{s*} a value high enough to spark the explosion, heat diffuses continuously from the container surface to the liquid. This results in a formation of an initial temperature distribution in both liquid and solid phases as illustrated in Figure 41. The initial temperature distribution is assumed to be a straight line distribution, and the thickness of the thermal boundary layer formed in the liquid phase is δ_ℓ. During the small explosion which starts the formation of the vapor phase, the temperatures of the liquid-vapor and solid-vapor interfaces, because of the heat of vaporization, drop immediately from the superheat temperature T_{s*} to the saturation temperature as shown in Figure 42. As a consequence of the heat transfer from the liquid to the vapor, the liquid near the interface is being cooled progressively from the interface toward the bulk and the thermal boundary layer increases in thickness as the thermal disturbance advances into the liquid. However, since the initial temperature in the liquid is not uniform, the temperature drop across the thermal boundary layer constantly decreases as the thermal boundary layer thickness increases.

2. ANALYSIS

The transient thermal boundary layer set up before the formation of a vapor film may be obtained by solving the following two conduction equations

$$\frac{\partial T_s}{\partial \tau} = \alpha_s \frac{\partial^2 T_s}{\partial x^2} \tag{46}$$

$$\frac{\partial T_\ell}{\partial \tau} = \alpha_e \frac{\partial^2 T_\ell}{\partial x^2} \tag{47}$$

with the initial conditions

$$T_s(x,0) = T_{s\infty} \quad \text{for } x < 0 \tag{48-a}$$

$$T_\ell(x,0) = T_{\ell\infty} \quad \text{for } x > 0 \tag{48-b}$$

and the boundary conditions

$$T_s(0,\tau) = T_\ell(0,\tau) \tag{49-a}$$

$$k_s \frac{\partial T_s(0,\tau)}{\partial x} = k_\ell \frac{\partial T_\ell(0,\tau)}{\partial x} \tag{49-b}$$

$$T_s(-\infty,\tau) = T_{s\infty} \tag{49-c}$$

$$T_\ell(\infty,\tau) = T_{\ell\infty} \tag{49-d}$$

The solutions to this problem is found as follows; solid temperature

$$\frac{T_s(x,\tau)-T_{s\infty}}{T_{s\infty}-T_{\ell\infty}} = -\frac{1+\operatorname{erf}\dfrac{x}{2\sqrt{\alpha_s\tau}}}{1+\sqrt{\dfrac{(\rho C_p k)_s}{(\rho C_p k)_\ell}}} \tag{50}$$

liquid temperature

$$\frac{T_\ell(x,\tau)-T_{\ell\infty}}{T_{s\infty}-T_{\ell\infty}} = \frac{\operatorname{erfc}\dfrac{x}{2\sqrt{\alpha_\ell\tau}}}{1+\sqrt{\dfrac{(\rho C_p k)_\ell}{(\rho C_p k)_s}}} \tag{51}$$

The actual temperature distribution in the solid near the container surface is assumed to be a straight line distribution as determined by

$$\frac{\partial T_s(0,\tau)}{\partial x} = \frac{T_{s\infty}-T_{\ell\infty}}{\sqrt{\pi\alpha_\ell\tau}\left[1+\sqrt{\dfrac{(\rho C_p k)_s}{(\rho C_p k)_\ell}}\right]} \tag{52}$$

The transient thermal-boundary layer thickness after a waiting time τ_o is obtained as

$$\delta_\ell = \frac{T_{s\infty}-T_s(0,\tau_o)}{\frac{\partial T_s(0,\tau_o)}{\partial x}} = \sqrt{\pi\alpha_s\tau_o} \tag{53}$$

Similarly, by assuming the actual temperature distribution in the liquid phase near the container surface to be a straight line, the transient thermal-boundary layer thickness is found as

$$\delta_\ell = \frac{T_s(0,\tau_o)-T_{\ell\infty}}{\frac{\partial T_\ell(0,\tau_o)}{\partial x}} = \sqrt{\pi\alpha_\ell\tau_o} \tag{54}$$

After the vapor film is formed, the temperature distribution in the solid may be obtained by solving the governing heat conduction Eq. (46) with the initial conditions .

$$T_s(x,0) = T_{sat} + (T_{sat}-T_{s\infty})\frac{x}{\delta_s} \quad \text{for } 0 > x > -\delta_s \tag{55-a}$$

$$= T_{s\infty} \quad \text{for } -\delta_s > x > -\infty \tag{55-b}$$

and the boundary conditions

$$T_s(0,\tau) = T_{sat} \tag{56-a}$$

$$T_s(-\infty,\tau) = T_{s\infty} \tag{56-b}$$

The temperature gradient at the solid surface is

$$\frac{\partial T_s(0,\tau)}{\partial x} = \frac{T_{sat}}{\sqrt{\pi\alpha_s\tau}} - \frac{T_{sat}-T_{s\infty}}{\delta_s}\,\mathrm{erf}\,\frac{\delta_s}{\sqrt{4\alpha_s\tau}} \tag{57}$$

Similarly as the phase growth progresses, the temperature distribution in the liquid is determined by the conduction Eq. (47) subject to the following initial and boundary conditions.

$$T_\ell(x,0) = T_{sat} - (T_{sat}-T_{\ell\infty})\frac{x}{\delta_\ell} \quad \text{for } 0 < x < \delta_t \tag{58-a}$$

$$= T_{\ell\infty} \quad \text{for } \infty > x > \delta_t \tag{58-b}$$

$$T_\ell(0,\tau) = T_{sat} \tag{59-a}$$

$$T_\ell(\infty,\tau) = T_{\ell\infty} \tag{59-b}$$

The x-coordinate is fixed on the liquid-vapor interface. The temperature gradient of the liquid at the liquid-vapor interface may be written as

$$\frac{\partial T_\ell(0,\tau)}{\partial x} = \frac{T_{sat}}{\sqrt{\pi\alpha_\ell\tau}} - \frac{T_{sat}-T_{\ell\infty}}{\delta_\ell}\,\mathrm{erf}\,\frac{\delta_\ell}{\sqrt{\pi\alpha_\ell\tau}} \tag{60}$$

Considering the heat balance on the lumped gas phase, the heat transferred from the solid surface and the heat transferred from the thermal boundary layer in the liquid phase are consumed as latent heat of vaporization at the liquid-vapor interface:

$$\rho_v h_{fg}\frac{dX}{d\tau} = k_s\frac{\partial T_s(0,\tau)}{\partial x} + k_\ell\frac{\partial T_\ell(0,\tau)}{\partial x} \tag{61}$$

or

$$\frac{dX}{d\tau} = \frac{k_s}{\rho_v h_{fg}}\left(\frac{T_{sat}}{\sqrt{\pi\alpha_s\tau}} - \frac{T_{sat}-T_{s\infty}}{\delta_s}\,\mathrm{erf}\,\frac{\delta_s}{\sqrt{4\alpha_s\tau}}\right) + \frac{k_\ell}{\rho_v h_{fg}}\left(\frac{T_{sat}}{\sqrt{\pi\alpha_\ell\tau}} - \frac{T_{sat}-T_{\ell\infty}}{\delta_\ell}\,\mathrm{erf}\,\frac{\delta_\ell}{\sqrt{4\alpha_\ell\tau}}\right) \tag{62}$$

The integration of Eq. (62) with respect to time τ gives

$$X(\tau) = \frac{\sqrt{\tau}}{\rho_v h_{fg}}\left\{\frac{2T_{sat}}{\sqrt{\pi}}\left[\sqrt{(\rho C_p k)_s} + \sqrt{(\rho C_p k)_\ell}\right] - \frac{\delta_\ell}{2\sqrt{4\alpha_\ell \tau}}\left[\frac{T_{sat}-T_{s\infty}}{\sqrt{(\rho C_p k)_s}} + \frac{T_{sat}-T_{\ell\infty}}{\sqrt{(\rho C_p k)_\ell}}\right]\right.$$

(63)

$$\left.\left(\frac{4\alpha_\ell \tau}{\delta_\ell^2}\operatorname{erf}\frac{\delta_\ell}{\sqrt{4\alpha_\ell\tau}} + \frac{2}{\sqrt{\pi}}\frac{\sqrt{4\alpha_\ell\tau}}{\delta_\ell}e^{-\frac{\delta_\ell^2}{4\alpha_\ell\tau}} - 2\operatorname{erfc}\frac{\delta_\ell}{\sqrt{4\alpha_\ell\tau}}\right)\right\}$$

The maximum thickness of vapor film is formed at τ_{max} which may be found by equating Eq. (62) to zero:

$$\frac{\operatorname{erf}\dfrac{\delta_\ell}{\sqrt{4\alpha_\ell\tau_{max}}}}{\dfrac{\delta_\ell}{\sqrt{4\alpha_\ell\tau_{max}}}} = \frac{2}{\sqrt{\pi}}\frac{\left[1+\sqrt{\dfrac{(\rho C_p k)_s}{(\rho C_p k)_\ell}}\right]\dfrac{T_{sat}}{T_{sat}-T_{\ell\infty}}}{1+\sqrt{\dfrac{(\rho C_p k)_s}{(\rho C_p k)_\ell}}\dfrac{T_{sat}-T_{s\infty}}{T_{sat}-T_{\ell\infty}}} \tag{64}$$

Since $\delta_\ell = \sqrt{\pi\alpha_\ell \tau_o}$ Eq. (64) may be rewritten as

$$\frac{\operatorname{erf}\sqrt{\dfrac{\tau_o}{\tau_{max}}}}{\sqrt{\dfrac{\tau_o}{\tau_{max}}}} = \frac{\operatorname{erf}\dfrac{\delta_\ell}{\delta_{max}}}{\dfrac{\delta_\ell}{\delta_{max}}} = \frac{2}{\sqrt{\pi}}\frac{\left[1+\sqrt{\dfrac{(\rho C_p k)_s}{(\rho C_p k)_\ell}}\right]\dfrac{T_{sat}}{T_{sat}-T_{\ell\infty}}}{1+\sqrt{\dfrac{(\rho C_p k)_s}{(\rho C_p k)_\ell}}\dfrac{T_{sat}-T_{s\infty}}{T_{sat}-T_{\ell\infty}}} \tag{65}$$

where δ_{max} is the maximum thickness of the vapor film.

At the time the temperature gradient in the liquid becomes negative, the vapor film starts to collapse and the vapor-liquid interface moves back toward the solid.

C. Transient Nucleate Boiling

1. STATEMENT OF THE PROBLEM

During the time the film boiling is in progress, the bulk temperature of the substrate decreases owing to heat transferred to the fluid through the vapor film. After the vapor film disappears completely from the solid surface

and the liquid adjacent to this is sufficiently superheated, two important processes follow: the formation of bubbles and the subsequent growth of these bubbles.

In Ref. 29 Jakob described the growth of a bubble on a heated surface as started by a small explosion. His conceptual model may be modified to suit the subcooled boiling at a heated surface as follows: As a bubble is detached from the surface, a volume of cold liquid rushes in and replaces the space previously occupied by the bubble at the superheated surface. This situation creates the initial condition at which the heating surface and the liquid are respectively at uniform temperatures $T_{s\infty}$ and $T_{\ell\infty}$. Subsequent to this moment, heat transfers from the heating surface to the liquid by pure conduction. This assumption is justified since the convection intensity near the heating surface is damped down due to the no slip boundary condition for a solid surface. As the waiting time increases, a thermal boundary layer is set up in the liquid. The temperature distribution in this thermal boundary layer is assumed to be linear for the sake of simplicity.

During the waiting period, a bubble is initiated with the cavity radius R_c. This bubble is in the condition of thermostatic equilibrium, which satisfies the equation

$$\Delta P = \frac{2\sigma}{R_c} \tag{66}$$

It temperature is uniform and equal to the surface temperature. Furthermore the bubble in waiting is in contact with the liquid having a linear distribution in temperature initiated during the waiting period. During the small explosion which starts the growth of a bubble the interface temperature, because of the heat of vaporization, drops immediately from the superheat temperature to T_{sat}, the saturation temperature corresponding to the vapor pressure of the bubble. As a consequence of the heat transfer from the liquid to the vapor bubble, the liquid envelope is being cooled progressively from the inside toward the outer boundary; a temperature boundary layer is created with a constantly decreasing temperature drop. This thermal boundary layer increases in thickness with the thermal wave, which advances from the vapor bubble interface into the liquid, has reached the outer limit of the hydrodynamic boundary layer. The decrease in thickness of the hydrodynamic boundary layer due to the evaporation at the interface is a small fraction of the total thickness. The conceptual model is shown in Figure 43.

2. ANALYSIS

For simplicity in the analysis, it is assumed that the one dimensional case may be converted to the three dimensional case by the introduction of a

curvature factor. The following assumptions are also imposed on the analysis:

(i) No convection in the liquid other than due to the bubble itself.

(ii) No change of mass of fluid due to change of phase through the vapor-liquid interface.

(iii) After initiation of the bubble, no effects on the bubble growth due to inertia and surface tension of the liquid.

(iv) Constant fluid properties.

(v) Spherical bubble surface.

(vi) Uniform bulk fluid temperature and pressure.

The results obtained above for transient film boiling for the temperatures gradients at the solid-liquid and liquid-vapor interfaces, Eqs. (57) and (60), may also be applied to the transient nucleate boiling. Using the criterion for bubble initiation from a gas filled cavity on a heating surface at constant temperature, Han and Griffith[27] have obtained the waiting period as

$$\tau_o' = \frac{\delta_\ell'^2}{\pi\alpha_\ell} = \frac{q}{4\pi\alpha_\ell}\left[\frac{R_c(T_s-T_{\ell\infty})}{T_s-T_{sat}\left(1+\frac{2\sigma}{R_c\rho_v h_{fg}}\right)}\right]^2 \tag{67}$$

Referring to the conceptual model shown in Figure 43 and including the effect of curvature, the governing heat balance equation for bubble growth is

$$\rho_v h_{fg}\left(4\pi R^2\frac{dR}{dt}\right)F_v = F_c F_s k_\ell (4\pi R^2)\frac{\partial T_\ell(0,\tau)}{\partial x} + F_b k_s (4\pi R^2)\frac{\partial T_s(0,\tau)}{\partial x} \tag{68}$$

where F_v = Volume fraction of the actual bubble

$$= 1 - \frac{1}{4}[2(1-\cos\phi) - \sin^2\phi\cos\phi] \tag{69}$$

F_s = Surface-area-in-contact-with-the-liquid fraction of the actual bubble

$$= \frac{1}{2}(1+\cos\phi) \tag{70}$$

F_b = surface-area-in-contact-with-the heating-surface fraction of the actual bubble

$$= \frac{\sin^2\phi}{4} \tag{71}$$

ϕ = contact angle

F_c = curvature factor where $1 < F_c < \sqrt{3}$ as presented in Ref. 27

The substitution of Eqs. (57) and (60) into Eq. (68) yields

$$\frac{dR}{dt} = \frac{F_c F_s k_\ell}{F_v \rho_v h_{fg}}\left(\frac{T_{sat}}{\sqrt{\pi\alpha_\ell \tau}} - \frac{T_{sat}-T_{\ell\infty}}{\delta_\ell'}\operatorname{erf}\frac{\delta_\ell'}{\sqrt{4\alpha_\ell\tau}}\right) + \frac{F_b k_s}{F_v \rho_v h_{fg}}\frac{T_{sat}}{\sqrt{\pi\alpha_s\tau}} - \frac{T_{sat}-T_{\ell\infty}}{\delta_s'}\operatorname{erf}\frac{\delta_s'}{\sqrt{4\alpha_s\tau}} \tag{72}$$

$$R(t) = \frac{2T_{sat}\sqrt{\tau}}{\rho_v h_{fg} F_v \sqrt{\pi}}\left[F_c F_s\sqrt{(\rho c_p k)_\ell} + F_b\sqrt{(\rho c_p k)_s}\right] - \frac{\delta_\ell'}{4\rho_v h_{fg} F_v\sqrt{\alpha_\ell}}\left[F_c F_s (T_{sat}-T_{\ell\infty})\sqrt{(\rho c_p k)_\ell} + F_b(T_{sat}-T_{s\infty})\sqrt{(\rho c_p k)_s}\right]\left[\frac{4\alpha_\ell\tau}{\delta_\ell'^2}\operatorname{erf}\frac{\delta_\ell'}{\sqrt{4\alpha_\ell\tau}} + \frac{2}{\sqrt{\pi}}\frac{\sqrt{4\alpha_\ell\tau}}{\delta_\ell'}e^{-\frac{\delta_\ell'^2}{4\alpha_\ell\tau}} - 2\operatorname{erfc}\frac{\delta_\ell'}{\sqrt{4\alpha_\ell\tau}}\right] \tag{73}$$

By equating Eq. (72) to zero, the maximum radius may be obtained as

$$\frac{\operatorname{erf}\dfrac{\delta_\ell'}{\sqrt{4\alpha_\ell \tau'_{max}}}}{\dfrac{\delta_\ell'}{\sqrt{4\alpha_\ell \tau'_{max}}}} = \frac{2}{\sqrt{\pi}} \frac{\left[1+\dfrac{F_b}{F_c F_s}\sqrt{\dfrac{(\rho C_p k)_s}{(\rho C_p k)_\ell}}\right]\dfrac{T_{sat}}{T_{sat}-T_{\ell\infty}}}{1+\dfrac{F_b}{F_c F_s}\sqrt{\dfrac{(\rho C_p k)_s}{(\rho C_p k)_\ell}}\;\dfrac{T_{sat}-T_{s\infty}}{T_{sat}-T_{\ell\infty}}} \tag{74}$$

or

$$\frac{\operatorname{erf}\dfrac{\tau_o'}{\tau'_{max}}}{\dfrac{\tau_o'}{\tau'_{max}}} = \frac{\operatorname{erf}\dfrac{\delta_\ell}{\delta_{max}}}{\dfrac{\delta_\ell}{\delta_{max}}} = \frac{2}{\sqrt{\pi}} \frac{\left[1+\dfrac{F_b}{F_c F_s}\sqrt{\dfrac{(\rho C_p k)_s}{(\rho C_p k)_\ell}}\right]\dfrac{T_{sat}}{T_{sat}-T_{\ell\infty}}}{1+\dfrac{F_b}{F_c F_s}\sqrt{\dfrac{(\rho C_p k)_s}{(\rho C_p k)_\ell}}\;\dfrac{T_{sat}-T_{s\infty}}{T_{sat}-T_{\ell\infty}}} \tag{75}$$

D. Discussion and Conclusion

Equations (61) and (73) describe respectively the transient growth of a vapor film and a bubble which either grows continuously from zero to a finite size (or thickness) within a finite time, or which grows during some initial time to a maximum size (or thickness) and then through recondensation diminishes to zero again. The magnitude of the maximum size (or thickness) and the time at which it occurs depend on the magnitude of the temperatures $T_{\ell\infty}$, $T_{s\infty}$, T_{sat} and the other parameters.

It is the purpose and primary interest of this study to determine the time $2\tau_{max}$, at which the vapor film has completely recondensated and the time τ_{max} at which the bubble has grown to the maximum size. At the moment $\tau = 2\tau_{max}$ the insulating substrate and the cryogenic fluid are in direct contact and soon the process of transient nucleate boiling follows. τ_{max} and τ'_{max} may be obtained from the transcendental Eqs. (64) or (65), and (74) or (75), respectively.

These equations indicate the significant parameters influencing the duration of the residence of a vapor film and a bubble on the insulating substrates: $(\rho C_p k)_s/(\rho C_p k)_\ell$ and dimensionless temperatures. For the purpose of optimization of the charge process of the cryogenic container, it is desirable that τ_{max} and τ'_{max} be as small as possible. The discussion of $\rho C_p k$, the new thermal

property of materials which is useful in selecting an insulating substrate, is given in detail in Ref. 13.

The investigation of Eqs. (64), (65), (74), and (75) reveals that for a given value of dimensionless temperatures $T_{sat}/T_{sat}-T_{\ell\infty}$ and $T_{sat}-T_{s\infty}/T_{sat}-T_{\ell\infty}$ a substrate-liquid system with lower $\rho C_p k$ ratio would be superior to those with large. $\rho C_p k$ ratio insofar as minimum residence times of the vapor film and bubble are concerned. That is to say, the prevention of excess boil-off of cryogenic liquid during the charge process by reducing the boiling phenomenon can be accomplished by lining the inside surfaces of such containers with a $\rho C_p k$ insulating material. This important conclusion is in agreement with the case of the pressurized-discharge process studied in Ref. 13.

REFERENCES

1. Clark, J. A., H. Merte, V. S. Arpaci, et al., Pressurization of Liquid Oxygen Containers, Progress Report No. 5, ORA Report 04268-5-P, NASA Contract No. NAS -8-825, The University of Michigan, February, 1963.

2. Clark, J.A., H.Merte, V. S. Arpaci, et al., Pressurization of Liquid Oxygen Containers, Progress Report No. 2 ORA Report 04268-2-P, NASA Contract No. NAS-8-825, The University of Michigan, November, 1961.

3. Clark, J.A., H. Merte, V. S. Arpaci, et al., Pressurization of Liquid Oxygen Containers, Progress Report No. 4, ORA Report 04268-4-P NASA Contract No. NAS-8-825, The University of Michigan, July, 1962.

4. Corty, C. and A.S. Foust, "Surface Variables in Nucleate Boiling," Chem. Eng. Prog. Symp., Series No. 17, 51, 1955.

5. Merte, H. and J. A. Clark, "Pool Boiling in an Accelerating System," Trans, ASME, J. Heat Transfer, 83, No. 3 (August, 1961), 223-242.

6. Clark, J. A., H. Merte, V. S. Arpaci, et al., Pressurization of Liquid Oxygen Containers, Final Report ORA Report 03583-3-F, Department of the Army Contract No. DA-20-018-506-ORD-254, The University of Michigan, March 1961.

7. Frederking, T.H.K. and J. A. Clark, "Natural Convection Film Boiling on a Sphere." Advances in Cryogenic Engineering 8, K. D. Timmerhaus, Editor, Plenum Press, New York (1963).

8. Bromley, L. A., "Heat Transfer in Stable Film Boiling," Chem. Eng. Prog., 46, (1958) 221.

9. Clark, J. A., H. Merte, V. S. Arpaci, et al., Pressurization of Liquid Oxygen Containers, Progress Report No. 3, ORA Report 04268-3-P, NASA Contract NAS-8-825, The University of Michigan, March, 1962.

10. Larsen, P. S., Clark, J. A., The Dynamics of Gas-Vapor Bubbles in Binary Systems, Technical Report No. 2, ORA Report 04268-7-T, NASA Contract No. NAS-8-825, The University of Michigan, December, 1963.

11. Thomas, P. D. and Morse, F. H., "Analytical Solution for the Phase Change in a Suddenly Pressurized Liquid-Vapor System," Advances in Cryogenic Engineering, 8, 1962.

REFERENCES (Continued)

12. Knuth, E. L., "Evaporation and Condensations in One-Component Systems," paper to be published in American Rocket Society, 1962.

13. Clark, J. A. "Transient Condensation on Insulating Substrates for Cryogenic Application," Advances in Cryogenic Engineering 7, pp. 360-366, 1961.

14. Yang, W. J., "Phase Change of One Component Systems in a Container," AIChE paper No. 62A-48, presented at the 6th National Heat Transfer Conference, Boston, Mass. August 11-14, 1963.

15. Yang, W. J., Larsen, P. S. and Clark, J. A., "Interface Heat and Mass Transfer in a Suddenly Pressurized, Multi-Component Liquid-Vapor System," manuscript in preparation.

16. Yang, W. J., Clark, J. A., "On the Application of the Source Theory to the Solution of Problems Involving Phase Change," ASME Paper No. 63-HT-14, presented at the 6th National Heat Transfer Conference, Boston, Mass. August 11-14, 1963.

17. Forster, H. K., "Diffusion in a Moving Medium With Time-Dependent Boundaries," J. AIChE, 3-4 pp. 534, 1957-58.

18. Carslaw, H. S., and Jaeger, J. C., Conduction of Heat in Solids. Oxford Univ. Press, 2nd ed., 1959.

19. Barakat, H., Clark, J. A., "Transient Laminar Free Convection Heat and Mass Transfer in Closed, Partially-Filled Liquid Containers" Technical Report No. 1, ORA Report 04268-6-T, NASA Contract No. NAS-8-825, The University of Michigan.

20. Bosnjakovic, F., "Evaporation and Liquid Superheating," NDA-24, Technische Mechanick und Thermodynamik, 1, No. 10 p. 358 (1930).

21. Plesset, M. S. and Zwick, S. A., "Growth of Vapor Bubbles in Superheated Liquids," J. Appl. Phys., 25, pp. 493-500 (1954).

22. Forster, H. K., and Zuber, N., "Growth of A Vapor Bubble in a Superheated Liquid," J. Appl. Phys., 25, p. 474 (1954).

23. Scriven, L. E., "On the Dynamics of Phase Growth," Chem. Eng. Sci. 10, p. 1-13 (1959).

24. Bankoff, S. G., "Bubble Dynamics at the Surface of an Exponentially Heated Plate," Industrial and Eng. Chem., Fundamentals, 1, No. 4 pp. 257-259 (1962).

25. Yang, W. J. and Clark, J. A., "On the Application of the Source Theory to the Solution of Problems Involving Phase Change, Part I Growth and Collapse of Bubbles," ASME paper 63-H-45, presented at the ASME-AIChE Heat Transfer Conference, Boston, Mass., August, 1963.

26. Zuber, N., "The Dynamics of Vapor Bubble in Non-Uniform Temperature Fields," Intern. J. Heat Transfer, 2, pp. 88-98 (1963).

27. Han, C. Y. and Griffith, P., "The Mechanism of Heat Transfer in Nucleate Pool Boiling," Tech. Report No. 19, MIT (1962).

28. Tachibana, F. and Fukui, S, "Heat Transfer in Film Boiling to Subcooled Liquids," Intern. Dvelop. in Heat Transfer, Part II, ASME, pp. 219-233 (1961).

29. Jakob, M., "Condensation and Evaporation, New Conceptions and Experiments," Z. Ver. Dtsch. Ing., 76, p. 1161 (1932).

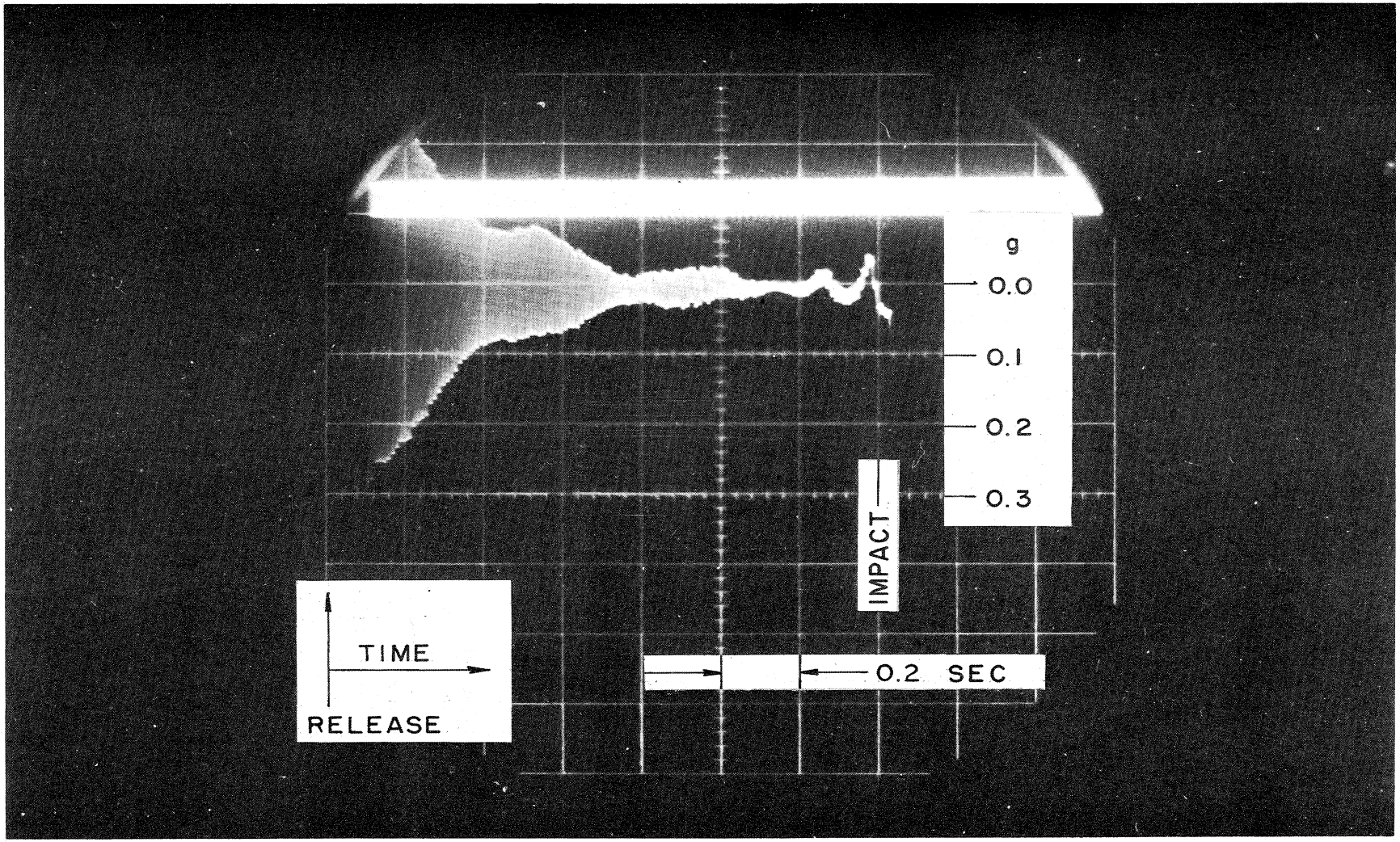

Figure 1. Accelerometer output from original test platform with free fall.

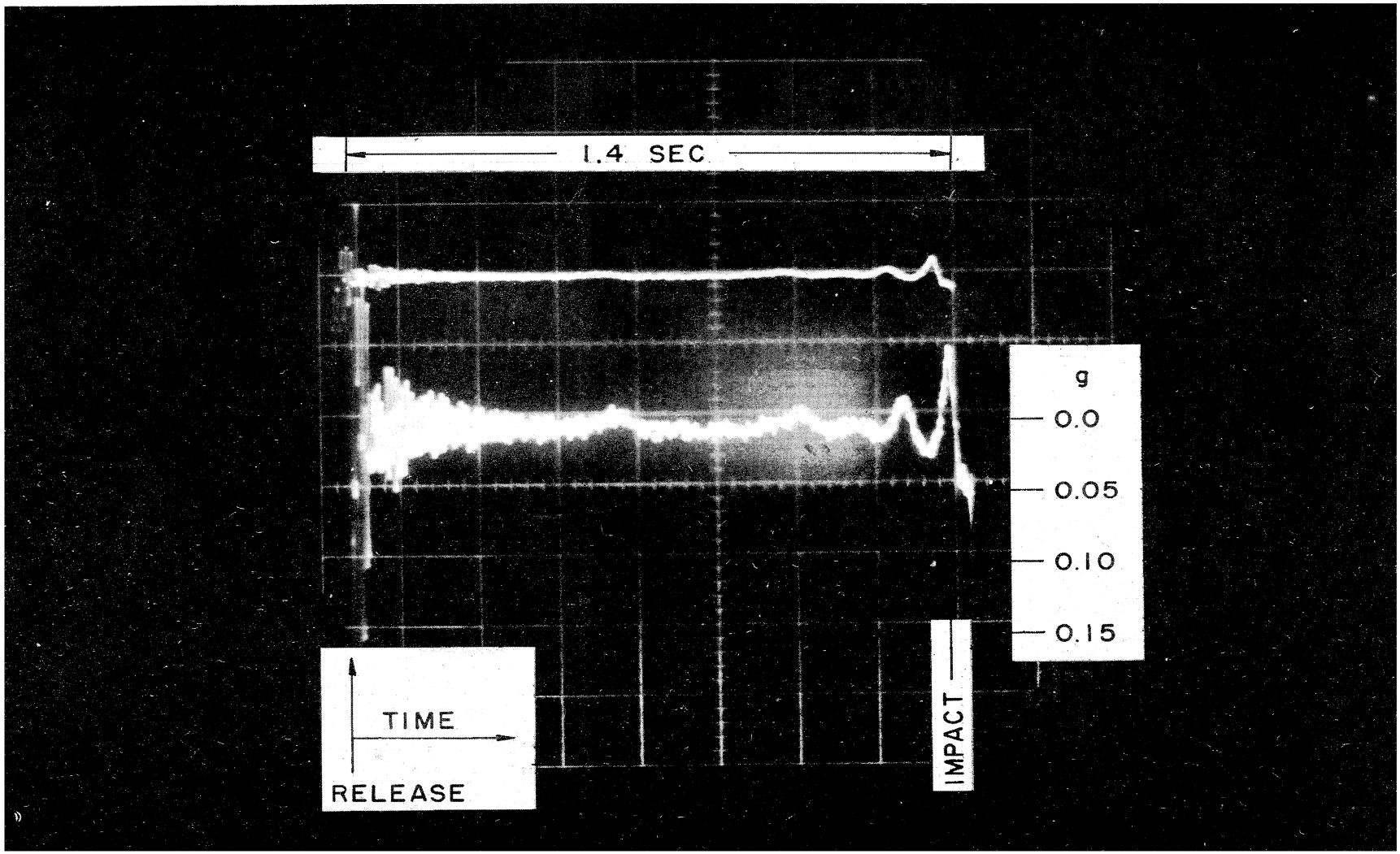

Figure 2. Accelerometer output from text platform with stiffener, with free fall.

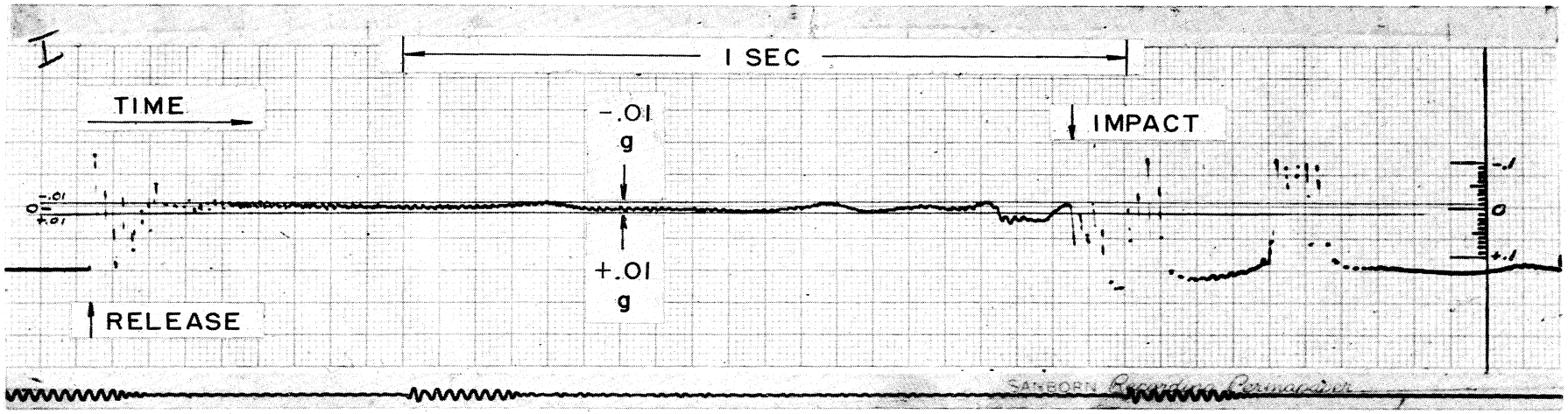

Figure 3. Accelerometer output from test platform during free fall.

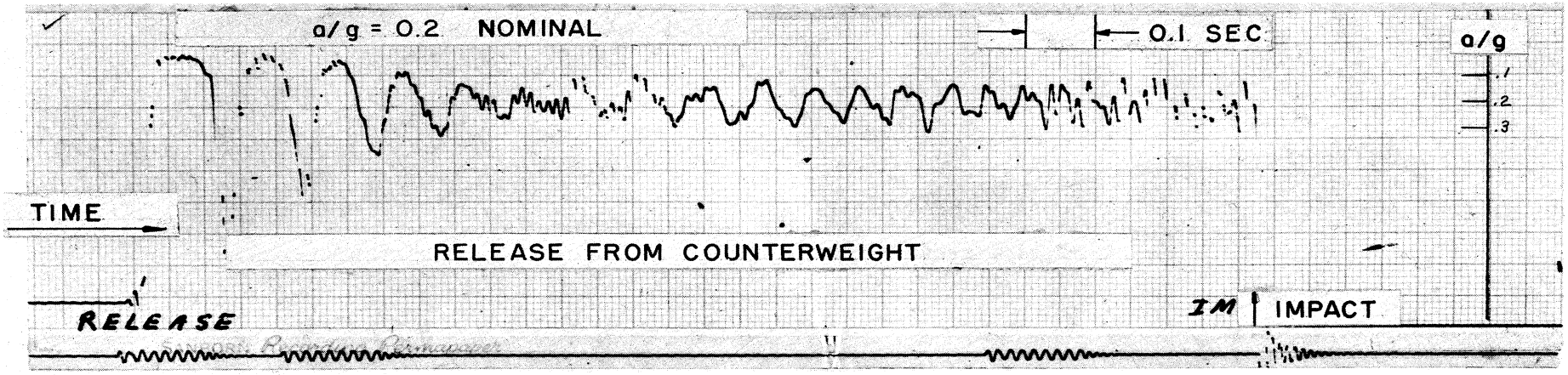

Figure 4. Accelerometer output from test platform with fractional gravity. Release from counter-weight.

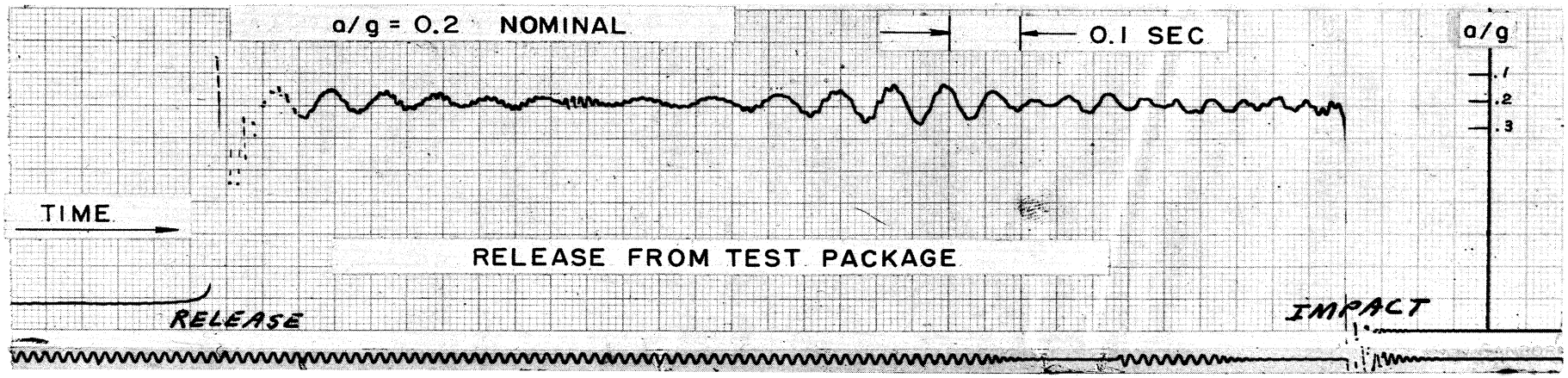

Figure 5. Accelerometer output from test platform with fractional gravity. Release from test platform.

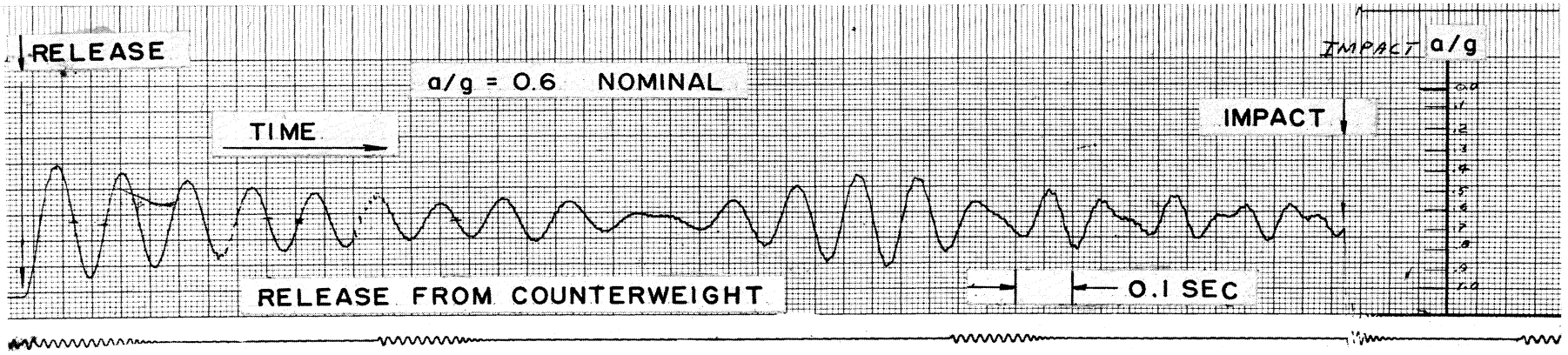

Figure 6. Accelerometer output from test platform with fractional gravity. Release from counter-weight.

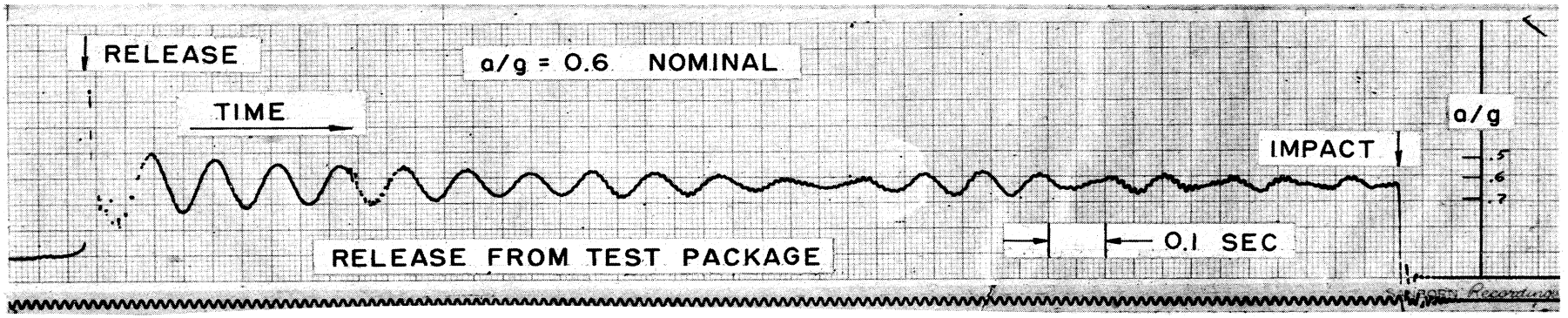

Figure 7. Accelerometer output from test platform with fractional gravity. Release from test platform.

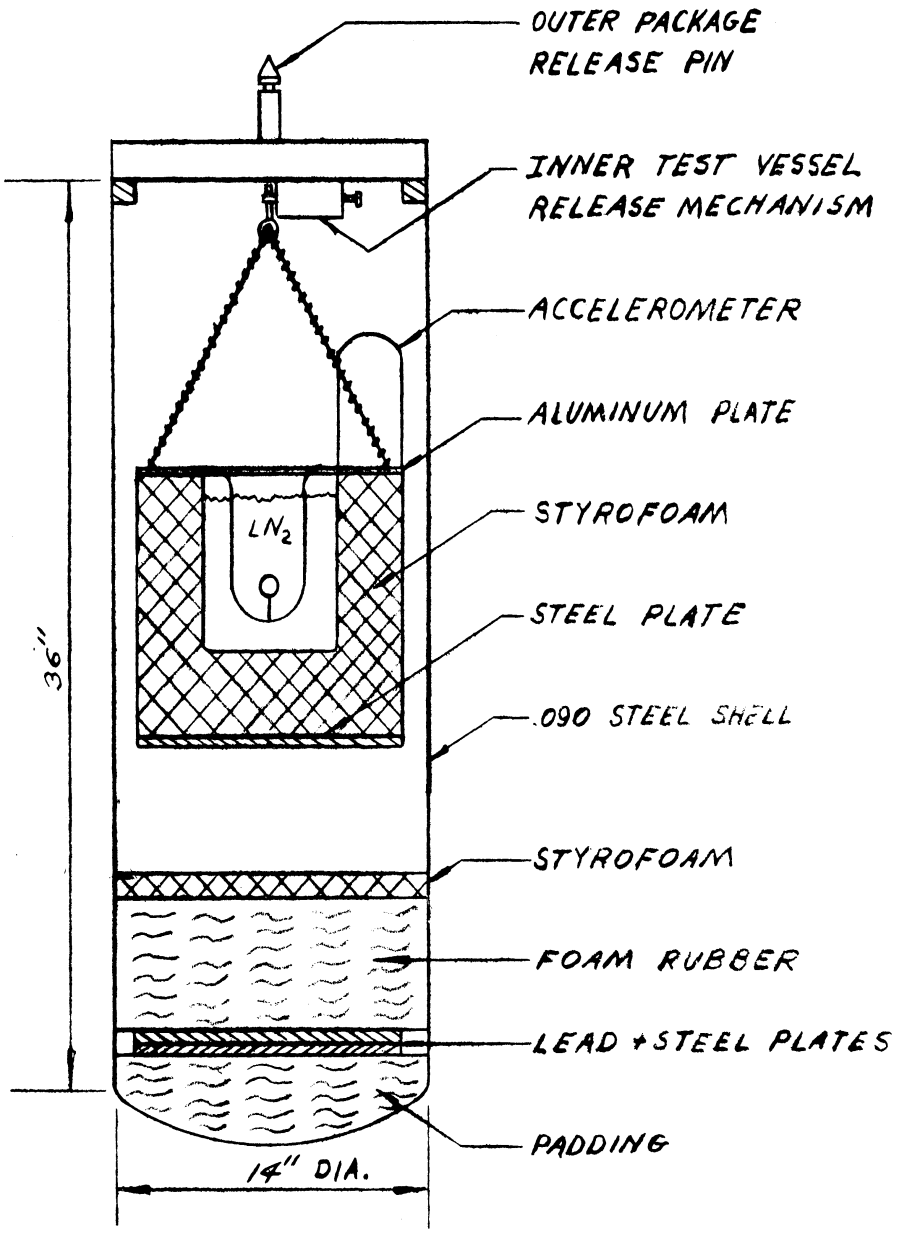

Figure 8. New test package.

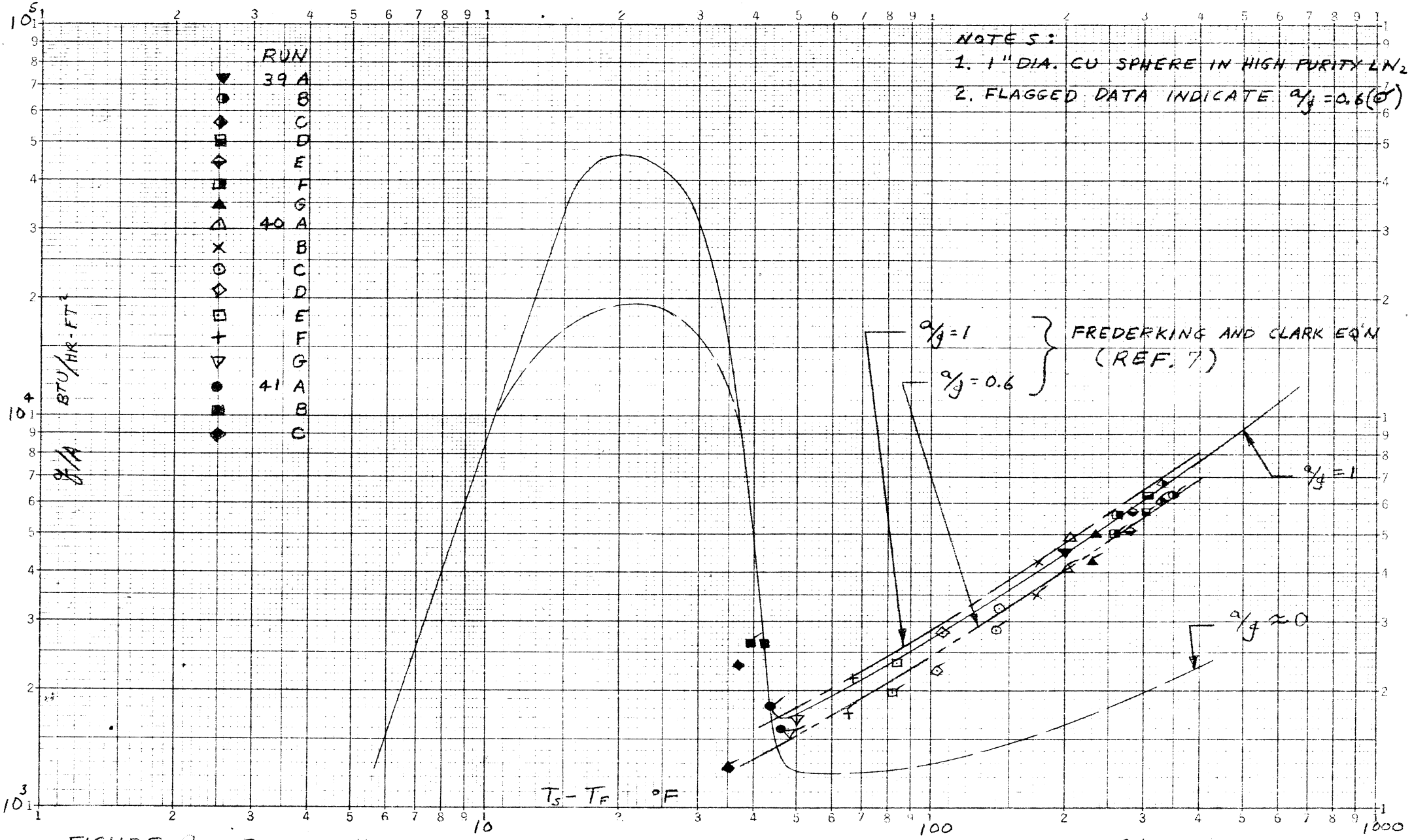

FIGURE 3. BOILING HEAT TRANSFER DATA IN THE FILM BOILING REGION FOR $q/q_f = 1$ & 0.6

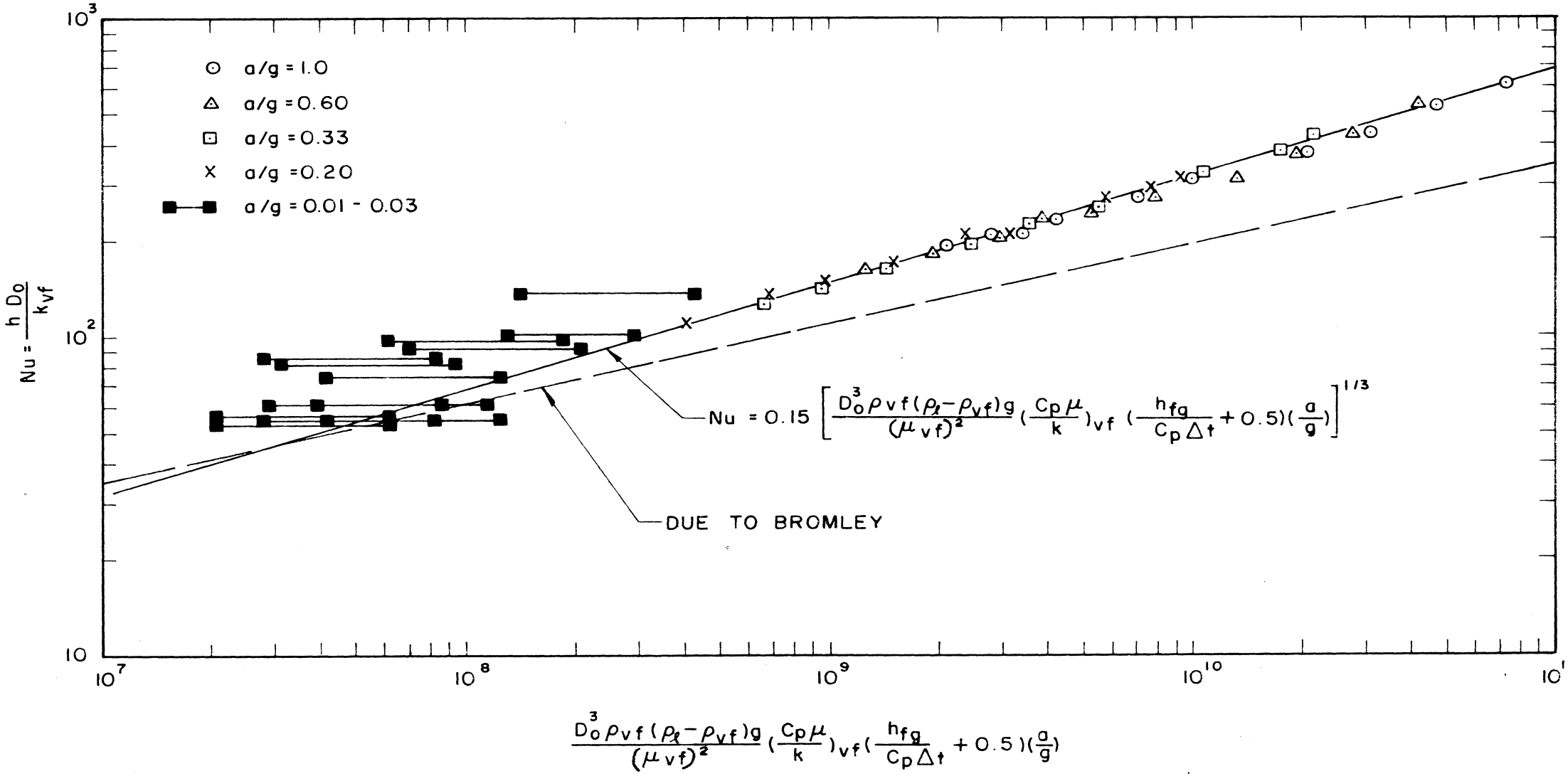

FIGURE 10. COMPARISON OF FRACTIONAL GRAVITY FILM BOILING DATA WITH 1" DIA. SPHERE FOR LIQUID NITROGEN WITH CORRELATIONS BY FREDERKING AND CLARK (7) AND BROMLEY (8).

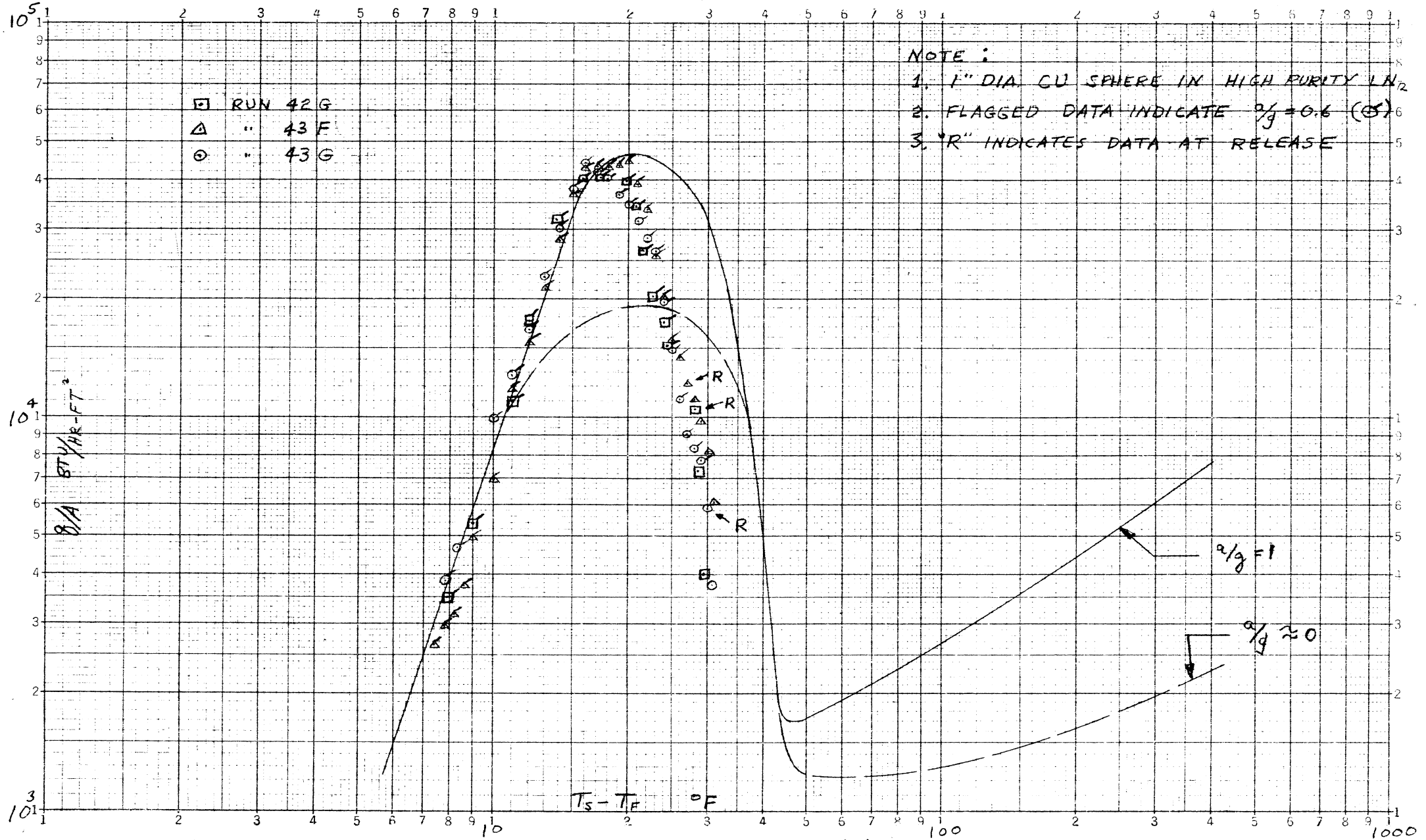

FIGURE 11. NUCLEATE AND TRANSITION BOILING FOR $a/g = 0.6$. SHIFT IN TRANSITION REGION.

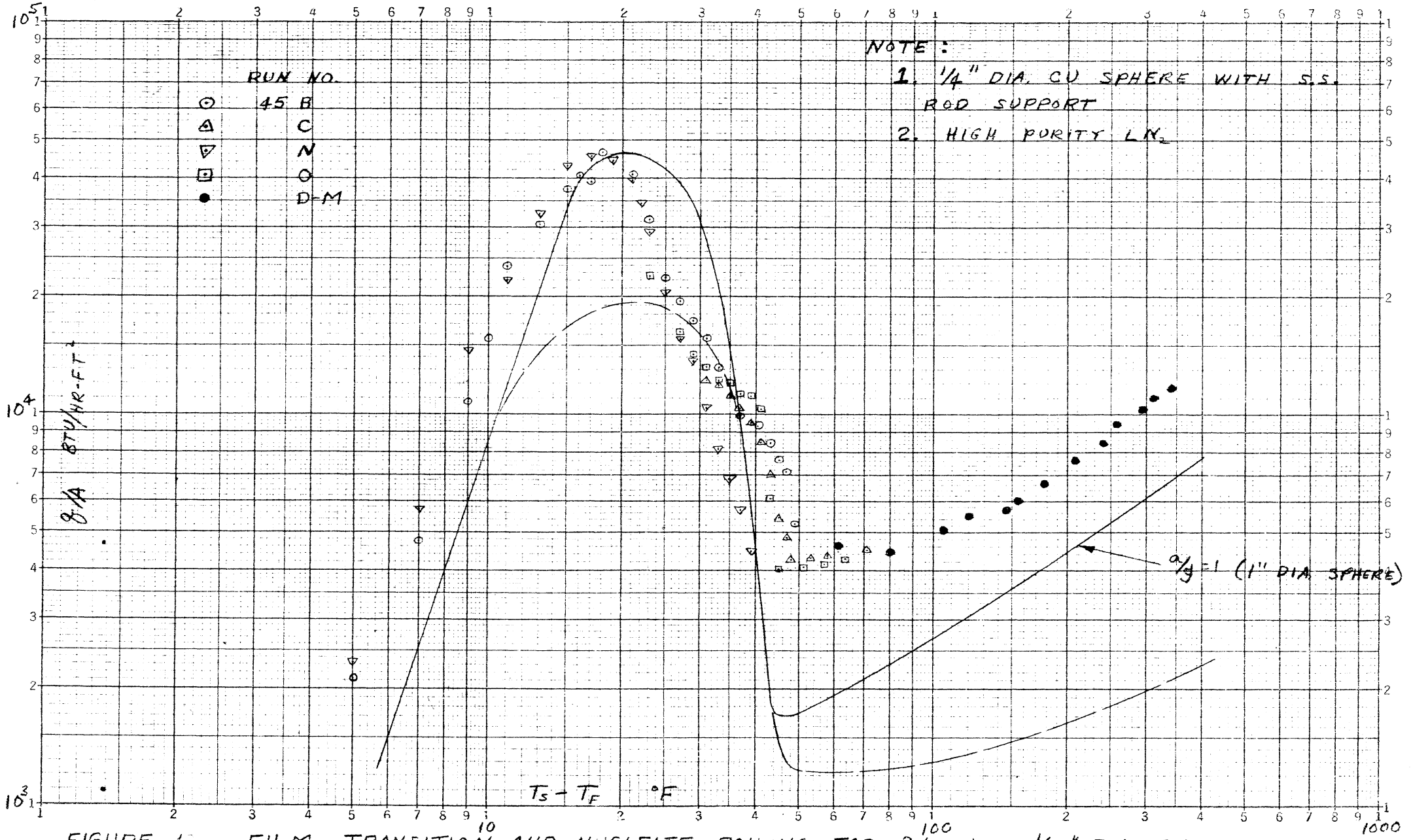

FIGURE 12. FILM, TRANSITION AND NUCLEATE BOILING FOR $q/g = 1$. 1/4" DIA. SPHERE.

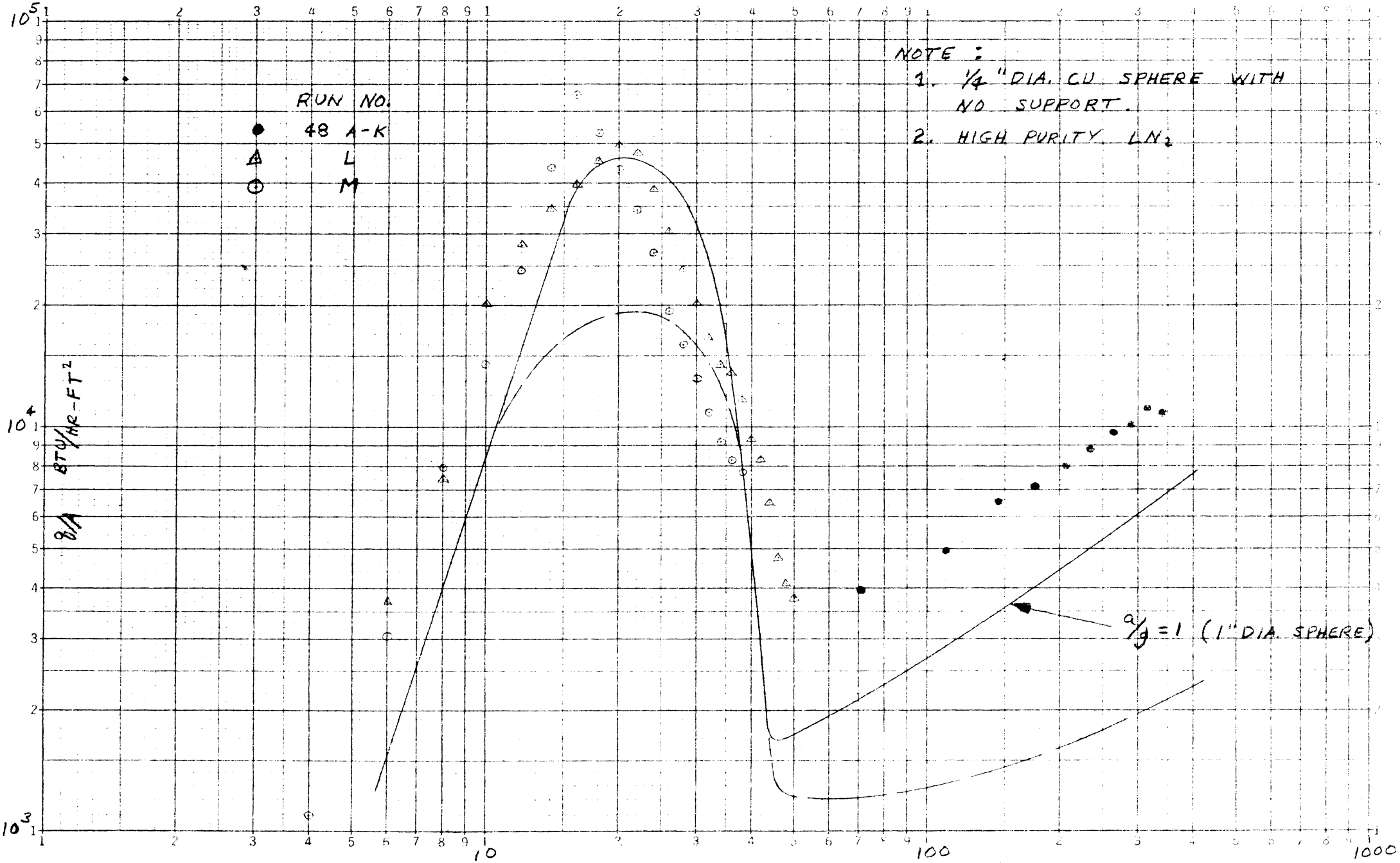

FIGURE 13. FILM, TRANSITION AND NUCLEATE BOILING FOR $q/g = 1$. 1/4" DIA SPHERE.

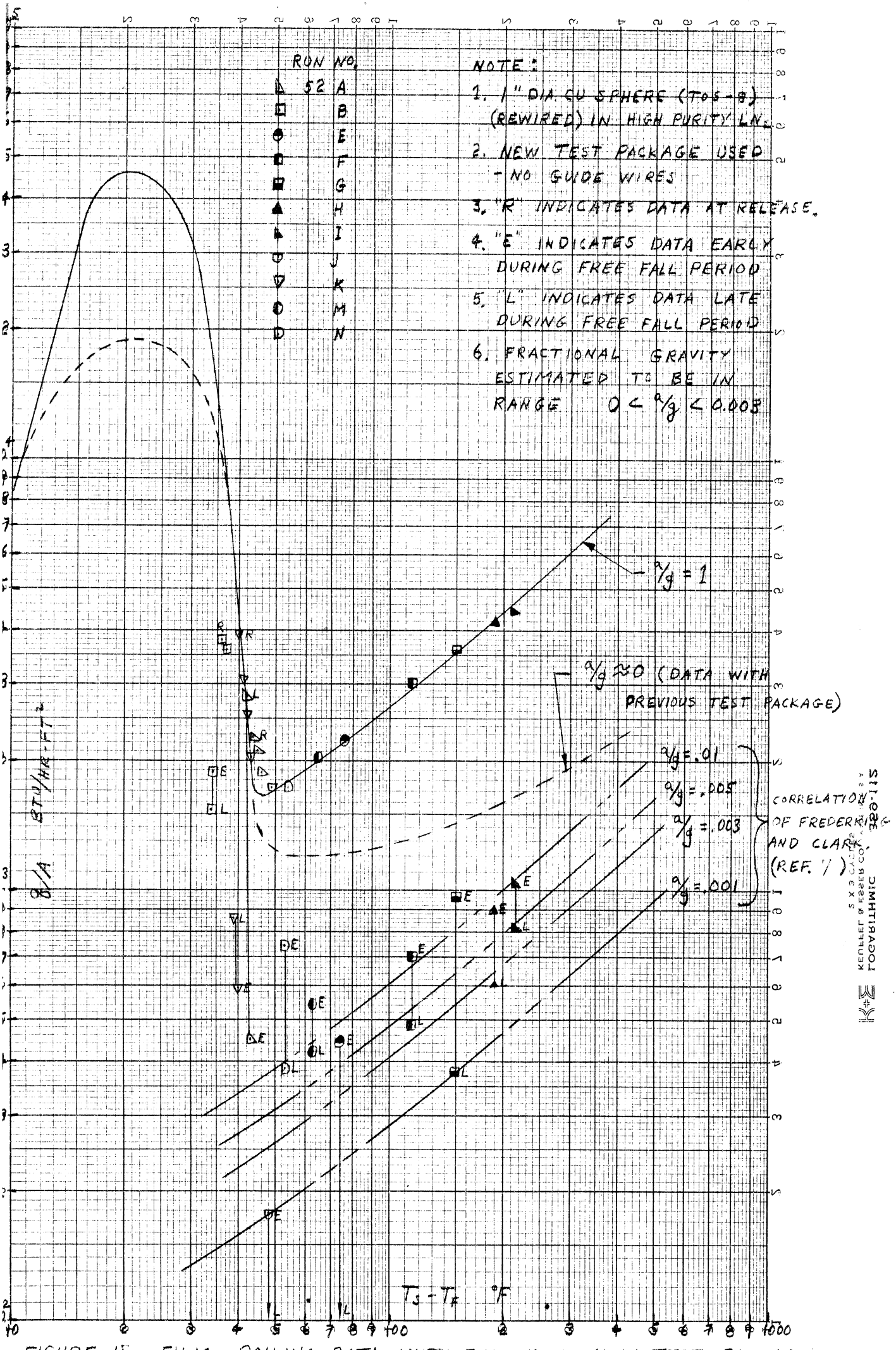

FIGURE 15. FILM BOILING DATA WITH FREE FALL. NEW TEST PACKAGE.

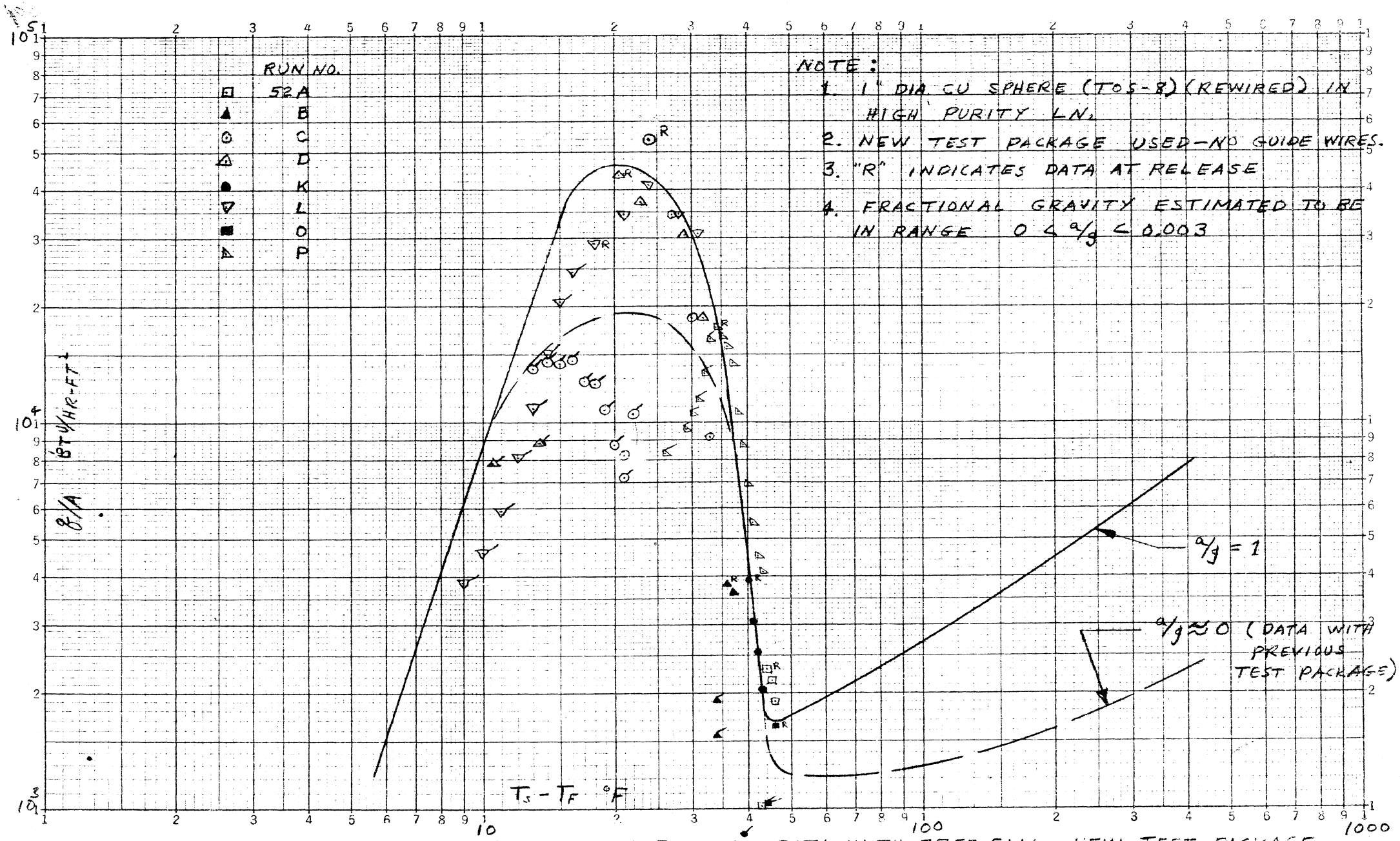

FIGURE 16. NUCLEATE AND TRANSITION BOILING DATA WITH FREE FALL. NEW TEST PACKAGE.

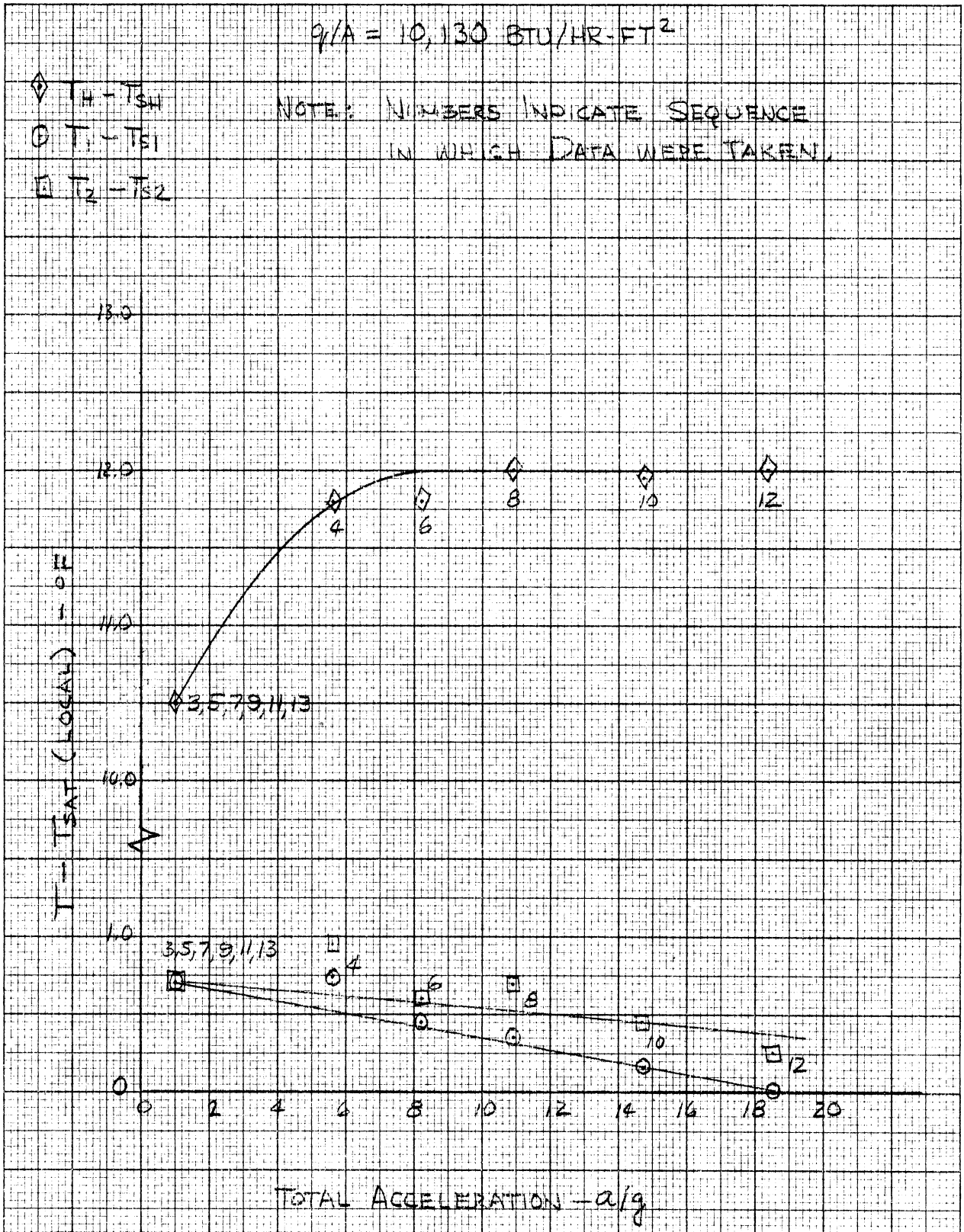

FIGURE 18. COMPOSITE PLOT FOR LIQUID DEPTH OF 2.5 INCHES. RUN NO. 32

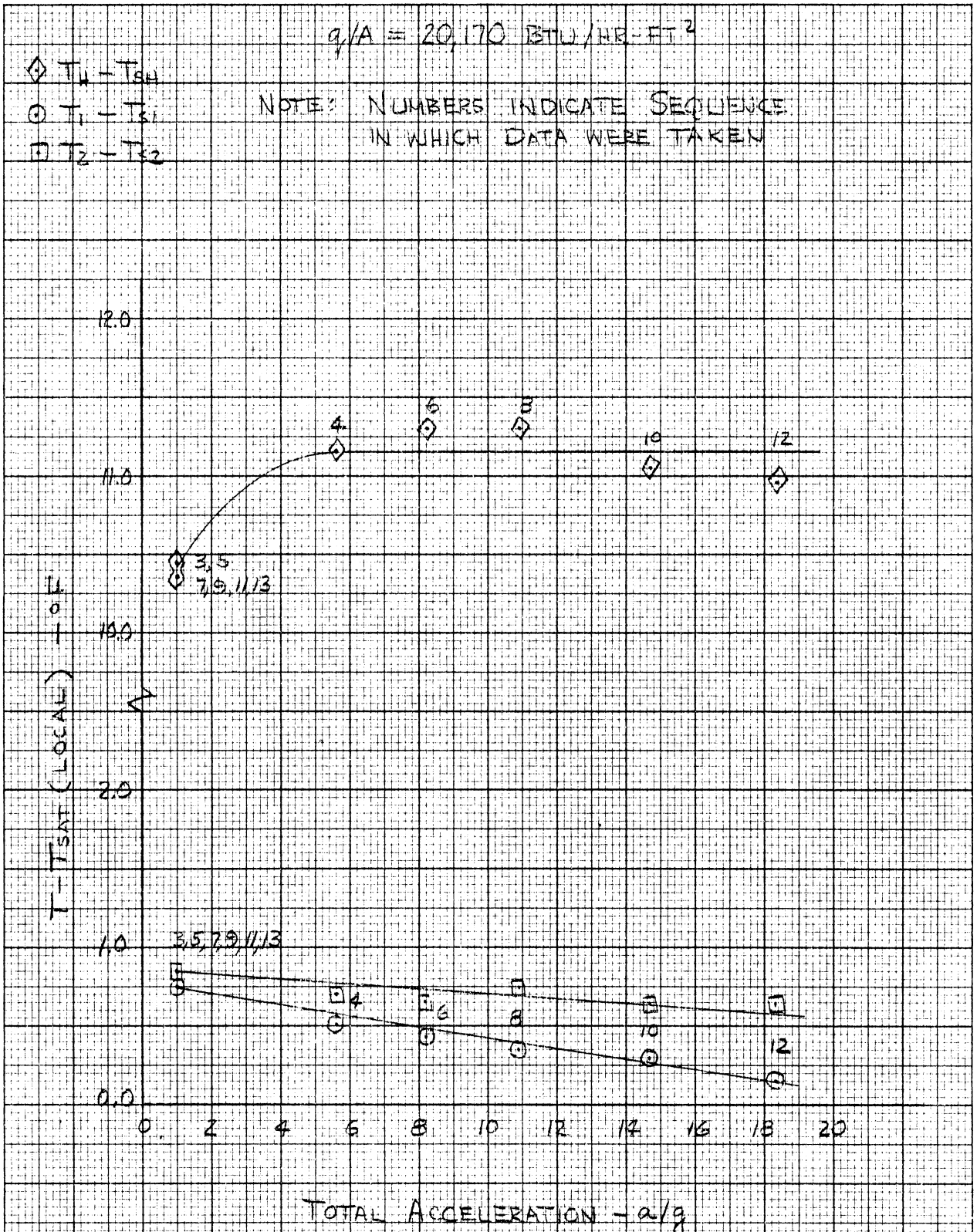

FIGURE 20. COMPOSITE PLOT FOR LIQUID DEPTH OF 2.5 INCHES. RUN NO 33

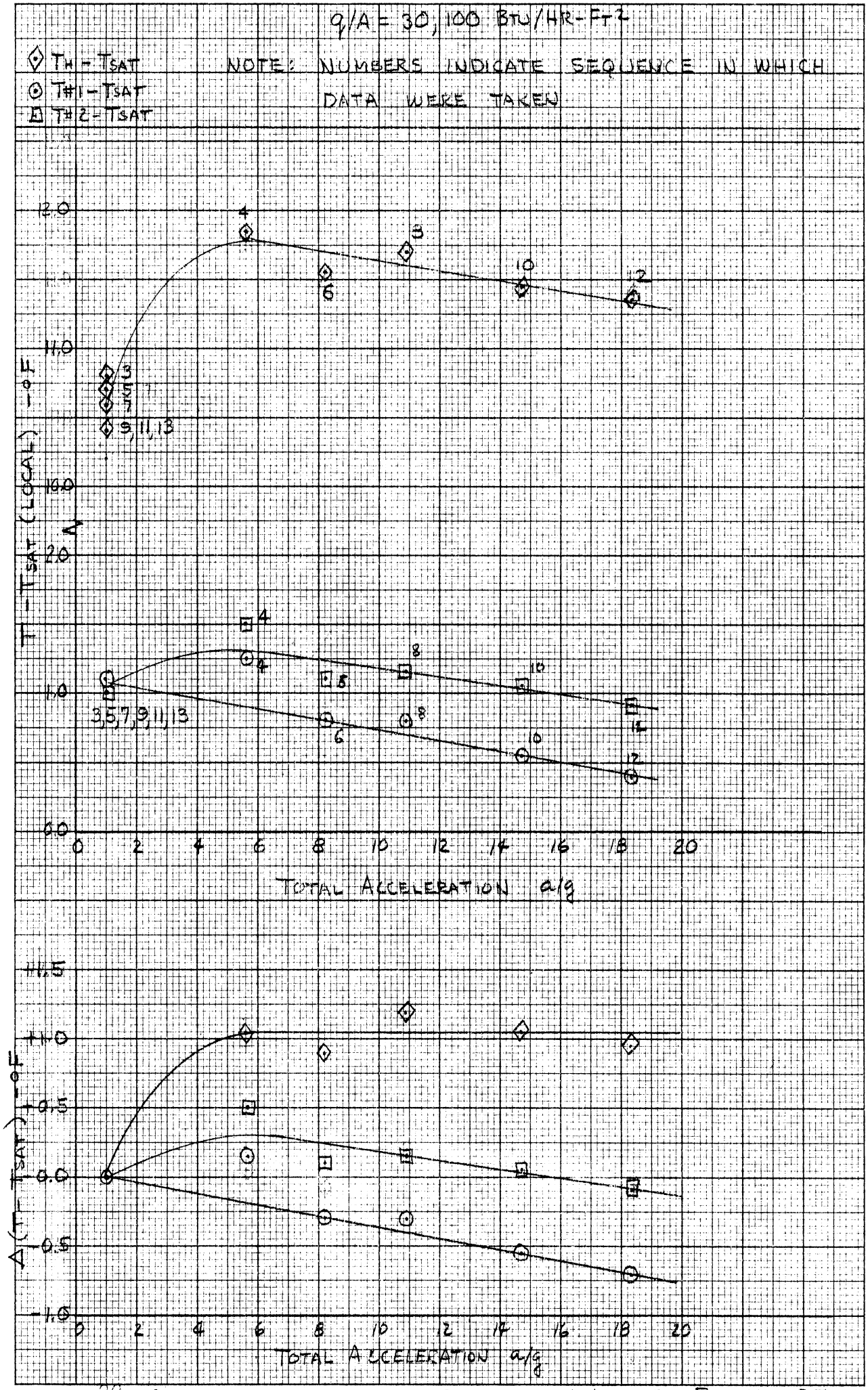

FIGURE 22, COMPOSITE PLOT FOR LIQUID DEPTH OF 2.5 INCHES. RUN NO. 35

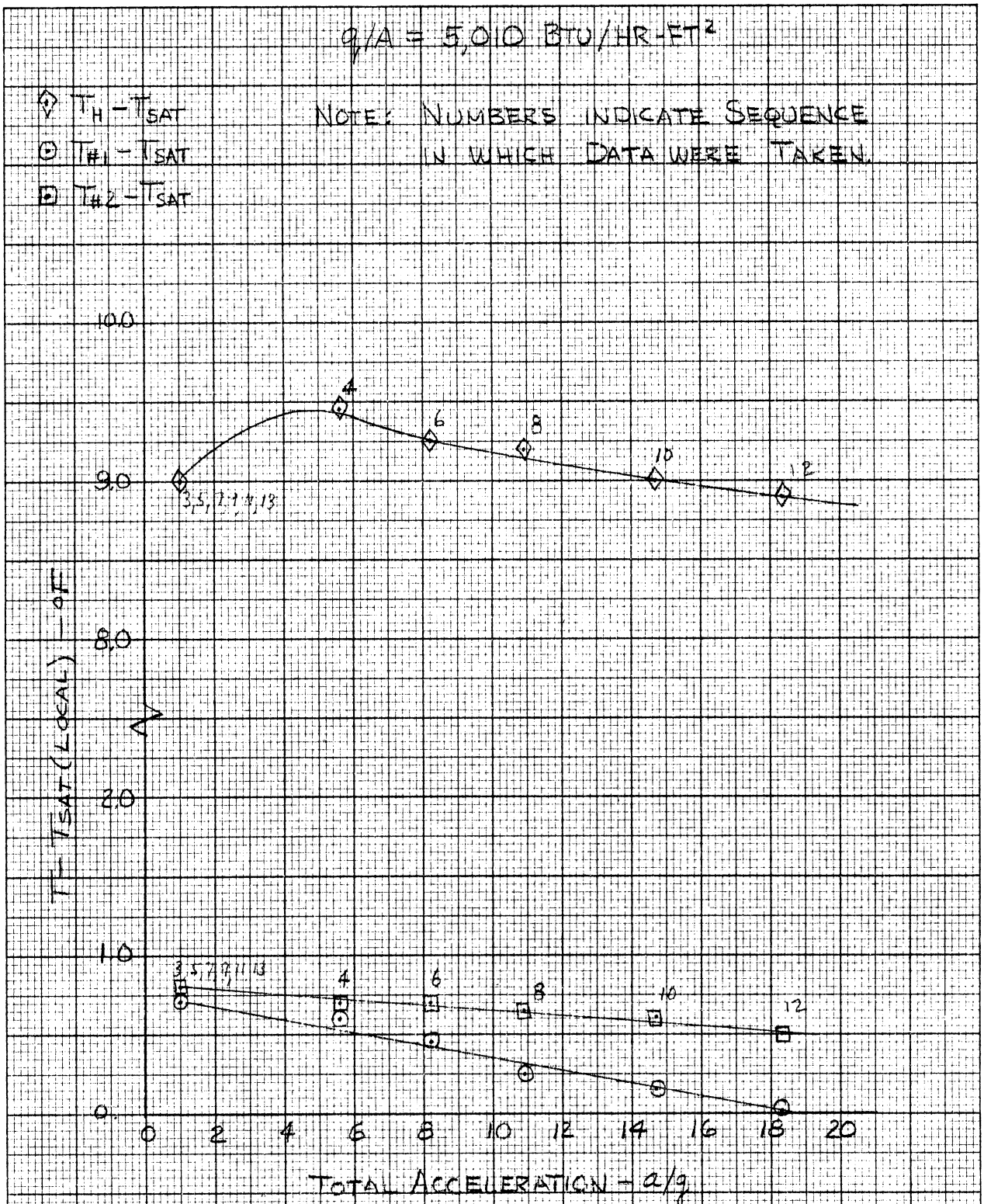

FIGURE 24. COMPOSITE PLOT FOR LIQUID DEPTH OF 2.5 INCHES. RUN NO. 36

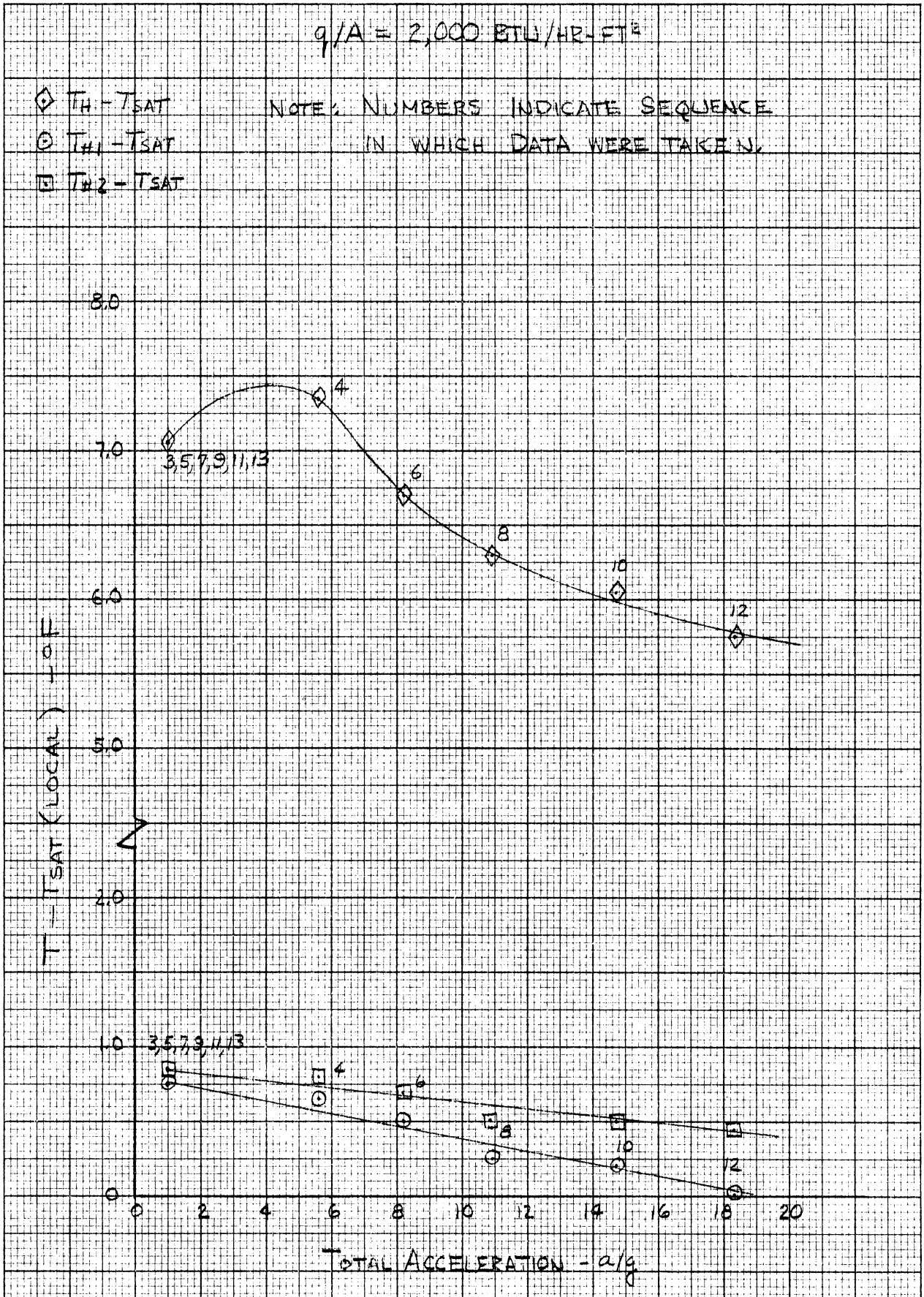

FIGURE 26. COMPOSITE PLOT FOR LIQUID DEPTH OF 2.5 INCHES. RUN NO. 37

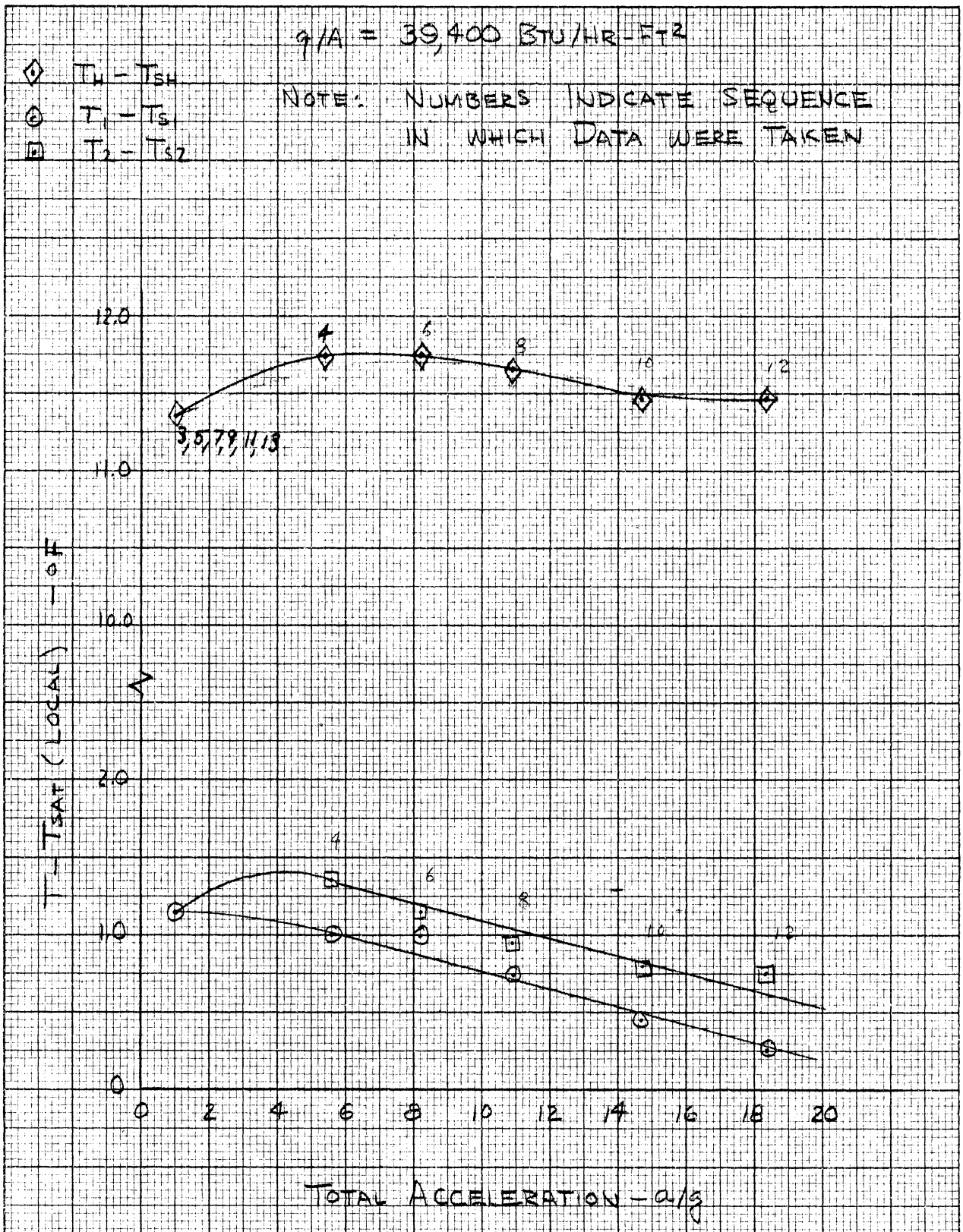

FIGURE 28. COMPOSITE PLOT FOR LIQUID DEPTH OF 2.5". RUN NO. 38

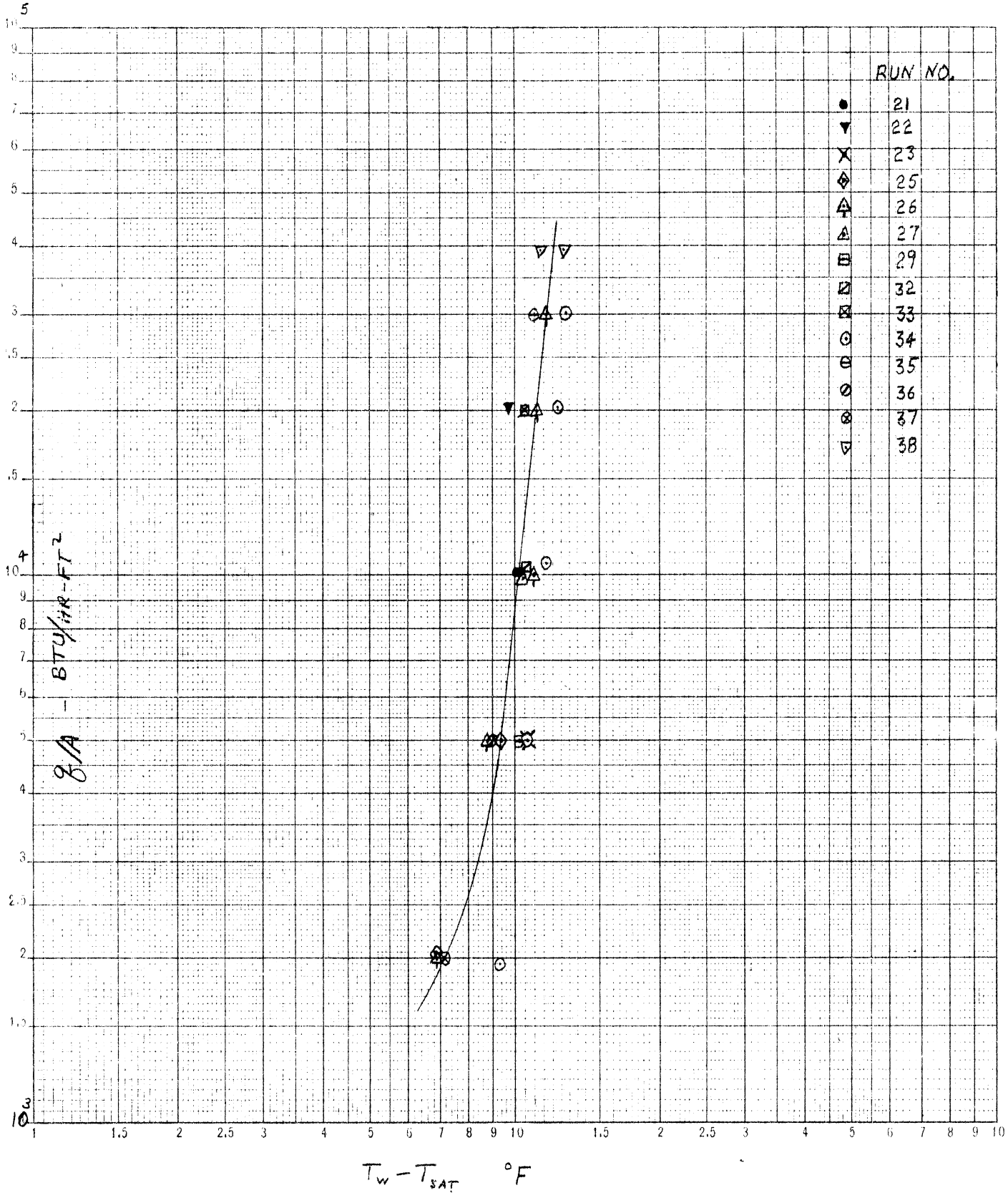

FIGURE 29 . HEAT FLUX vs. $T_w - T_{SAT}$ FOR SATURATED LIQUID NITROGEN AT $a/g = 1$.

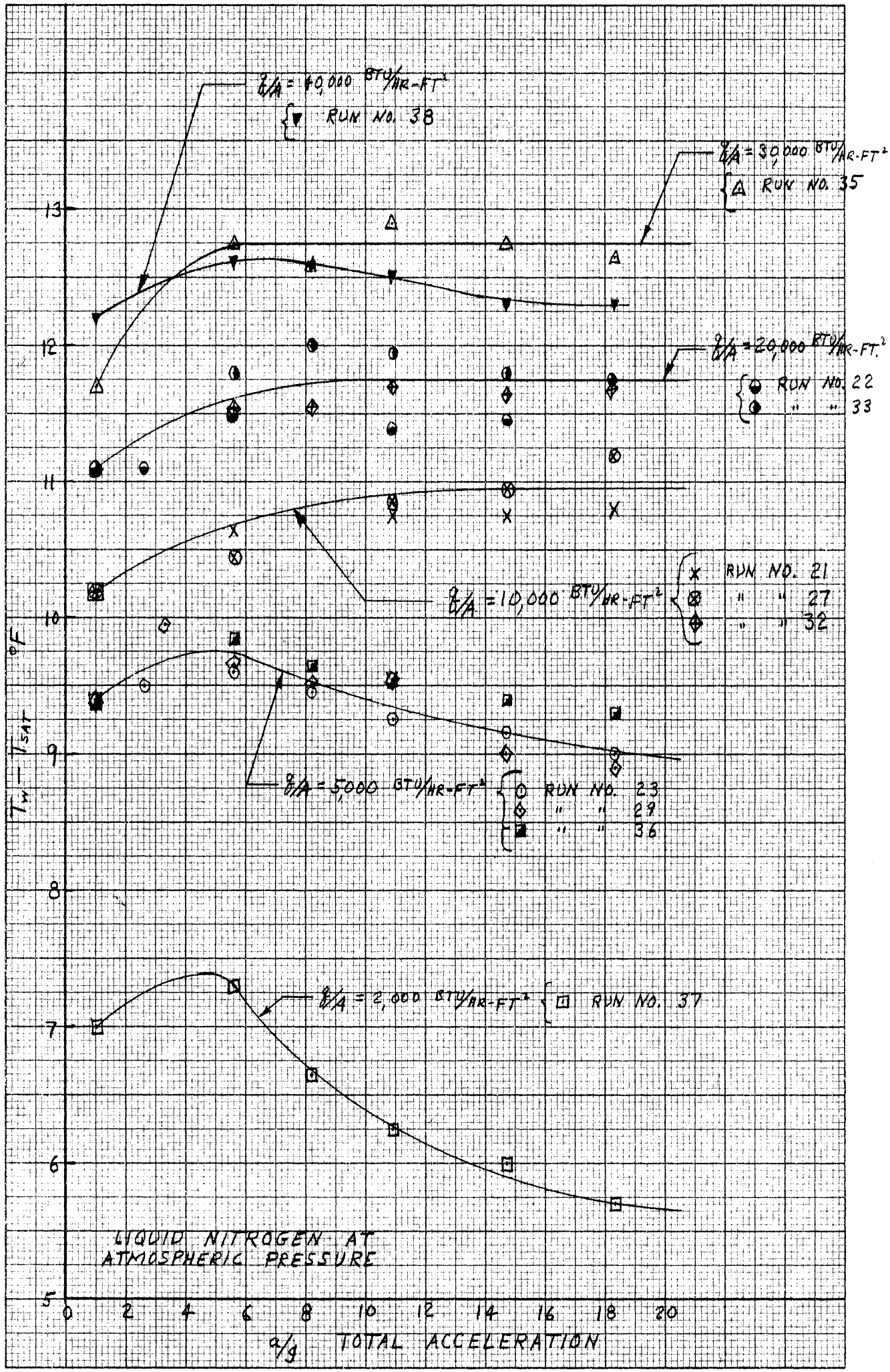

FIGURE 30. VARIATION OF $T_w - T_{SAT}$ WITH SYSTEM ACCELERATION AT VARIOUS LEVELS OF HEAT FLUX.

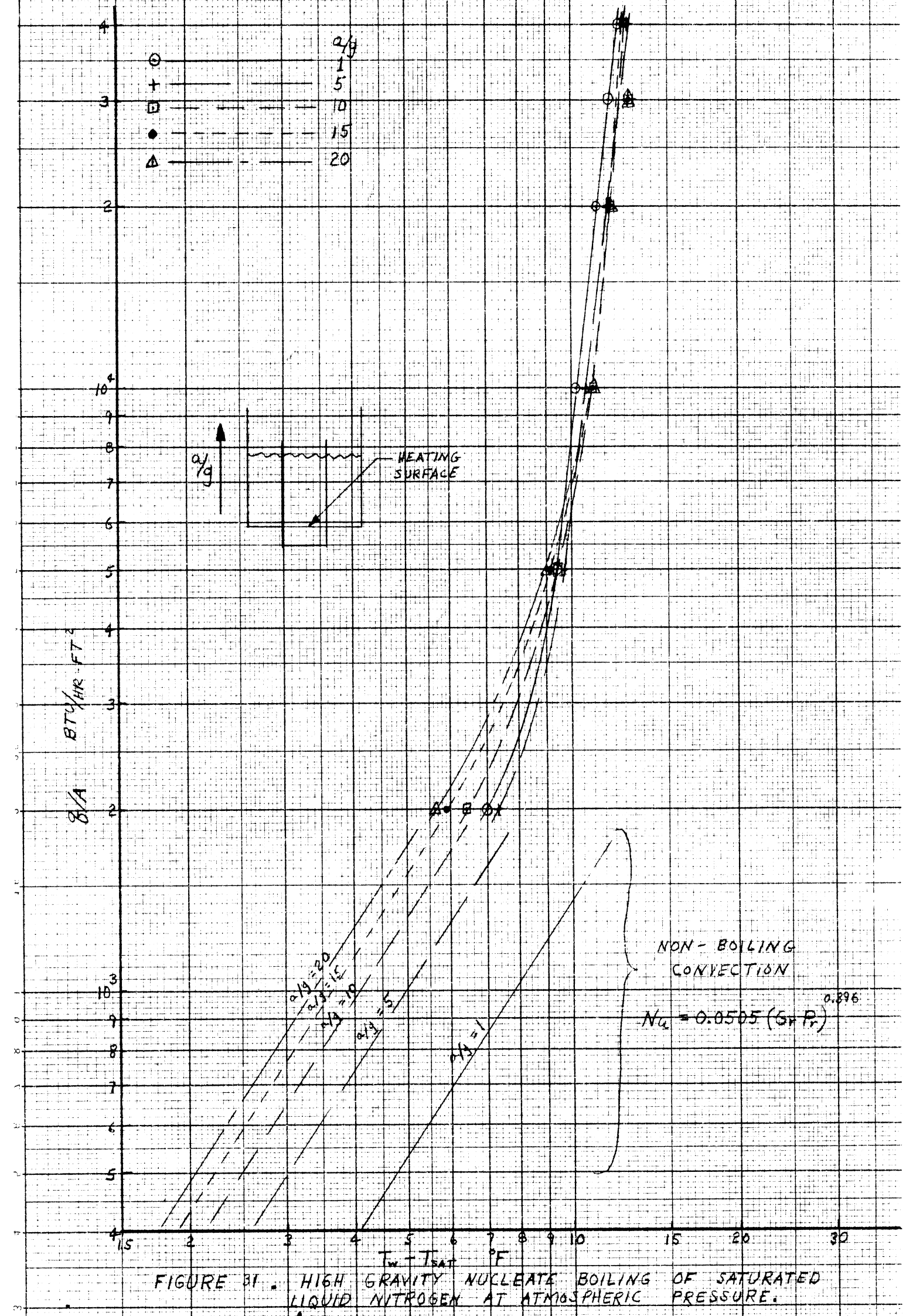

FIGURE 31. HIGH GRAVITY NUCLEATE BOILING OF SATURATED LIQUID NITROGEN AT ATMOSPHERIC PRESSURE.

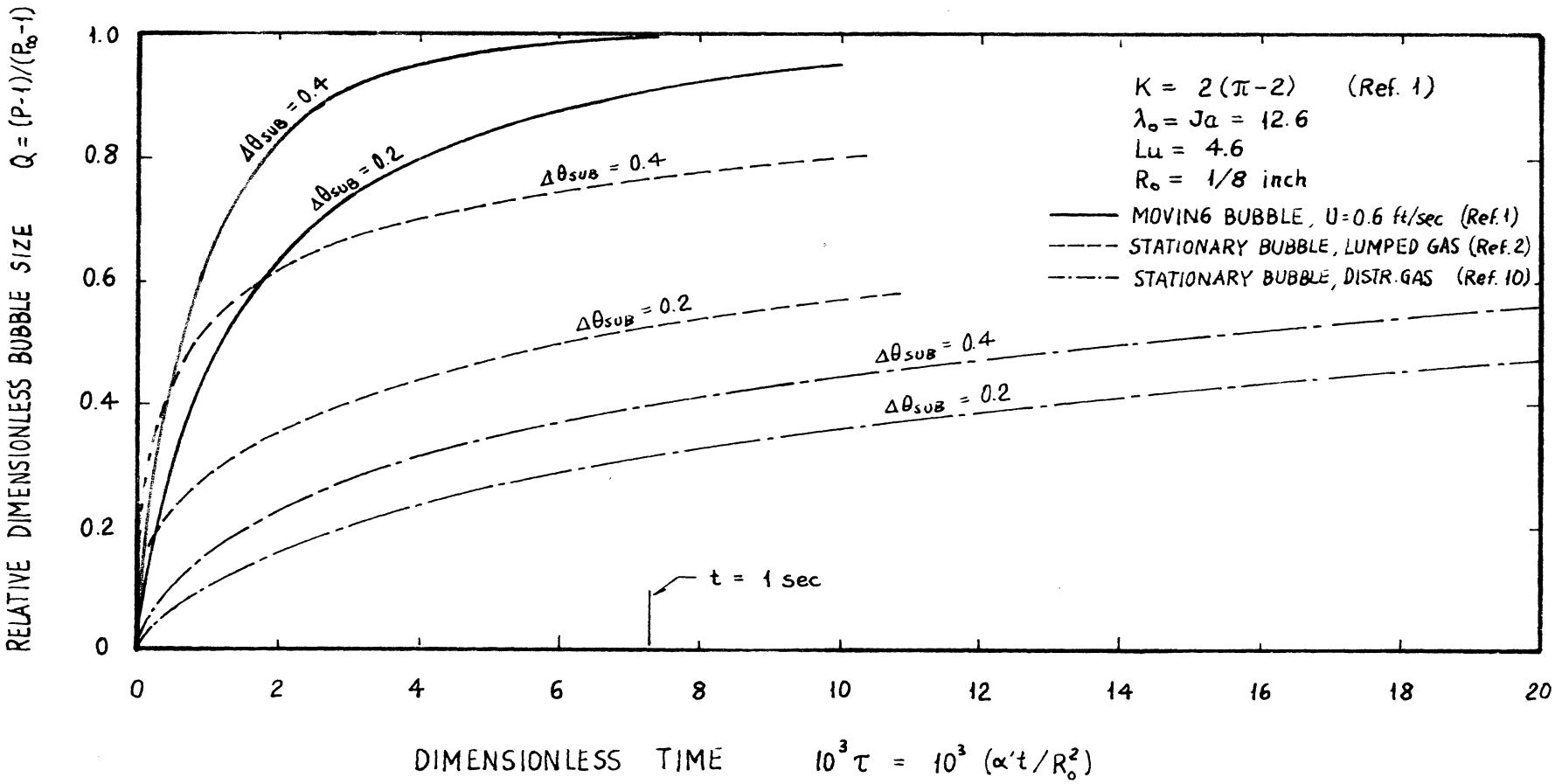

FIGURE 32. RELATIVE DIMENSIONLESS BUBBLE GROWTH. HELIUM IN LIQUID OXYGEN 3.1 atm.

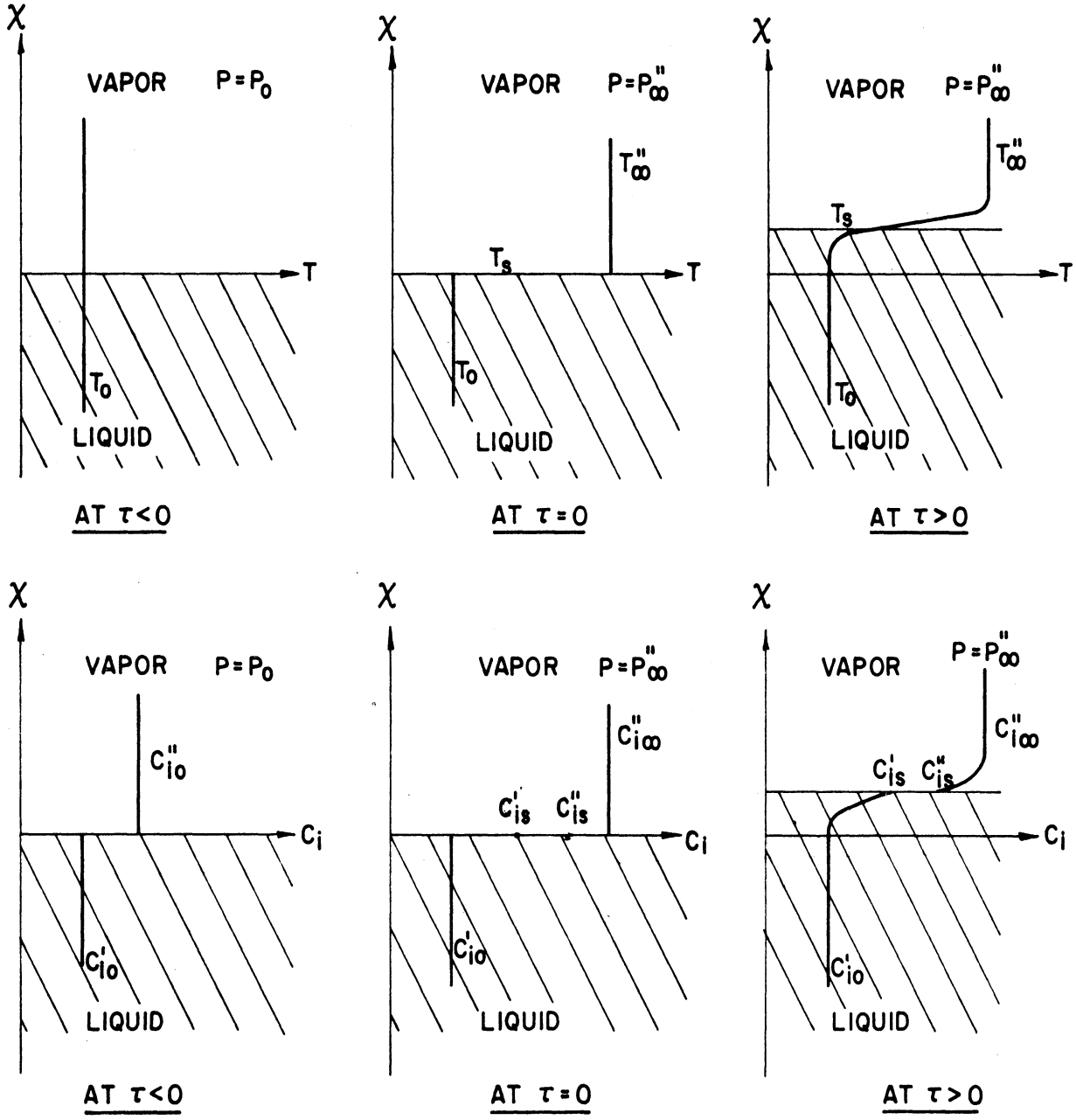

Figure 33. Schematic illustration of temperature and concentration distributions in the liquid and vapor regions at several different times.

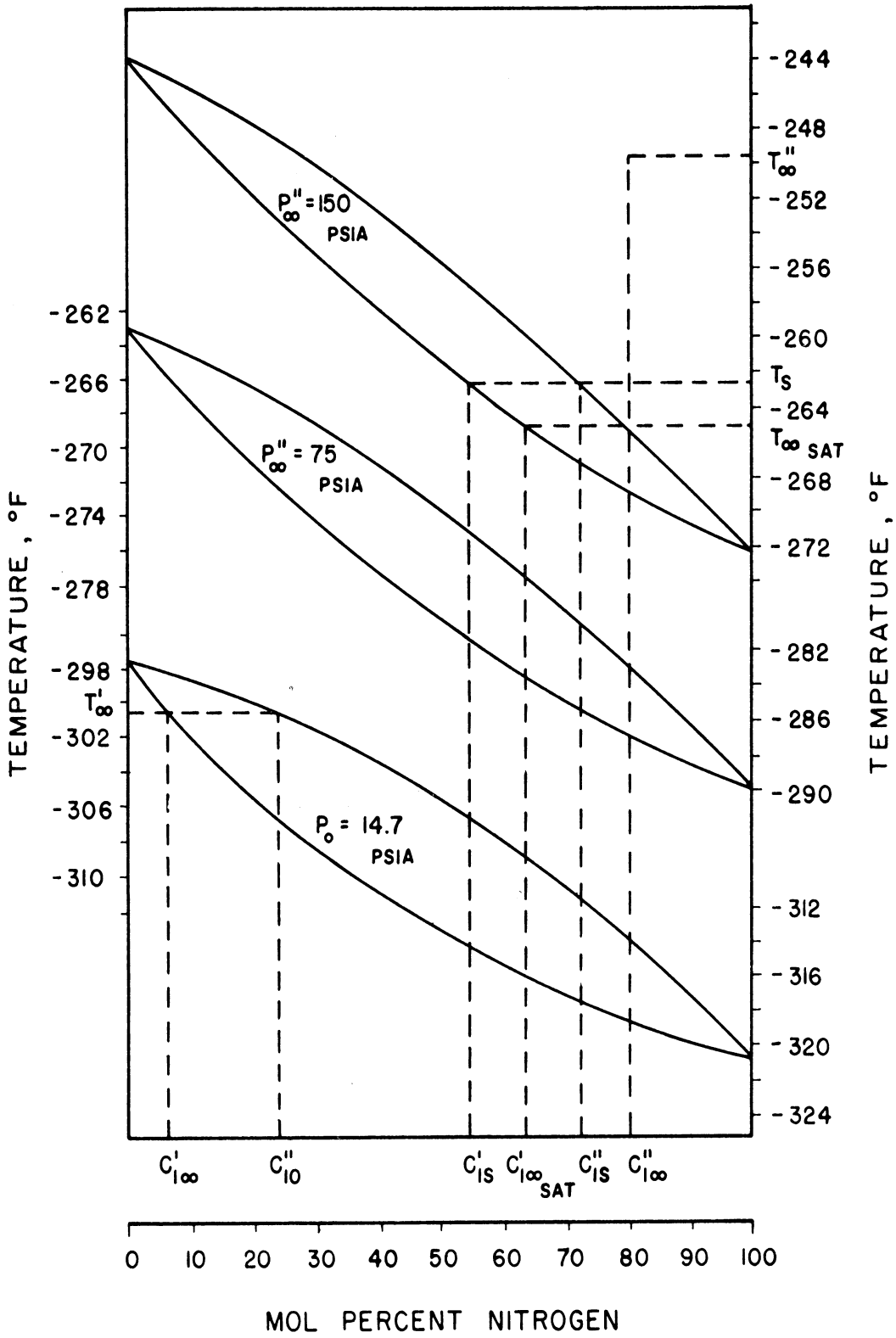

Figure 34. Equilibrium diagram of oxygen-nitrogen mixtures.

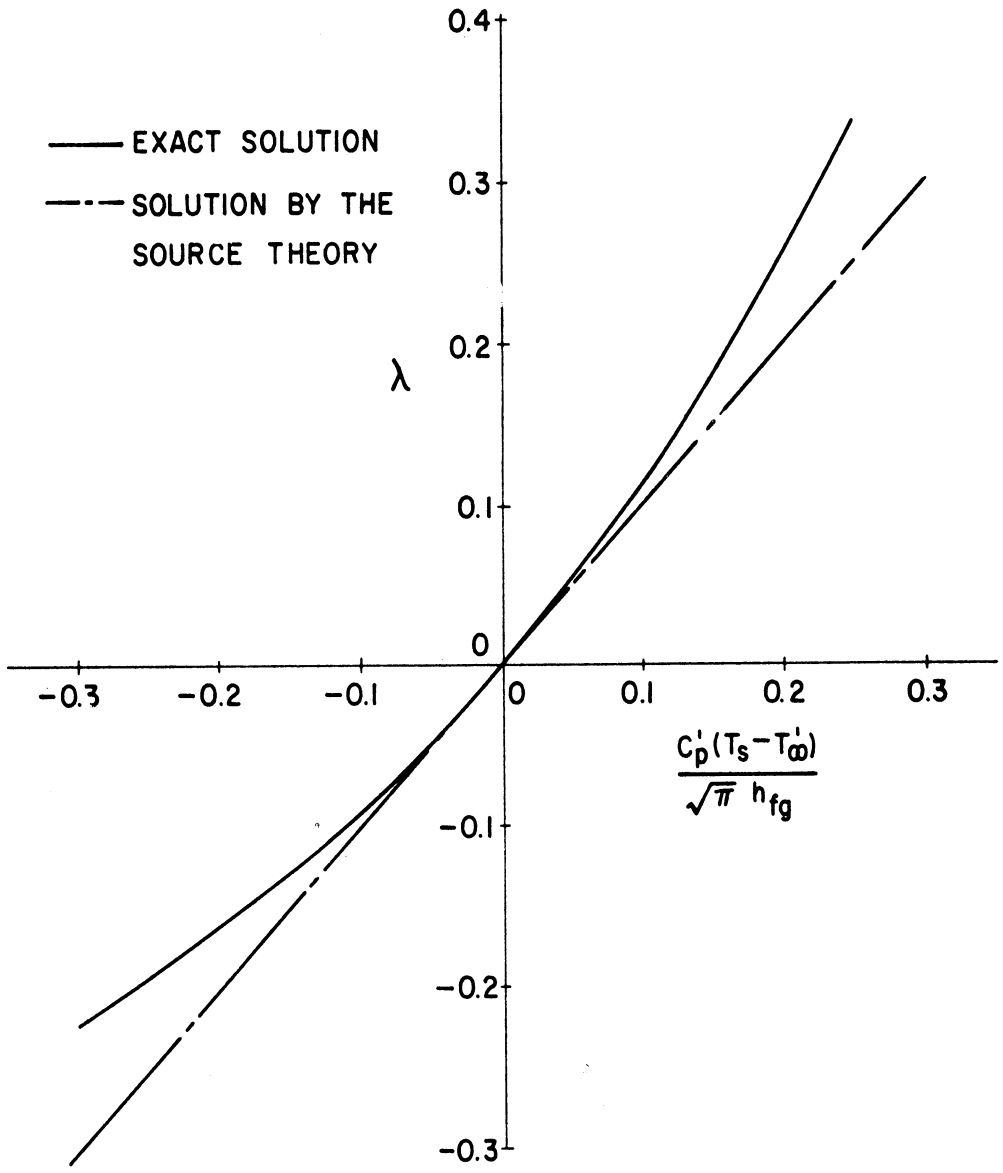

Figure 35. Growth-rate parameter of one-component systems with gas phase lumped.

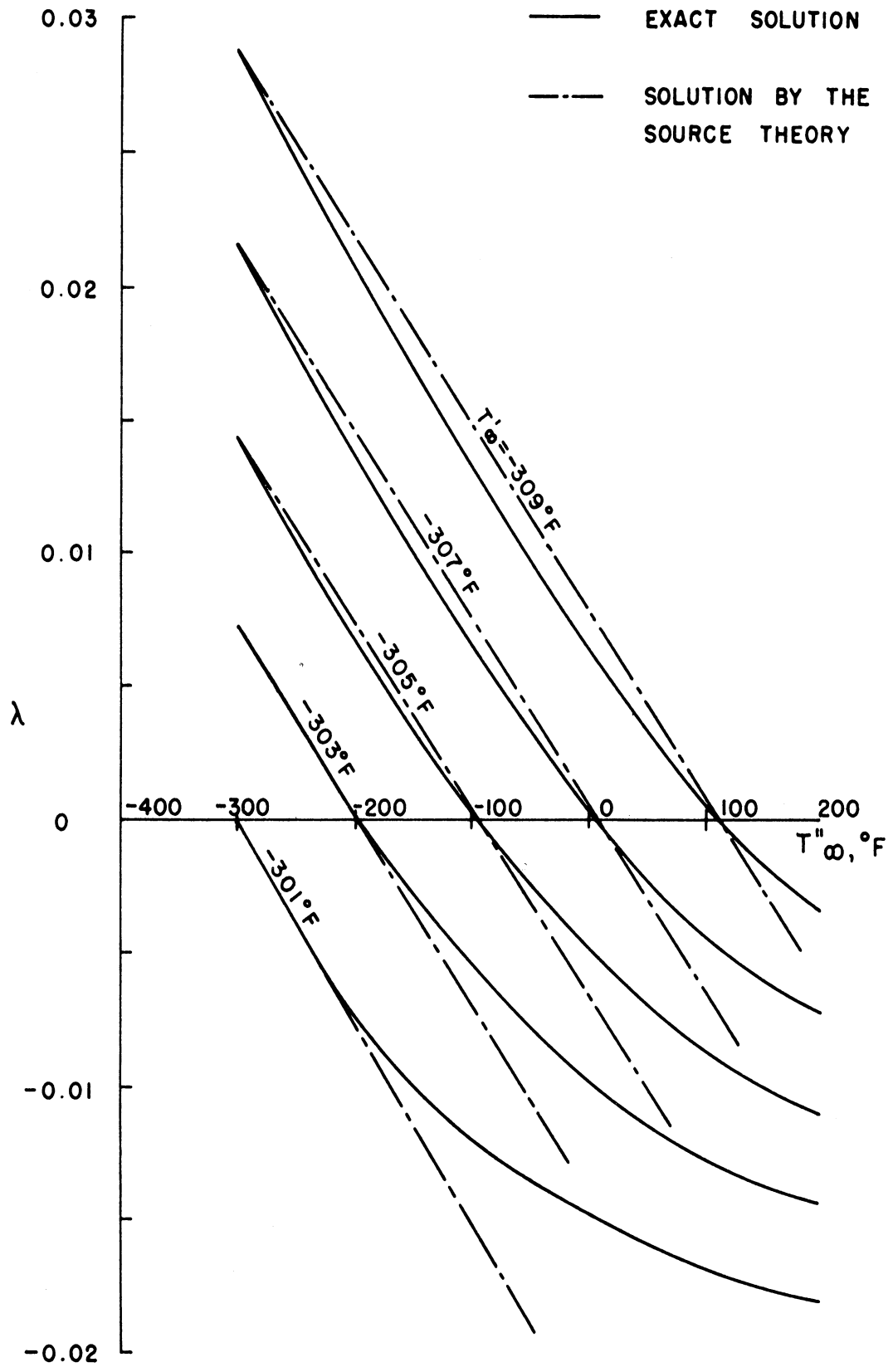

Figure 36. Growth rate parameter of liquid-vapor nitrogen system pressurized from 1 atm. to 3 atm.

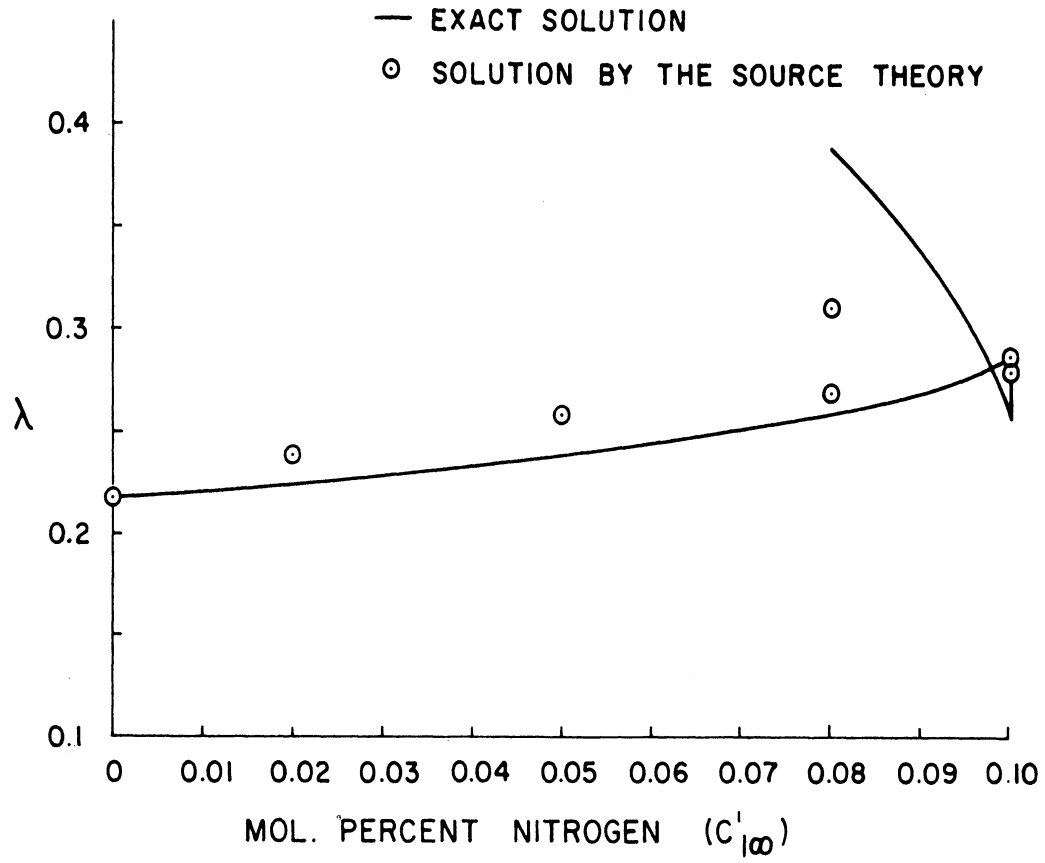

Figure 37. Growth-rate parameter of helium-nitrogen system pressurized from 4 atm. to 20 atm. $T'_{\infty} = T_{sat}$ (corresponding to 4 atm., $C'_{l\infty}$) and $C'_{l\infty} = C'_{l\infty_{sat}}$.

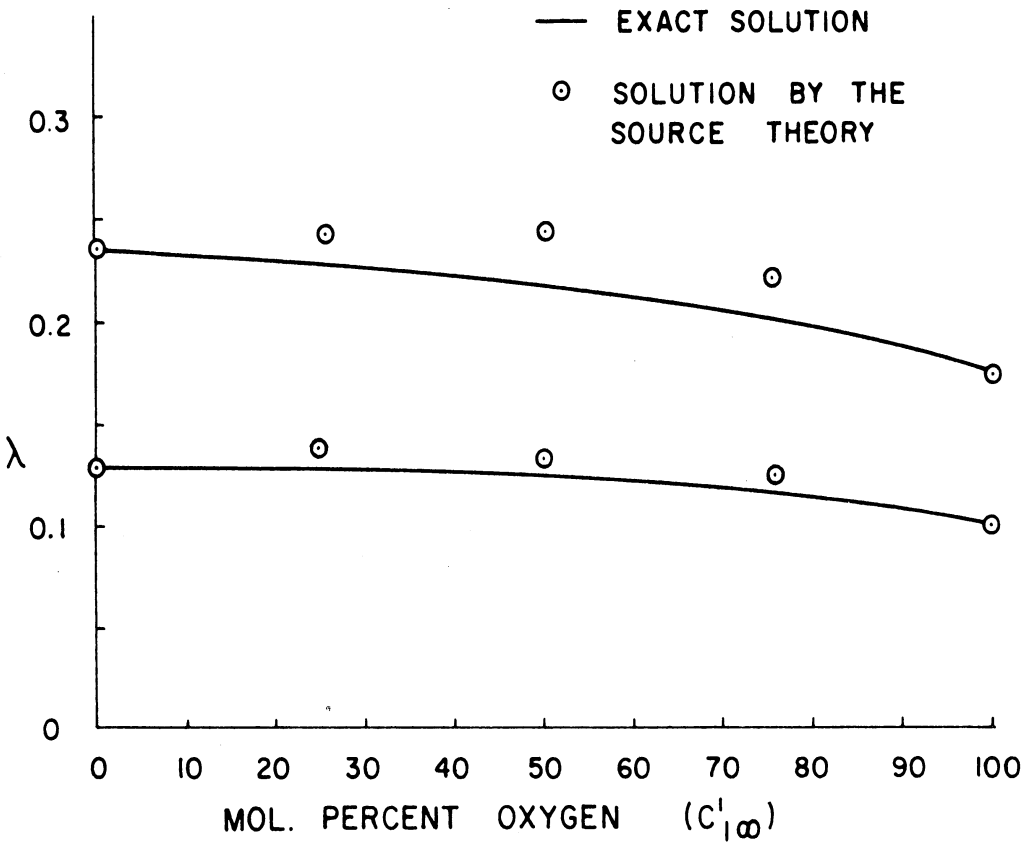

Figure 38. Growth-rate parameter of oxygen-nitrogen system pressurized from 14.7 psia to 75 psia and 150 psia. $T'_\infty = T_{sat}$ (corresponding to 14.7 psia, $C'_{i\infty}$) and $C'_{i\infty} = C'_{i\infty_{sat}}$.

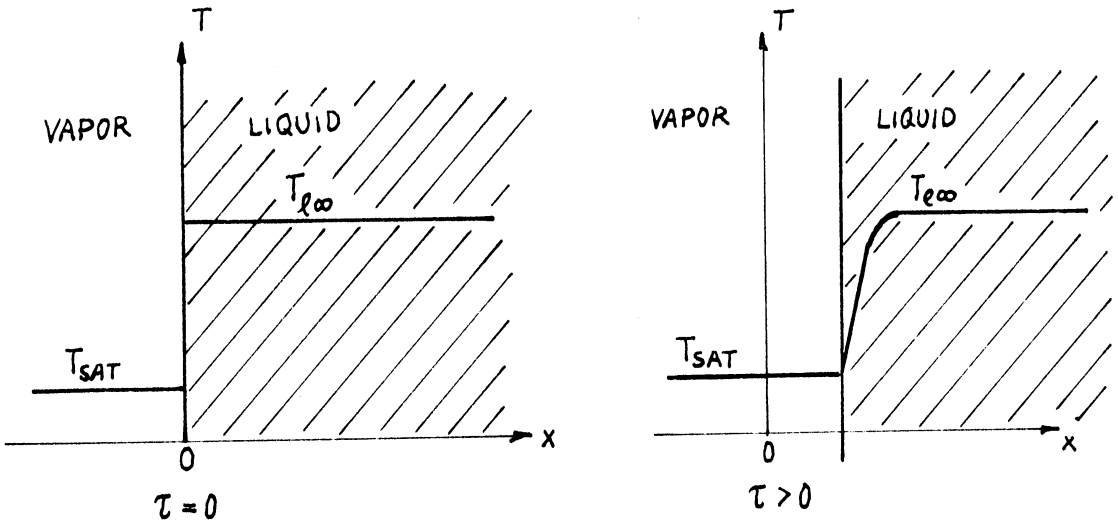

FIGURE 39. PHASE GROWTH IN A UNIFORM TEMPERATURE FIELD

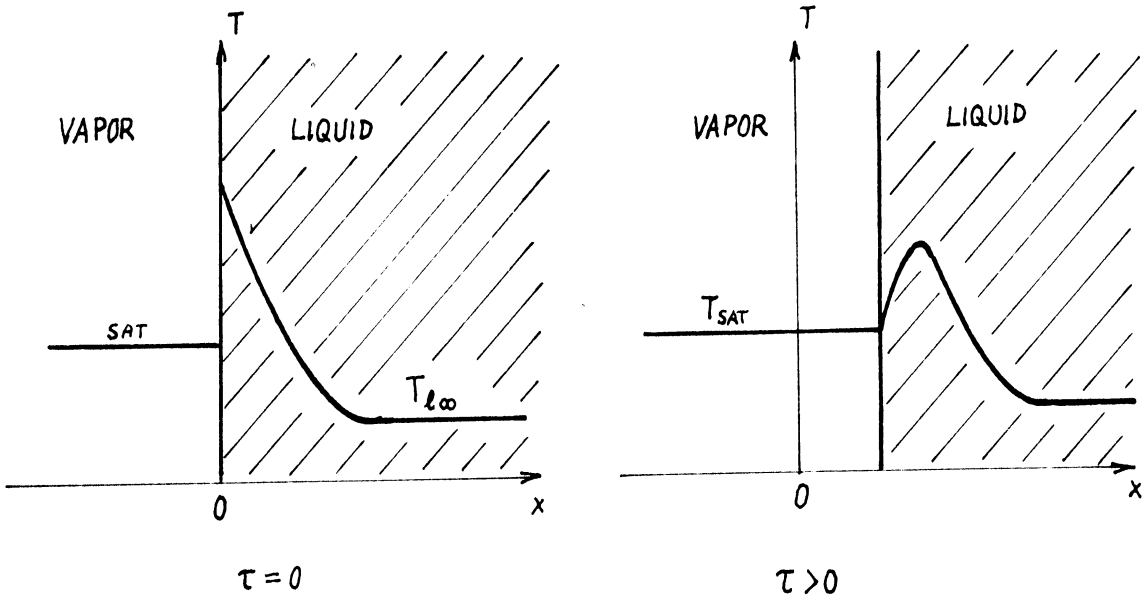

FIGURE 40. PHASE GROWTH IN A NONUNIFORM TEMPERATURE FIELD

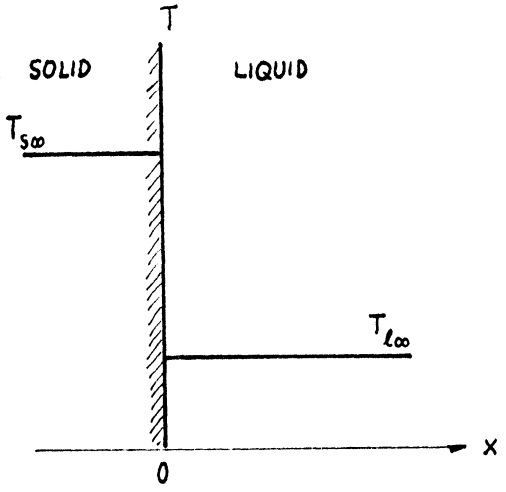

The moment at which a liquid is filled into a container.

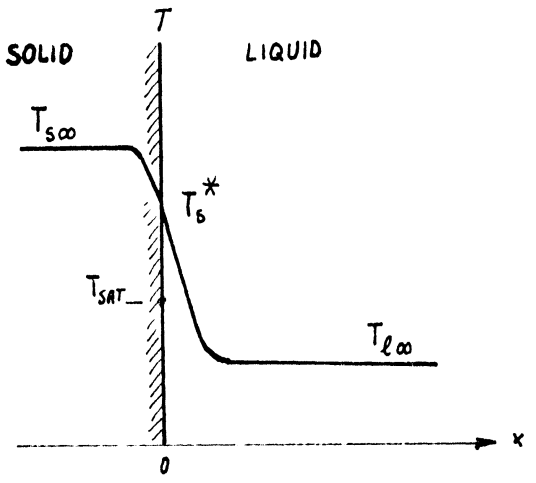

The moment immediately before the formation of vapor film or the growth of bubble.

Fig. 4.1 Conceptual Model of Heat Diffusion Before Phase Change

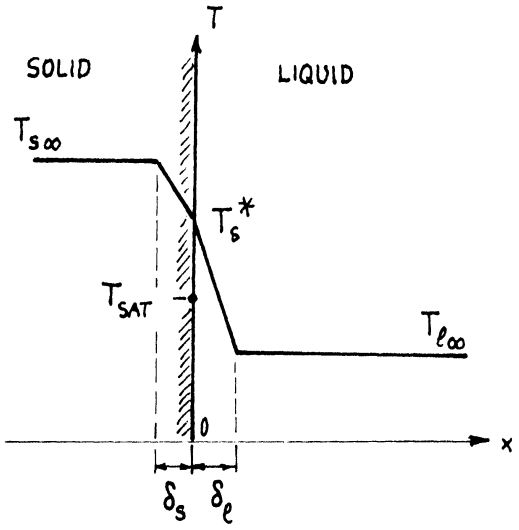

$\tau = 0$

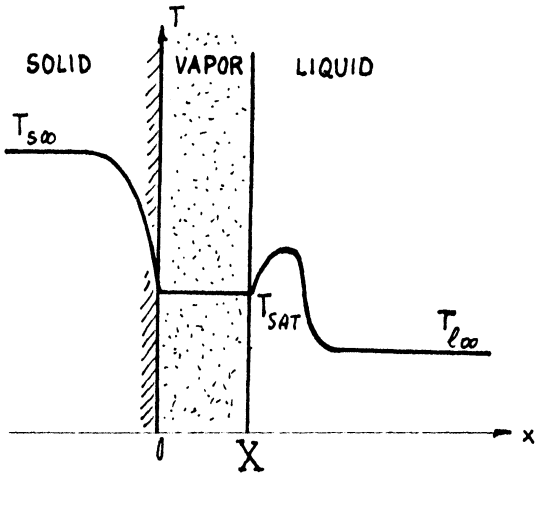

$\tau > 0$

Fig. 4.2 Conceptual Model of Phase Growth in Film Boiling On A Nonuniform Temperature Field.

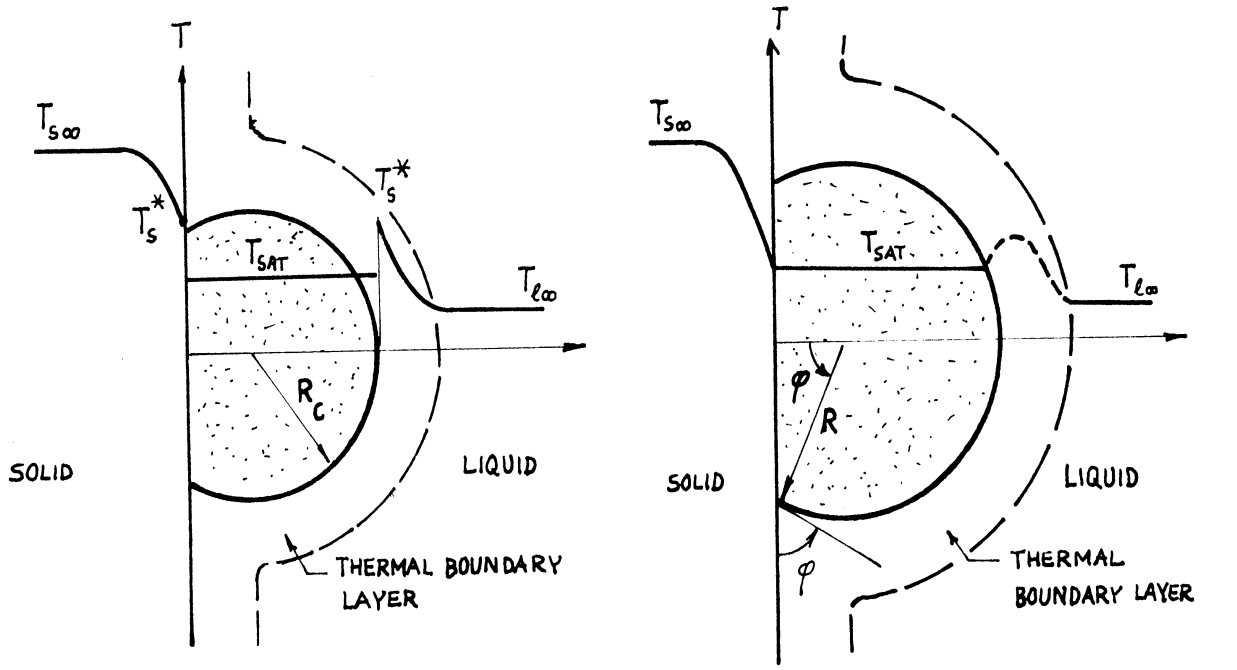

FIGURE 43. CONCEPTUAL MODEL OF A BUBBLE GROWTH IN A NONUNIFORM TEMPERATURE FIELD